CELLULAR MECHANISMS OF AUDITORY PROCESSING IN THE INFERIOR COLLICULUS

An in vivo patch-clamp study

Mei Lian Tan

CELLULAR MECHANISMS OF AUDITORY PROCESSING IN THE INFERIOR COLLICULUS

Cover: "44 days" (H.P. Theeuwes & M.L. Tan)

Printed by Ipskamp Drukkers, Enschede
ISBN: 978-90-9024454-9

CELLULAR MECHANISMS OF AUDITORY PROCESSING IN THE INFERIOR COLLICULUS

An in vivo patch-clamp study

CELLULAIRE MECHANISMEN VAN AUDITIEVE VERWERKING IN DE COLLICULUS INFERIOR

Een in vivo patch-clamp studie

PROEFSCHRIFT

ter verkrijging van de graad van doctor aan de
Erasmus Universiteit Rotterdam
op gezag van de
rector magnificus

Prof.dr. H.G. Schmidt

en volgens besluit van het College voor Promoties.

de openbare verdediging zal plaatsvinden op
woensdag 16 september 2009 om 15.30 uur

door

Mei Lian Tan

geboren te Utrecht

PROMOTIECOMMISSIE

Promotoren:	Prof.dr. J.G.G. Borst Prof.dr. L. Feenstra
Overige leden:	Prof.dr. M.A. Frens Dr. T.J.H. Ruigrok Prof.dr.ir. J.H.M. Frijns

The research in this thesis was financially supported by a Neuro-Bsik Grant and by the Heinsius Houbolt Fund.

Publication of this thesis was financially supported by:
ALK-Abelló B.V., Artu Biologicals, Atos Medical B.V., Beltone Netherlands B.V., Beter Horen B.V., Carl Zeiss B.V., Daleco Pharma B.V., Decos Systems B.V., EmiD audiologische apparatuur, GlaxoSmithKline, de Nationale Hoorstichting / Sponsor Bingo Loterij, de Nederlandse Vereniging voor KNO-heelkunde en Heelkunde van het Hoofd-Halsgebied, Olympus Nederland B.V., Oticon B.V., Schoonenberg Hoorcomfort, Veenhuis Medical Audio B.V.

aan mijn ouders

voor Thijs en Hugo-Max

CONTENTS

Chapter 1	General introduction and outline of the thesis	**9**
Chapter 2	Expression of vesicular glutamate transporters 1 and 2 in the mouse inferior colliculus	**27**
Chapter 3	Membrane properties and firing patterns of inferior colliculus neurons: an in vivo patch-clamp study in rodents	**39**
Chapter 4	Comparison of responses of neurons in the mouse inferior colliculus to current injections, tones of different durations and sinusoidal amplitude-modulated tones	**67**
Chapter 5	Cellular mechanisms of FM tuning in the mouse inferior colliculus	**99**
Chapter 6	General discussion	**119**
Summary		**133**
Samenvatting		**137**
Dankwoord		**142**
Curriculum Vitae		**146**
List of publications		**147**
List of abbreviations		**148**
References		**150**

Chapter 1

General introduction

Normal hearing is essential for optimal communication and survival of animal species. In The Netherlands hearing loss continues to be a growing problem in health care. For an individual it is a large social limitation, to society it is an economic burden. The prevalence of hearing loss in The Netherlands is estimated at 1.3 million and the costs for Dutch health care in 2003 were estimated to be 639 million euros (Kramer et al. 2006). The list of etiologic factors for hearing loss is extensive and some causes are better understood than others (Bauer and Jenkings 2005). Central auditory hearing disorders are still poorly understood, which is mainly due to a lack of consequent and reliable tests to quantify the severity of hearing loss and the difficulty to localize the pathophysiological substrate. In addition, many aspects of basic cell physiology within the normal auditory system are still unresolved, while pathophysiological mechanisms behind hearing loss need to be clarified.
Situated at the level of the midbrain, the inferior colliculus (IC) plays a prominent role within the auditory pathway. The IC is an essential relay station between lower auditory nuclei and thalamus/auditory cortex. In the IC, ascending and descending, excitatory and inhibitory inputs are processed. Most studies in literature are based on intracellular recordings from brain slices (in vitro) or extracellular recordings in awake or anaesthetized animals (in vivo). How cell characteristics of the IC contribute to sound processing is largely unknown. In this thesis the relative contribution of synaptic inputs and membrane properties to responses of IC neurons to sounds are examined. For this purpose, the in vivo patch-clamp technique was used to investigate IC neuron responses to constant current injection and stimulation with different types of sound. This introduction includes an overview of the central auditory pathway, a description of a few central auditory hearing disorders, background information of anatomy and physiology of the IC and an outline of the thesis.

The central auditory pathway

The central auditory pathway starts at the cochlear nerve, which leads to the cochlear nucleus (CN) in the brainstem. From there on, a highly organized complex of several inter- and intra-nuclear connections exist between the superior olivary complex (SOC) in the medulla, the lateral lemniscus (LL) in the pons, the inferior colliculus at midbrain level, the medial geniculate body of the thalamus and the auditory cortex (Fig. 1.1).

Cochlear nucleus

The cochlear nucleus (CN) is the first auditory nucleus in the brainstem. It contains a tonotopic map (maintained from the tonotopic map of the cochlea) with low frequencies in the lateral regions and high frequencies in the medial part of the CN (Hudspeth 2000). A massive divergence of cochlear nerve projections has been found, with a great variety in structure and function of postsynaptic neurons. In addition, there are abundant inhibitory neurons that shape the primary excitatory input. The incoming auditory signal usually consists of a complex pattern with spectral, temporal and spatial aspects. In the CN this complex pattern is decomposed when different cell types distribute the sound information to specific targets more downstream in the auditory pathway (Winer and Schreiner 2005). The CN can be divided into

three subnuclei: the dorsal cochlear nucleus (DCN), the anteroventral cochlear nucleus (AVCN) and the posteroventral cochlear nucleus (PVCN) (Paxinos and Watson 1998; Ramón y Cajal 1995; Santi and Mancini 2005).

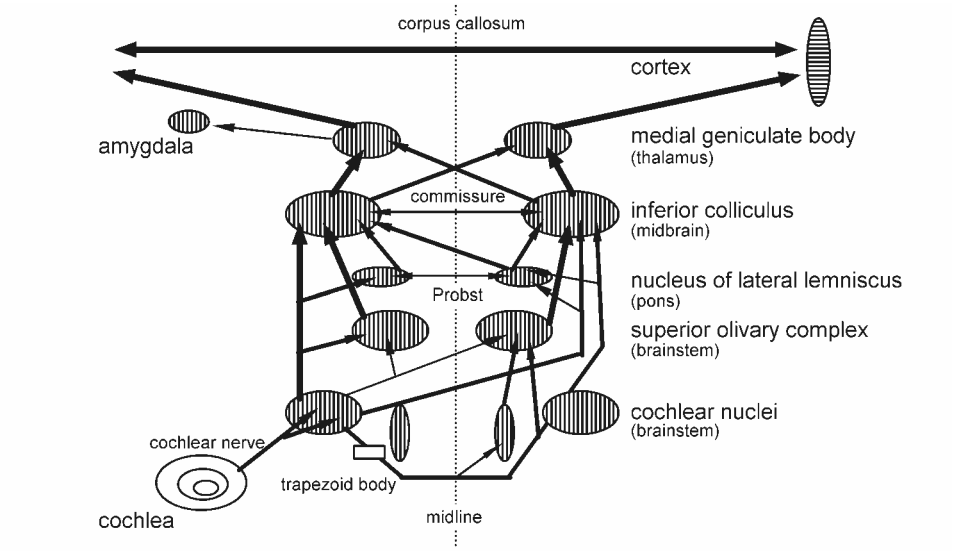

Figure 1.1 A schematic overview of the nuclei and ascending pathways of the central auditory system.
All nuclei are bilaterally present. Most of them (except the superior olivary complex) have bilateral ascending projections. Contralateral communication via fibers of a commissure is only seen in the nuclei of the lateral lemniscus (commissure of Probst) and the inferior colliculi. See also text for subdivisions of each nucleus (adapted and modified from Winer and Schreiner 2005).

Several cell types can be identified from either histological studies or from responses to sound. In the DCN, apart from giant cells and granule cells, the most prominent cell type is the fusiform (or pyramidal) cell with a pyramidal cell body and extensive dendritic tree. These cells show a pauser/buildup pattern consisting of a delayed discharge after stimulus onset or onset response followed by an abrupt decrease of spikes and subsequent increase in spike rate. Apart from excitatory inputs from the cochlear nerve, some of these neurons receive inhibitory inputs from other types of neurons, such as stellate, vertical, Golgi and cartwheel cells, which contain the inhibitory neurotransmitters GABA or glycine. In the PVCN, a different type of cell has been found. Octopus cells mainly respond with an onset type of firing pattern containing one spike or a burst of spikes at the beginning of the stimulus. Bushy and stellate cells have been found in mostly in AVCN (Santi and Mancini 2005). In contrast with fusiform cells, spherical bushy cells contain 1 or 2 short dendrites with little or no inhibition. Therefore, the firing pattern is rather similar to the auditory nerve input; they show a primary-like response, which means a sustained response throughout the tone, with a gradual decrease in spikes until a steady state is reached. Stellate (multipolar) cells are characterized by a chopper response containing several clustered spike bursts, with the first spike burst having the highest number of action

potentials. A third type of neuron in the AVCN is the globular bushy cell (Cant 1992). All these different cell types are present in different parts of the CN. Each cell type has intrinsic neuronal properties, a specific firing pattern and shows a different frequency-response area with a broad, narrow, symmetrical or asymmetrical tuning curve (Oertel 1991; Webster 1995). As a result, structure and function of these cells are closely related, and each cell type has its own, unique contribution to the processing of the auditory signal. From this point on, several parallel pathways arise (Frisina and Walton 2001), although the projecting neuron in the CN and the receiving target cell type in downstream auditory structures of the brainstem and midbrain may not have a strictly one-to-one basis (Winer and Schreiner 2005).

Superior Olivary Complex

The SOC is the first nucleus in which binaural inhibitory and excitatory inputs are integrated. In this nucleus, information about interaural time differences (ITD) that stems from the medial superior olive (MSO) and about interaural level differences (ILD) that originates from the lateral superior olive (LSO) converges (Webster 1995). This information is used to localize sound. LSO neurons mostly integrate monaural intensity differences between left and right ear for high frequencies and transmit this information to the lateral lemniscus and inferior colliculus. LSO neurons receive excitatory inputs from the ipsilateral AVCN (Santi and Mancini 2005; Winer and Schreiner 2005). In most species the medial nucleus of the trapezoid body (MNTB) is present. Neurons in this nucleus receive excitatory inputs from the contralateral AVCN and have inhibitory projections to the LSO. Interestingly, the presence of MNTB in humans has been questioned for a long time. In a recent post-mortem study of human brainstems this structure has been identified with Nissl stainings and is comparable with the MNTB of other low-frequency hearing mammals (Kulesza 2008), but this result has been questioned (Hilbig et al. 2009). Neurons in the MSO, the second main nucleus within the SOC, compare sound delays between both ears, mainly at lower frequencies (Yin and Chan 1990).
In contrast with the somatosensory and visual systems, there are many descending subcortical connections in the auditory system. Bilateral and topographical descending connections from the olivary nuclei, peri-olivary cell groups surrounding the SOC and the nuclei of the trapezoid body onto different parts of the cochlear nucleus are present (Spangler et al. 1987). These descending projections are preserved in the IC and auditory cortex (Winer and Schreiner 2005).

Nucleus of the lateral lemniscus

Three nuclei can be found in the lateral lemniscus: a dorsal (DNLL), an intermediate (INLL) and a ventral nucleus (VNLL) (Paxinos and Watson 1998; Ramón y Cajal 1995). DNLL neurons are mostly GABAergic (>85%), while VNLL neurons are mainly glycinergic (>80%). Except for the INLL, in which GABAergic and glycinergic cells constitute <20% of the neurons, the nucleus of the lateral lemniscus plays an important inhibitory role within the auditory system (Saint Marie et al. 1997). Neurons in the dorsal and ventral nuclei also show distinct temporal properties (spiking patterns of onset and duration)

suggesting that they shape the timing information towards their downstream targets, which include the bilateral inferior colliculi. This is supported by neuroanatomical studies that show that the DNLL has mostly bilateral projections to the central nucleus of the IC (CNIC), whereas the VNLL has ipsilateral monaural connections with the CNIC (Winer and Schreiner 2005). The nuclei of the lateral lemniscus communicate via fibers of the commissure of Probst (Santi and Mancini 2005). Transsection of this commissure decreases the precision of sound localization, especially in the horizontal plane (Ito et al. 1996).

Inferior Colliculus

The anatomy and physiology of the IC will be discussed in detail below.

Thalamus

The thalamus is situated between midbrain and forebrain. The lateral geniculate body is part of the visual system, whereas the medial geniculate body (MGB) is involved in the auditory system. The ventral division of the MGB is characterized by Golgi type I and II cells (Santi and Mancini 2005). Interestingly, the number of Golgi type II/GABAergic neurons in the MGB differs across species, suggesting that auditory processing is different for each type of species. Again, there is a systematic tonotopy of frequency distribution, mostly in the ventral part, which receives inputs from the CNIC and auditory cortex (Hudspeth 2000; Santi and Mancini 2005). Compared with other auditory nuclei, the function of the MGB is probably least understood. Most likely it plays a role in multimodality processing (Frisina and Walton 2001). The dorsal part of the MGB is believed to be part of attention and temporal processing, while the medial division of the MGB has afferent inputs from non-auditory sources such as the vestibular system. This medial part of the MGB projects to any part of the auditory cortex, but also to non-auditory cortex and amygdala which is essential in learning processes (Winer and Schreiner 2005).

Auditory Cortex

The auditory cortex (AC) consists of millions of neurons that are arranged in six layers. Interneurons or other neurons such as pyramidal cells vertically link the layers. Primary regions receive topographic projections from the auditory thalamus. In humans, the primary auditory cortex is located in the upper bank of the temporal lobe (Santi and Mancini 2005). There are numerous projections to all subcortical structures that have been mentioned above. In the AC, subdivisions differ among species and its functions are just as diverse. Higher order communication such as comprehending and initiating speech or vocalizations is ultimately the net result of integration and evaluation of behavioral significance, which differs between species (Hudspeth 2000; Winer 2005).

Central auditory hearing loss

Histo-anatomical studies may show important connections between auditory nuclei, but there are still numerous gaps in our knowledge how central auditory processing actually takes place, let alone what the pathophysiological mechanisms are behind central auditory hearing loss. In the past years, clinicians are increasingly more aware of the existence of central auditory hearing disorders but the available diagnostic tools and therapeutic options are rather limited. Apart from tumors and cerebrovascular accidents (which can be identified by radiological imaging), the pathophysiology of central auditory hearing loss is much less well defined, compared with the peripheral auditory system. Oto-acoustic emissions (OAEs), which reflect the function of outer hair cells in the cochlea, auditory brainstem response (ABR), pure tone and speech audiograms are tools that can be used to differentiate between peripheral and central auditory deficits. Middle and long latency-evoked potentials represent synchronous activity of large groups of neurons at the level of the auditory midbrain and cortex. In clinical practice, however, these are much less used since they are considerably more depending upon attention and subject state (awake, sedated or under anesthesia) compared with the hearing tests mentioned above (Brown 2005).
Auditory neuropathy and central auditory processing disorders are two types of central hearing loss that are diagnosed more and more frequently. Patients with auditory neuropathy complain of hearing loss, have normal outer hair cell function (normal OAEs), normal radiological imaging studies of the auditory system but have no measurable ABR waveforms, show poor speech perception and miss middle ear acoustic reflexes such as the stapedius reflex (Tibesar and Shallop 2005). Several synonyms for this disease have arisen over the years and it has been argued that the actual diagnosis "auditory neuropathy" should only be reserved for disorders at the level of the spiral ganglion cells and fibers of the auditory nerve (Rapin and Gravel 2003). Confusingly, sometimes this term has also been used to indicate more complex disorders of the central auditory system, the so-called "auditory processing disorders" (APDs). In the past thirty years, APDs have been described as interaction deficits between peripheral and central auditory pathways. Patients generally suffer from problems with sound localization, speech discrimination, auditory pattern recognition and temporal processing. In these patients, auditory processing is typically much worse than can be expected or predicted from normal tone audiograms and OAEs. Relatively normal tone audiograms or OAEs and brain stem response, but poor speech perception is one of the possible findings in APD. The prevalence of APD is estimated as high as 7% in childhood. Several underlying diseases have been described for APD, such as neurological disorders, infectious disease, trauma, intoxication, prematurity, cerebrovascular disorders, and metabolic disease. Several reports also mention APD as part of developmental abnormalities such as dyslexia, language impairment and learning disabilities (Bamiou et al. 2001). Until now, the pathophysiological mechanism behind this disease is poorly understood (ASHA 1996).
In general, it is not surprising that our knowledge of the central auditory system is limited compared with the more accessible peripheral system. Consistent (psycho-) physiological tests (such as middle and long-latency evoked potentials) are more complex towards the auditory cortex and are

difficult to interpret, compared with more objective tests (such as OAEs, brainstem audiometry or pure tone audiograms), since these tests are not (yet) fully developed until after approximately 10 years of age (Brown 2005).
One particular type of sensorineural hearing loss due to aging (presbyacusis) deserves to be mentioned separately. This type of hearing loss can be expected to claim a large portion of health care in the near future due to the increase in the aging population in general. The severity and time course of presbyacusis may be subjected to multiple variables, of which some are better understood than others. Anatomical, physiological, and audiological changes have been described in patients and animal models. Environmental factors, such as socioeconomic status and cultural barriers, other external factors, such as lifestyle and noise-exposure, as well as internal factors, such as genetics and cognitive variables play an important role in etiology and severity (Willott et al. 2001). As mentioned before, both in humans and in animal models, morphological anatomical changes have been found, both in the peripheral and in the central auditory system. Deterioration of outer and inner hair cells in the organ of Corti (cochlea), as well as a loss of eighth nerve fibers, but also changes in the brainstem and midbrain have been reported (Kashima ML et al. 2005). A decrease in the inhibitory neurotransmitter gamma-amino butyric acid (GABA) has been found at the level of the inferior colliculus (IC). This is expressed by a decrease in the relative number of cells containing GABA, a decrease in GABA content, GABA release and GABA receptors. All taken together, these changes lead to a decrease in inhibition that may contribute to the inability of speech discrimination and of performing other higher complex auditory tasks (Caspary et al. 1995). Possible causes for these changes are unknown. A chronic, progressive functional deafferentation due to a peripheral loss of input can be hypothesized.
Treatment options to restore and rehabilitate sensorineural hearing disorders comprise conventional external hearing aids. These have been extended with cochlear implants and, more recently, brainstem and midbrain implants (Eisenberg et al. 1987; House et al. 1979; Lim et al. 2008; Schwartz et al. 2008). In my opinion, to optimize treatment possibilities for hearing rehabilitation, we should gain more insight into the underlying pathophysiological mechanisms. This, in turn should be preceded by an increase in basic knowledge in physiology.

Anatomy of the IC

Grossly taken, the IC can be subdivided into a central nucleus that has a strictly auditory function, a lateral cortex that most probably has a multisensory function and a dorsal cortex of which the function is not yet clear. Analogous to the cochlea, cochlear nucleus and olivary complex, tonotopy is preserved in the IC. Low frequencies are represented in dorsolateral regions and high frequencies in ventromedial regions. From the size of the inferior colliculus, one can expect that this structure has a prominent role in the auditory system, since it is one of the largest auditory nuclei (Winer and Schreiner 2005). The IC contains more neurons than all other subcortical auditory nuclei combined; therefore the IC can be seen as an important sound-processing factory (Kulesza et al. 2002). The IC receives inputs from nearly all parts of the cochlear nucleus, olivary complex, lateral

lemniscus and auditory cortex. In addition, there are several intracollicular and commissural projections. This is the site where all auditory brainstem information converges and integration takes place. Although limited, behavioral studies indicate several functions of the IC in sound localization, attention and speech discrimination. The IC also seems involved in acousticomotor behavior such as the startle reflex, audiogenic seizures and is subjective to nociceptive influences (Winer and Schreiner 2005).
Like many other brain structures, the exact boundaries of each subdivision cannot be easily delineated. In literature, subdivisions have been identified with neuroanatomical and electrophysiological studies. However, electrophysiological recordings are best interpreted when post-mortem immunohistology is subsequently performed to identify cell localization. Most immunohistological studies include Nissl or myelin stains, Golgi impregnations or molecular methods such as the use of antibodies against calcium binding proteins or immunohistochemical assays for the metabolic marker cytochrome oxidase and, more recently, nicotinamide adenine dinucleotide phosphate-diaphorase (NADPH-d). Functional mapping of sound-evoked activity can be obtained when it is combined with immunohistochemical assays for uptake of 2-deoxyglucose in presynaptic endings or staining for c-fos protein in neurons (Loftus et al. 2008; Nudo and Masterton 1986; Paxinos and Watson 1998; Ramón y Cajal 1995; Saint Marie et al. 1999).

Central Nucleus

The largest nucleus within the IC is called the central nucleus (CNIC), which is a paired structure connected by a commissural arch (ICC). A unique organization is found in the CNIC due to the presence of fibrodendritic laminae. Based on dendritic branching and histological arrangements, two main morphological types of neurons have been identified in the CNIC in all species: disk-shaped (named "flat" in rats) and stellate cells ("less-flat" in rats) (Oliver 2005). Disk-shaped cells are highly oriented cells with parallel dendritic fields. Stellate cells that have a more spherical, radiating dendritic arbor alternate them. The cells are tonotopically organized from dorsolateral (low frequencies) to ventromedial direction (high frequencies) (Friauf 1992; Saint Marie et al. 1999). As stated before, the CNIC has an important auditory function and is connected with nearly all other nuclei within the auditory system. The CNIC receives ascending excitatory inputs from the medial superior olive (MSO), lateral superior olivary nuclei (LSO), and (dorsal and anteroventral) cochlear nucleus (DCN and AVCN). To a much lesser extent, GABAergic inhibitory inputs originate in the dorsal nuclei of the lateral lemniscus (DNLL), while glycinergic inhibitory inputs come from the ipsilateral LSO. A third important inhibitory input is from the ventral nuclei of the lateral lemniscus (VNLL) that may contain glycine, GABA or both (Fig. 1.2) (Merchán et al. 2005; Oliver 2005).

Lateral Cortex

The CNIC is surrounded by a few other structures. The lateral cortex (also known as external nucleus or external cortex) is situated laterally to the central nucleus and contains two or three layers, depending upon the species (Loftus et al. 2008). It receives inputs from the ipsilateral CNIC, lateral lemniscus, auditory cortex, spinal cord and somatosensory cortex. Stellate cells are predominantly present in this part of the IC. The exact function of this subnucleus is not yet known, but it most probably contributes to multimodal integration (Oliver 2005; Paxinos and Watson 1998; Ramón y Cajal 1995).

Dorsal Cortex

Dorsal to the CNIC lies the dorsal cortex (DC) (Paxinos and Watson 1998; Ramón y Cajal 1995). It can be subdivided into four layers and is characterized by neurons with axons without laminar organization, unlike the CNIC. It receives inputs from the neocortex and commissure of the IC and, to a lesser extent, from the DCN and DNLL. The function of the DC is uncertain (Oliver 2005).

Intracollicular projections within IC

The two inferior colliculi are connected through a commissural arch. Several tracer studies strongly support the idea that homotopic regions of both colliculi are activated even when only one colliculus has received incoming inputs from lower brainstem regions. Since tonotopy shows that CNIC and DNIC neurons project bilaterally at similar characteristic frequency, the function of the commissural projections may well be to amplify frequency selectivity (Saldaňa and Merchán 2005).

Ascending projections from IC

The main ascending target of the IC is the medial geniculate body (MGB) of the thalamus. This structure has a dorsal, ventral and medial division (Paxinos and Watson 1998; Ramón y Cajal 1995). Each division receives specific inputs from lower nuclei of the IC or brainstem and project to the auditory cortex and amygdala. Especially in the ventral division, tonotopy is preserved due to the strong inputs from the CNIC (Hudspeth 2000; Santi and Mancini 2005). MGB neurons show tonic or burst firing patterns after intracellular current injections and can be altered when glutamate, GABA and acetylcholine are applied. Auditory responses in the MGB are diverse and it can be questioned whether these responses originate in the MGB itself or result from the IC inputs. Since GABAergic cells are a minority in the MGB, inhibition is suggested to largely be a midbrain contribution. Sharpness of tuning, response latencies and reliability of responses to sound differ across MGB subdivisions and between species. Response latencies can be as short as <10 ms or may take up >100 ms. Temporal responses include onset, sustained, offset, onset-offset or a variety of patterns (Wenstrup 2005). Response latencies, temporal responses and sharpness of frequency tuning can be altered by anesthesia (Calford 1983; Edeline et al. 1999).

Descending projections from IC to other auditory nuclei

Main descending targets terminate in the ipsilateral DNLL, contralateral SOC and bilateral CN, while minor terminations are made in INLL, VNLL and other perilemniscal regions (Malmierca et al. 1996). Since most DNLL projections towards IC use the inhibitory neurotransmitter GABA, it is thought that this feedback system contributes to shaping the response of IC neurons. (A similar feedback pathway can be seen in the SOC and the medial olivocochlear system (MOC) that is situated nearby the SOC and both project to the contralateral outer hair cells in the cochlea.) Other circuits include the cochlear nucleus where giant cells and fusiform cells in the DCN receive bilateral inputs from the IC (Schofield and Cant 1999). Granule cells in the fusiform cell layer not only receive ipsilateral inputs from the IC, but they receive other afferent auditory and somatosensory inputs as well (Thompson 2005).

Descending projections to IC

There are three systems of descending projections to the IC: the cortico-collicular system from the auditory cortex, the thalamotectal system from the thalamic regions and the amygdala-collicular system. An important role for the cortico-collicular system is thought to be feedback (Winer 2005). The physiological impact of the last two systems has been suggested to be part of multimodal sensory integration (Casseday and Covey 1996), but this theory still requires more experimental evidence (Santi and Mancini 2005; Winer 2005).

Connections with non-auditory structures

Behavioral studies show that the IC has multiple connections with structures that are not strictly part of the auditory system but have essential biological relevance (Casseday and Covey 1996). Projections from the IC to non-auditory nuclei include the superior colliculus (SC) and paralemniscal regions that play a role in pinna movement that is used in most animals for sound localization. Other non-auditory pathways include pontine reticular formation, facial motor nucleus and spinal cord that are involved in the acoustic startle reflex that is prompted by brief loud sounds. Connections between IC and periaqueductal gray enable vocalizations through projections to nucleus ambiguus, nucleus retroambiguus and SC that turn over abdominal, pharyngeal and laryngeal musculature. In addition, the IC has indirect inputs to the amygdala via the SC that contribute to emotional behavior (Thompson 2005).
From this short overview it becomes apparent that auditory perception is a complex, yet highly organized entanglement of intertwined functions and the net result of integration of inhibitory, excitatory, converging, diverging, ascending and descending projections. Next to auditory cortex, the IC appears to be the largest processing 'factory' in the auditory system, where projections from all other auditory nuclei converge. It is therefore the focus of the research described in this thesis.

Physiology of the IC

The two most common techniques that have been used to examine cell physiologic properties of neurons in the IC are intracellular or patch-clamp recordings on brain slices (in vitro) or extracellular recordings in awake or anaesthetized animals (in vivo). Each technique has revealed different aspects that are important for processing auditory information and each technique has its benefits as well as its limitations.

In vitro patch-clamp recordings

In the late 70's Neher and Sakmann first developed the patch-clamp technique and in 1981 Hamill et al further improved this technique, which is now used as method of choice for single cell physiology (Hamill et al. 1981; Neher and Sakmann 1976; Verkhratsky et al. 2006). Within the IC, the patch-clamp technique has been used in pharmacological studies, which have shown that glutamate is the main excitatory neurotransmitter from ascending, descending and intrinsic inputs, while GABA and glycine are the principal inhibitory neurotransmitters (Kelly and Caspary 2005). This technique also allows us to measure firing patterns both spontaneously and artificially induced by current injections. In vitro, depolarizing and hyperpolarizing current injections in IC neurons have shown at least six different types of firing patterns, but a correlation between physiology and histological type or localization within the IC has not yet been observed. Although the classification of firing patterns is somewhat arbitrary, a gross distinction can be made between the following types of CNIC neurons that have been characterized by a variety of potassium- (K^+) channels. Sustained-regular cells (with constant interspike intervals) have been found in the majority of cells. Cells with this type of firing pattern have K^+-channels that are 4-aminopyridine- (4-AP) and tetraethylammonium (TEA)-sensitive (Sivaramakrishnan and Oliver 2001). These cells may play a role in encoding sound-duration. Onset cells (with one action potential just after the onset of current injection) may be more involved in precise timing of repetitive stimuli and have low- and high-threshold voltage dependent K^+- channels. Rebound-regular cells are similar to sustained-regular, but show a calcium-dependent rebound spike that may play a role in ongoing sound stimuli with the ability to time the end of a stimulus. Koch and Grothe reported that rebound spiking can also be induced by the mixed cation current I_h, which is a hyperpolarization-activated sodium/potassium current (Koch and Grothe 2003).
Adapting cells (with increasing interspike intervals) have been described to have a different calcium-dependent K^+-channel that is apamin-sensitive. Buildup-pauser and burst cells show similar firing patterns as in the cochlear nucleus (Bal et al. 2002; Peruzzi et al. 2000; Sivaramakrishnan and Oliver 2001). Onset, sustained-regular and rebound-adapting neurons have also been found in the cortical structures of the IC (Peruzzi et al. 2000). Between cells, differences in membrane characteristics have been found, such as input resistance, time constant, membrane excitability, resting membrane potential, etc. These are best examined with the patch-clamp method (Ahuja and Wu 2007; Basta and Vater 2003; Koch and Grothe 2003; Wu et al. 2004; Xie et al. 2007). Within the three subnuclei of the IC, differences in passive

membrane properties and firing patterns have also been described (Li et al. 1998). Due to the scarcity of studies in lateral and dorsal cortex it is difficult to determine whether these differences in membrane properties actually lead to functional differences compared with CNIC. In any case, the advantages of in vitro studies are that intracellular or patch-clamp recordings can be performed in specific areas within the IC that are visually easily accessible, guided by anatomic atlases (Paxinos and Watson 1998; Ramón y Cajal 1995). Membrane properties and ion channels can be studied in the presence or absence of drugs, and recordings are on average long lasting and stable with low access resistance (Koch and Grothe 2003; Margrie et al. 2002; Sivaramakrishnan and Oliver 2001; Sun and Wu 2008). Clearly, the largest disadvantage of existing studies is that auditory stimulation is not possible in brain slices. Current injections cannot accurately mimic auditory stimulation. So the question arises: if different ion channels and membrane characteristics determine all these firing patterns, how do they contribute to sound processing?

Sound-evoked extracellular recordings

Extracellular recordings in anaesthetized or awake animals show that pure tone auditory stimulation results in firing patterns that are similar to those observed with current injections in vitro, including onset, sustained, adapting and chopper responses (Palombi and Caspary 1996; Pollak et al. 1978; Rees et al. 1997). With extracellular recordings, the membrane potential remains unknown and it is very difficult to obtain information about sub-threshold fluctuations in the membrane potential. Another disadvantage of extracellular recordings is that there is a clear selection bias (Margrie et al. 2002). Since extracellular units are obtained by monitoring spike activity while lowering a recording pipette, neurons that show few or no action potentials will not be selected for recording. With this technique a tonotopic map has been found in the central nucleus, with cells responding to high frequency sounds in dorso-lateral direction and cells responding to low frequency sounds in ventro-medial direction (Saint Marie et al. 1999). In the dorsal and lateral cortex this tonotopy has been studied to a lesser extent. Traditionally, we refer to the characteristic frequency (CF) as the frequency for which a response can be obtained at the lowest sound pressure level (SPL) and the best frequency (BF) as the frequency with the most spikes at a given SPL (Winer and Schreiner 2005). In general, the DC has a low frequency ("broadly tuned") selectivity, which means that cells may respond to a broad range of frequencies. CNIC neurons show excitatory tuning curves that are surrounded by inhibitory areas. These tuning curves can be divided into four classes. Class I neurons are similar to the excitatory responses with lateral inhibition that have been seen in auditory nerve fibers; class II are strongly dominated by inhibition; class III neurons have small and weak inhibition; class IV neurons have complex, sometimes multiple excitatory and inhibitory regions. Sharpness in tuning increases with spectral frequency selectivity and from psychophysical tests the idea of 'critical bands' has arisen that are important for speech perception. These critical bands can be translated to tone discrimination in noisy environment, identification of vowels and animal vocalizations, and are based on the spectral filter properties of ICC neurons. Spectral tuning at the level of the IC is the net result of facilitation and inhibition of spectral

receptive fields from lower brainstem nuclei. Next to spectral coding, sound intensity coding has been found in the CNIC that is also an important aspect of speech perception. However, it is likely that more peripherally located sites, such as inner hair cells and synapses formed by the auditory nerve fibers, have a larger contribution to the dynamic range of the auditory system than that this phenomenon arises at midbrain level. It has not been clear to what extent spectral and sound intensity coding are present in the dorsal and lateral cortex of the IC (Ehret and Schreiner 2005). When higher communication is dissected into complex sounds, it appears that temporal modulations are essential for auditory perception of speech or other vocalizations. These modulations include frequency (FM), amplitude (AM) and duration modulations. We have learnt from extracellular work how cells respond to each of these complex sounds. For instance, cells can be selective for FM sweeps in upward or downward direction, or to FM sweeps alone compared with pure tones. The response to FM sweeps is referred to as the FM tuning of a cell. A preference for upward over downward sweeps was observed more often in the external nucleus compared with the central nucleus in bats (Gordon and O'Neill 2000). In the mouse CNIC, a concentrically arranged map of sweep speed has been described, with the representation of downward and of slow speeds mainly in the center of a frequency band lamina (Hage and Ehret 2003). Direction selectivity is already present at the cochlear nucleus (Britt and Starr 1976), but it is not clear whether FM selectivity is additionally shaped at the level of the midbrain.

Other important features of temporal processing include "periodicity coding" for amplitude-modulated (AM) sounds ("pitch" in speech perception) and "duration tuning" for sounds with different durations (Brand et al. 2000; Eggermont 2001; Ehrlich et al. 1997; Langner and Schreiner 1988; Perez-Gonzalez et al. 2006; Rees and Moller 1983; Schreiner and Langner 1988). AM tuning is mostly determined by the ability to synchronize the spectral envelope that modulates the basic carrier. A tonotopic map for periodicity has been found and is called 'periodotopy'. Low modulation frequencies are found in medial regions, whereas high modulation frequencies are represented in lateral parts of the CNIC (Rees and Langner 2005). In bats, duration tuning is biologically relevant, because best durations of neurons are near the range of their biosonar call durations that are used during hunting. It is important for cells to be able to detect the end of a sound. Rebound excitation has been observed to be part of this mechanism. A large role for side-band inhibition has been suggested in many studies, but cannot be adequately measured with extracellular recordings (Gordon and O'Neill 1998; Rees and Langner 2005). Considering the relatively large inhibitory inputs from DNLL, ipsilateral LSO and VNLL, it is likely that the IC is the first site where temporal processing of FM, AM and duration modulated sounds is prominent because this structure receives bilateral excitatory and inhibitory inputs from all lower auditory nuclei (Fig. 1.2). One of the main disadvantages of extracellular recordings is that characteristics such as the basic membrane properties of a cell cannot be studied with this method, in contrast with intracellular work in brain slices. With this method observation of spontaneous inhibitory and excitatory inputs is limited, therefore the mechanisms behind auditory processing can only be studied partially.

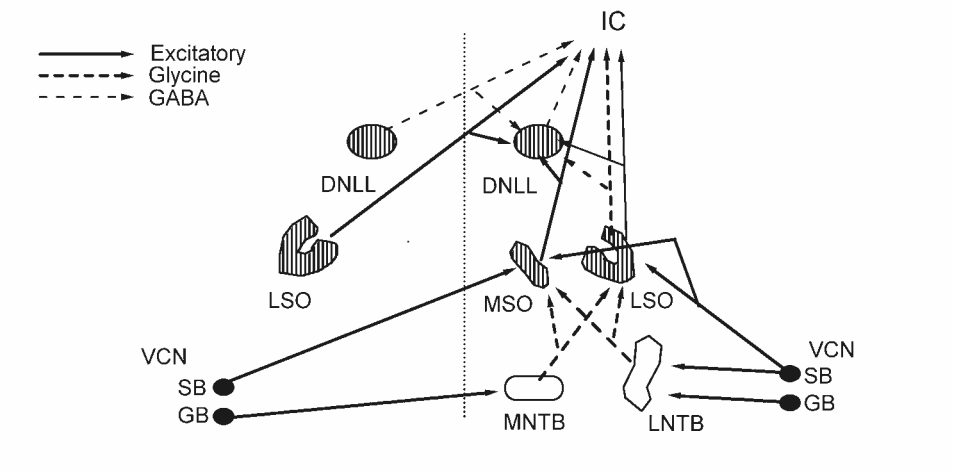

Figure 1.2 Ascending pathways toward the inferior colliculus.
Binaural ascending excitatory and inhibitory inputs towards IC originate from the ventral cochlear nucleus (VCN), medial and lateral nucleus of trapezoid body (MNTB, respectively LNTB), medial and lateral superior olive (MSO and LSO) and dorsal nucleus of lateral lemniscus (DNLL). SB = spherical bushy cell, GB = globular bushy cell (adapted from Schofield 2005).

In vivo patch-clamp technique

To circumvent the disadvantages of existing techniques mentioned above, we used the 'in vivo patch-clamp' technique to study the role of cell properties and synaptic excitation and inhibition during processing of sound in an intact auditory system. This technique has been used since 1996 in bats (Covey et al. 1996). In bats, the IC is located on the surface of the brain, unlike the situation in humans, where the IC is fully covered by cerebellum. However, the echolocating system of the bat is a unique, highly specialized system, for which there is no analogue in the human auditory system. The 'in vivo patch-clamp' technique has also been used in other superficial structures such as sensorimotor and auditory cortex (Deweese and Zador 2004; Liu et al. 2007; Margrie et al. 2002; Metherate and Ashe 1994), but not in the rodent inferior colliculus, which is partly covered by cerebellum (Paxinos and Watson 1998). Electrophysiological measurements with sharp electrodes are generally more subjected to background noise (Neher and Sakmann 1976; Verkhratsky et al. 2006), which may be less the case of in vivo studies (Pedemonte et al. 1997). Patch-clamp is, in fact, a more reliable tool to measure membrane properties of a single cell in an intact system. Especially in small cells, patch-clamp recordings are stable and last longer compared with recordings with sharp electrodes. Apart from the advantage of studying membrane properties of a single cell in an intact system, it is possible to measure spontaneous excitatory and inhibitory inputs, synaptic integration, as well as subthreshold auditory evoked responses.

Overall aim of the study

The main focus of this thesis is to discover which factors determine auditory processing at the level of the midbrain (IC). First of all, can the classification system of different cell types that has been used for current injections on brain slices be extrapolated into an intact auditory system in vivo? How are these cell types determined? What is the contribution of basic cell characteristics (i.e. membrane resistance, membrane time constant, resting membrane potential, and firing threshold) to the firing pattern of a cell? How do firing patterns caused by current injections relate to firing patterns that are sound evoked? Are cell types specialized in encoding certain aspects of sound? What is the role of inhibition in shaping sounds of different durations (duration tuning), amplitude-modulated sounds (AM tuning) and frequency-modulated sounds (FM tuning)? How does the integration of excitatory and inhibitory inputs affect the shape of the incoming signal? What is the role of membrane properties in duration tuning, AM tuning and FM tuning? Finally, we discuss whether it is possible to make a cellular model for auditory processing in the IC from the obtained results.

Outline of the Thesis

In this thesis we have obtained a first inventory of auditory evoked responses in the rodent IC measured with the in vivo patch clamp technique. With this technique we have tried to bridge the gap between auditory evoked extracellular work and intracellular in vitro results.

The dorsocaudal approach that we use hampers visual identification of the central nucleus of the inferior colliculus during electrophysiological experiments. **Chapter 2** describes a post-mortem method to confirm the localization of recorded neurons with biocytin injection in the cell and the immunohistochemical markers vGlut1 and vGlut2 to identify the central nucleus.

Chapter 3 describes different firing patterns of IC neurons after constant current injections in vivo. We examine to what extent basic membrane properties such as resting membrane potential, action potential threshold, membrane resistance, membrane time constant and the presence of a voltage-dependent sodium / potassium "hyperpolarization-activated " channel (I_h) contribute to the firing pattern of a cell.

In **Chapter 4** these basic membrane properties are further explored during stimulation with sounds of different duration (duration tuning) and amplitude-modulated sounds (AM tuning).

Finally, **Chapter 5** illustrates that spectro-temporal integration of synaptic responses, especially synaptic inhibition as well as summation of excitation, plays an important role in processing frequency-modulated (FM) sounds.

In **Chapter 6** we recapitulate the underlying mechanisms for central auditory processing in the IC midbrain, with the main conclusion being that the auditory responses in the IC are very diverse. In this thesis we have set the first steps in understanding the IC by dissecting the responses at the cellular level while using current injections and simple sound stimuli with just a spectral, temporal or single modulated (AM and FM) variable. Topics for future research will be discussed in this chapter. How decoding of complex stimuli will lead to recognition, processing and eventually perception are questions that remain to be answered.

Chapter 2

Expression of vesicular glutamate transporters 1 and 2 in the mouse inferior colliculus

M.L. Tan, H.P. Theeuwes, L. Feenstra, J.G.G. Borst

To be submitted

ABSTRACT

At present there is no consensus method for parceling the inferior colliculus (IC), but cytochrome oxidase histochemistry has often been used to determine the boundaries of its central nucleus. We compared vesicular glutamate transporter type 1 and 2 (vGLUT1 and vGLUT2) staining with cytochrome oxidase histochemistry in the mouse IC. Both cytochrome oxidase activity and vGLUT1 staining were higher in the central region of the IC and in the superficial, small-celled layer of the lateral cortex, whereas vGLUT2 had a largely complementary distribution to vGLUT1. These data show that regions of the IC with a greater density of vGLUT1-positive synaptic terminals have higher metabolic activity. In addition, since vGLUT1 and cytochrome oxidase revealed similar borders of the central nucleus of the IC, we conclude that vGLUT1 is a useful alternative to cytochrome oxidase activity as a marker for the central nucleus of the IC.

INTRODUCTION

The inferior colliculus (IC) integrates auditory information from ascending and descending pathways. It is an important relay station where several parallel streams originating from the cochlear nucleus converge before transmitting information to the thalamus and auditory cortex. The IC can be subdivided into a central nucleus, dorsal cortex and lateral cortex (also called external nucleus or external cortex). Within the IC, the central nucleus is the main target for inputs from the cochlear nucleus, the superior olivary complex (SOC) and the nuclei of the lateral lemniscus (Cant 2005; Schofield 2005). Functionally, cells in the central nucleus are characterized by their large, short-latency response to tones and their sharp tuning (Aitkin et al. 1975). Morphologically, the central nucleus can be defined either by the presence of disc-shaped (also called flat or bipolar) neurons, or by higher cytochrome oxidase activity, a marker for metabolic activity (Loftus et al. 2008; Oliver 2005). However, both morphological methods for defining the borders of the central nucleus have their limitations. Complete analysis of individual neuron morphology throughout the IC is not practical for routine use. Also, the area receiving direct inputs from the cochlear nucleus is larger, both in the lateral and in the rostral direction, than the area with disc-shaped neurons (Oliver 2005). Cytochrome oxidase histochemistry is more readily performed, but delineating the boundaries of the central nucleus is not unambiguous (Cant and Benson 2005). In addition, cytochrome oxidase activity can change rapidly. This change does not necessarily obey the original central nucleus boundaries and can even be induced by non-auditory stimuli (Poremba et al. 1997). Other measures of activity, such as fos expression or incorporation of 2-deoxyglucose are laborious and depend on the choice of an appropriate stimulus (Oliver 2005).

The large, short-latency response to tones and sharp tuning of neurons in the central nucleus is thought to result from their direct innervations by the cochlear nucleus and SOC (Cant 2005; Schofield 2005). Similarly, the central area with high cytochrome oxidase activity corresponds to the lemniscal projection zone (Cant and Benson 2006). Since both the physiological and the histochemical definition of the central nucleus are based on its inputs, the molecular composition of the glutamatergic terminals within the IC may be used for its parcellation. We therefore compared cytochrome oxidase histochemistry with immunocytochemistry of vesicular glutamate transporter 1 and 2 (vGLUT1 and vGLUT2; (Fremeau et al. 2004).

MATERIALS AND METHODS

Animal procedures were performed in accordance with guidelines provided by the animal committee of the Erasmus MC. Six young-adult (25- or 26-days-old) C57/Bl6 mice were intracardially perfused with 0.9% NaCl in 0.02 M phosphate buffer (PB) under deep pentobarbital anesthesia, followed by 4% paraformaldehyde in 0.12 M PB and 10% sucrose in 0.1 M PB. Brains were post-fixed in 4% paraformaldehyde, gelatin-embedded and sectioned at 40 µm in the coronal plane using a freezing microtome.

In two mice, all sections containing the IC were stained with antibodies against vGLUT1. In the other four, sections stained with vGLUT1 antibodies were alternated with staining of vGLUT2 and/or cytochrome oxidase immunohistochemistry. Sections were incubated with primary antibody against either vGLUT1 (AB5905; 1:5000, guinea pig IgG; Chemicon International, Inc., Temecula, USA) or vGLUT2 (AB5907; 1:2000) in Tris-buffered saline with 2% normal horse serum and 0.4% Triton X-100. The specificity of these antibodies for glutamatergic synaptic vesicles has been previously characterized (Liu et al. 2005; Rodriguez-Contreras et al. 2006) and staining patterns generally matched those obtained with other antibodies directed against vGLUT1 or vGLUT2 (Fremeau et al. 2004). Secondary antibody was biotinylated anti-guinea pig IgG (1:200; Vector Labs; Burlingame, USA). Sections were processed free-floating, employing a standard avidin–biotin–immunoperoxidase complex method (ABC, Vector Laboratories, USA) with diaminobenzidine (0.05%) as the chromogen and counterstained with thionin. Cytochrome oxidase immunohistochemistry, which provides a measure for the endogenous mitochondrial cytochrome oxidase activity, was done according to Jaarsma et al. (Jaarsma et al. 2000).

Sections were photographed using a Leica DM-RB microscope with 1.6x (N.A. 0.05) and 100x (N.A. 1.30) objectives and a Leica DC300 CCD camera. After Gaussian filtering and spectral separation of the brown DAB signal from the blue thionin stain, the boundaries of the central nucleus were obtained in ImageJ (v1.34s) by binary thresholding vGLUT1 staining intensity. Control experiments in the absence of the thionin stain showed that the thionin stain did not affect the location of the central nucleus boundaries. The threshold was obtained using the Otsu criterion, which divides the histogram of the pixel intensity into two classes by minimizing the inter-class variance (Otsu 1979). Following removal of single pixel regions using erosion/dilation, a single, contiguous region was obtained with the built-in wand tool in ImageJ. The same procedure was followed for vGLUT2- or cytochrome oxidase-stained slices, except that for vGLUT2 staining the central region was the region with low intensity. Surface areas of the CNIC were calculated in ImageJ. A 3D reconstruction was made using Neurolucida (version 4.6) and NeuroExplorer software (version 3.23b; MicroBrightField, Williston, VT).

RESULTS

Figure 2.1 shows consecutive sections of the mouse IC that were stained for cytochrome oxidase activity, vGLUT1 or vGLUT2. Cytochrome oxidase staining appeared to label mostly neuropil. The labeling was more prominent in the central region of the IC, with additional reactive patches at the superficial small-celled layer of the lateral cortex (Fig. 2.1A; n = 3 mice), in accordance with previous studies (Cant and Benson 2005; Chernock et al. 2004; Gonzalez-Lima and Cada 1994; Poremba et al. 1997; Willott 2001).

Antibodies against both vGLUT1 and vGLUT2 produced punctate labeling in the IC, consistent with labeling of presynaptic terminals (Fig. 2.1B, C). The number of vGLUT1-positive puncta was much greater in the central region than in lateral or dorsal regions (Fig. 2.1B). This region also included medial and lateral bands that extended in the dorsomedial direction, with the lateral band almost reaching the dorsal surface of the IC (Fig. 2.1B). The medial band formed the border of the central nucleus and the periaqueductal gray. In addition, there was a band of more intense vGLUT1 staining at the superficial, small-celled layer of the lateral cortex (n = 6 mice). DAB intensity in vGLUT1 staining was about 50% larger in the CN compared to the rest of the IC, similar to the about two-fold increase seen with cytochrome oxidase (Fig. 2.1A; (Gonzalez-Lima and Cada 1994)).

Staining of vGLUT2 was largely complementary to vGLUT1, with high intensities in dorsal and lateral cortex and low intensities in the central region (Fig. 2.1C; n = 2 mice). The density of vGLUT2-positive puncta appeared higher than of vGLUT1-positive puncta in most regions of the IC (Fig. 2.1B and C), but confocal analysis of simultaneous staining for both vGLUT1 and -2 is needed for quantification and for estimating the fraction of boutons that contain both types of transporters.

The staining intensities of each slice were thresholded to obtain the boundaries of the central nucleus. In a second mouse each section was stained for vGLUT1 and, following thresholding (Fig. 2.1D) the central nucleus was reconstructed. Figure 2.2 shows the 3D-reconstruction of the IC and central nucleus localization based on vGLUT1 staining. From a dorsal view, the central nucleus is cone-shaped, while from a frontal view it is horseshoe-shaped. We measured a volume of 3.8 mm^3 for the entire IC, somewhat larger than in an earlier microscopic study (Willott et al. 1994), but in agreement with a recent MRI study (Yu et al. 2005). The volume of the central nucleus as defined by vGLUT1 immunocytochemistry was about 0.6 mm^3 (0.57 - 0.67 mm^3; n = 2 mice), about 15% of the total volume of the IC, which is consistent with the volume of the region of the IC that shows an increased MRI signal following activation by broad-band noise (Yu et al. 2005).

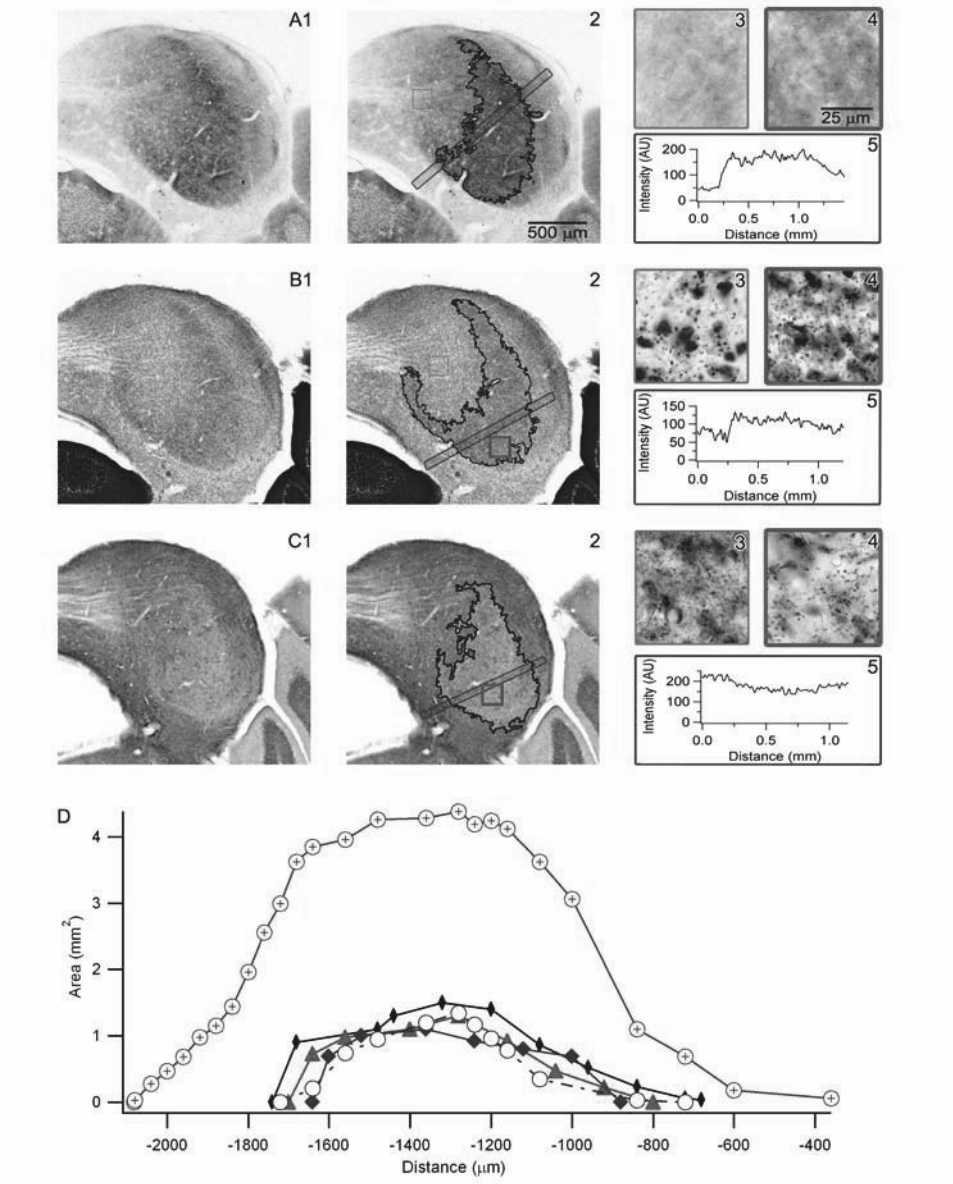

Figure 2.1 Comparison of staining of the mouse inferior colliculus (IC) for cytochrome oxidase activity (A) and vGLUT1 (B), or vGLUT2 (C) proteins.
*(*A1*): Cytochrome oxidase staining of IC (level: interaural –1320 µm).*
*(*A2*): As (*A1*), but showing thresholding of central region. The green and red squares show regions with low and high cytochrome oxidase staining, shown at higher magnification in (*A3*) and (*A4*), respectively.*
*(*A5*): Average staining intensity along the long edge of the blue rectangle shown in (*A2*).*

*(*B1*): Anti-vGLUT1 staining with Nissl counterstaining (level: interaural –1280 µm).*
*(*B2*): As (*B1*), but showing regions defined by binary thresholding. The green and red squares show regions with low and high density of punctate staining, shown at higher magnification in (*B3*) and (*B4*), respectively.*
*(*B5*): Average vGLUT1 staining intensity along the long edge of the blue rectangle shown in (*B2*).*

*(*C1*): Anti-vGLUT2 staining with Nissl counterstaining (level: interaural –1240 µm).*
*(*C2*): As (*C1*), but showing boundaries of the central region with lower intensity of vGLUT2 staining, as defined by binary thresholding. The green and red squares show regions with high and low density of punctate staining, shown at higher magnification in (*C3*) and (*C4*), respectively.*
*(*C5*): Average vGLUT2 staining intensity along the long edge of the blue rectangle shown in (*C2*).*

*(*D*): Area plot of the IC and of the central area, as defined by binary thresholding, of two different mice. For the first mouse, the green circle with cross reflects total surface area of outlined IC and grey open circles show the surface of the central nucleus according to vGLUT1 staining. For the second mouse, black diamonds depict the total surface area of the central area, as based on cytochrome oxidase staining (*A2*), red triangles show the CNIC surface area, as defined by vGLUT1 staining (*B2*) and blue diamonds show total surface area of the central region based on vGLUT2 staining (*C2*).*

Scale bar in A2 *also applies to* A1, B1-2 *and* C1-2*. Scale bar in* A4 *also applies to* A3, B3-4 *and* C3-4*.*

DISCUSSION

Generally speaking, the boundaries of the central nucleus of the mouse IC determined in this study were similar to those seen in earlier studies (Frisina and Walton 2001; Gonzalez-Lima and Cada 1994; Meininger et al. 1986), except we observed further dorsomedial extension of the medial band with vGLUT1 staining (Fig. 2.1B). This band may correspond to the medial part of the lateral lemniscus bundle (Meininger et al. 1986), or be due to cortical inputs (Coleman and Clerici 1987; Winer 2005) and anterograde injections are needed to establish its origin. Similar to a recent study in rat (Altschuler et al. 2008), our study shows that vGLUT2 staining has higher intensities in dorsal and lateral cortex compared with the central nucleus (Fig. 2.1C) and vGLUT2-positive puncta appear higher than of vGLUT1-positive puncta in most regions of the IC (Fig. 2.1B and C).

The similarity between vGLUT1 and cytochrome oxidase staining shows that metabolic activity is higher in regions where vGLUT1-positive terminals are concentrated. No significant differences in transport rates or substrate affinity have been observed between the two transporters, arguing against a causal relation between the presence of vGLUT1 and a higher metabolic activity.

Although the boundaries of the central nucleus of the IC were similar when defined by cytochrome oxidase and vGLUT1 staining, vGLUT1 immunocytochemistry has some advantages. VGLUT1 immunocytochemistry is more readily combined with other stainings and is not dependent on enzymatic activity of the material. Moreover, vGLUT1 immunocytochemistry presumably defines the central nucleus by its input properties, rather than by its metabolic activity level. Based on the known expression patterns of vGLUT1 and vGLUT2 obtained from in situ hybridizations and immunohistochemistry, it seems likely that the contralateral ventral cochlear nucleus (VCN) is the most important source of vGLUT1-positive inputs. The central nucleus predominantly receives inputs from the brainstem, with minor or no inputs from the neocortex and modest input from the medial nucleus of the geniculate body and the contralateral IC (Oliver 2005). The VCN is the most important source of ascending excitatory inputs to the IC (Cant 2005). In situ hybridizations show that the cochlear nucleus mostly expresses vGLUT1, whereas the SOC and the IC itself mostly express vGLUT2 (Atlas 2004-2006; Fremeau et al. 2001; Herzog et al. 2001). The VCN has more prominent vGLUT1 expression than the DCN (Friedland et al. 2006). Therefore, the VCN is most likely the predominant source of vGLUT1 input in the central region.

Possible sources of the vGLUT1-positive band in the lateral cortex include the dorsal cochlear nucleus (Ryugo et al. 1981), the cerebral cortex (Fremeau et al. 2004; Winer 2005), or non-auditory inputs (Oliver 2005).

VGLUT2 distribution is largely complementary to vGLUT1 in many brain areas (Fremeau et al. 2001; Herzog et al. 2001), including the IC (Fig. 2.1B, C; (Kaneko et al. 2002)). An important source of vGLUT2 inputs in the dorsal and lateral cortex are the intracollicular connections (Atlas 2004-2006). A possible cause of the horseshoe shape of the central nucleus in the frontal plane is the predominance of inputs from the contralateral IC in the dorsomedial region, since the contralateral dorsomedial region is clearly highlighted when the entire central nucleus or all commissural fibers are labeled (Saldaña and Merchán 2005). Cortical inputs, which are mostly

vGLUT1 expressing (Fremeau et al. 2004), represent most of the descending inputs throughout the IC (Winer 2005). Our observation that the lateral and dorsal cortexes stain more prominently for vGLUT2 therefore suggests that non-cortical inputs outnumber cortical inputs. We conclude that vGLUT1 is potentially a very useful marker for the central nucleus of the IC, but that anterograde tracings from input regions to the IC are needed to definitively establish that the vGLUT1-positive region in the IC accurately represents the region that receives inputs from the CN.

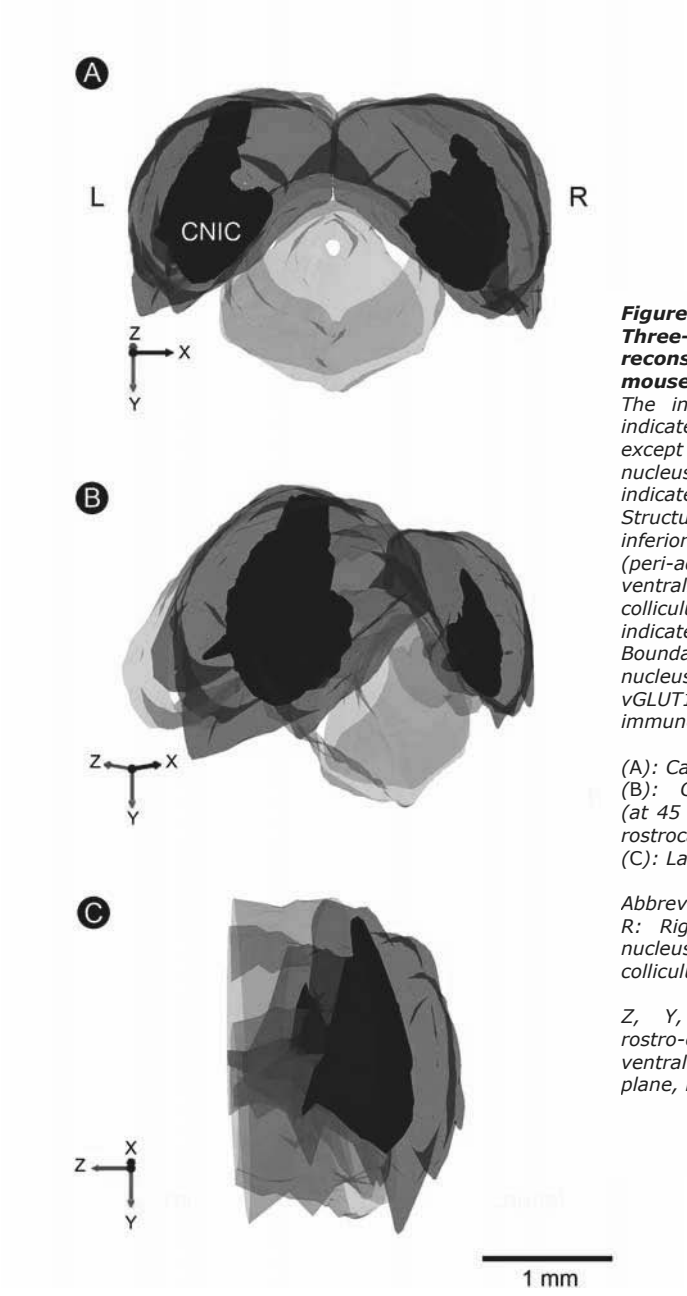

Figure 2.2
Three-dimensional reconstruction of the mouse IC.
The inferior colliculus is indicated in light blue, except for the central nucleus, which is indicated in dark-blue. Structures outside of the inferior colliculus (peri-aqueductal grey, ventrally, and superior colliculus, rostrally) are indicated in grey. Boundaries of the central nucleus were based on vGLUT1 immunocytochemistry.

(A): Caudal view.
(B): Caudo-lateral view (at 45 degrees angle with rostrocaudal axis).
(C): Lateral view.

Abbreviations L: Left, R: Right, CNIC: central nucleus of the inferior colliculus.

Z, Y, X indicate the rostro-caudal, dorso-ventral and medio-lateral plane, respectively.

Chapter 3

Membrane properties and firing patterns of inferior colliculus neurons: an in vivo patch-clamp study in rodents

M.L. Tan, H.P. Theeuwes, L. Feenstra, J.G.G. Borst

J Neurophysiol 98:443-453, 2007

ABSTRACT

The inferior colliculus (IC) is a large auditory nucleus in the midbrain, which is a nearly obligatory relay center for ascending auditory projections. We made in vivo whole-cell patch-clamp recordings of IC cells in young-adult anaesthetized C57/Bl6 mice and Wistar rats to characterize their membrane properties and spontaneous inputs. We observed spontaneous spikelets in both rat (18%) and mouse (13%) IC neurons, which suggests that IC neurons may be connected via electrical synapses. In many cells, spontaneous postsynaptic potentials were sufficiently large to contribute to spike irregularity. Cells differed greatly in the number of simultaneous spontaneous postsynaptic potentials that would be needed to trigger an action potential.
Depolarizing and hyperpolarizing current injections showed six different types of firing patterns: buildup, accelerating, burst-onset, burst-sustained, sustained and accommodating. Their relative frequencies were similar in both species. In mice, about half of the cells showed a clear depolarizing sag, suggesting that they have the hyperpolarization-activated current I_h. This sag was observed more often in burst and in accommodating cells than in buildup, accelerating or sustained neurons. Cells with I_h had a significantly more depolarized resting membrane potential. They were more likely to fire rebound spikes and generally showed long-lasting afterhyperpolarizations following long depolarizations. We therefore suggest a separate functional role for I_h.

INTRODUCTION

The inferior colliculus (IC) integrates auditory information from ascending and descending pathways in the auditory system. It is the first site in which the several parallel streams that originate from the cochlear nucleus converge. In patch-clamp recordings in slices of the inferior colliculus of young animals a variety of firing patterns have been observed during constant-current injections reviewed by Wu (Wu 2005). An important distinction is made based on the amount of accommodation. Many cells show sustained firing during current injection, whereas other cells accommodate rapidly or show onset firing. In addition, cells can be classified based on firing regularity or on the presence of rebound, burst, or buildup firing in response to constant-current injections (Bal et al. 2002; Peruzzi et al. 2000). Interestingly, many of these firing patterns can be directly attributed to the presence of unique potassium conductances: buildup neurons have an A-type current, onset cells a special high-threshold tetraethylammonium (TEA)-sensitive current, rebound cells express different types of calcium-dependent potassium currents and cells with a sustained-regular firing pattern express mainly delayed-rectifier-type potassium currents (Sivaramakrishnan and Oliver 2001). The hyperpolarization-activated mixed cation current I_h also contributes to the different firing patterns. Onset and adapting neurons have larger I_h currents than sustained neurons in the IC and I_h gates more rapidly in onset and sustained cells than in non-accommodating cells (Koch and Grothe 2003), presumably because these cells express the HCN1 subunit (Koch et al. 2004; Notomi and Shigemoto 2004). I_h may also contribute to rebound firing and to an afterhyperpolarization following long depolarizations (Koch and Grothe 2003).

In earlier intracellular or patch-clamp studies from the IC of cats, bats or guinea pigs (Casseday et al. 1994; Covey et al. 1996; Kuwada et al. 1997; Nelson and Erulkar 1963; Pedemonte et al. 1997), the responses to current injection were not studied, thus it is not yet known whether the firing patterns observed in rodent slices can be observed in vivo as well. We therefore investigated firing patterns in both young-adult rats and mice using in vivo patch-clamp recordings.

MATERIALS AND METHODS

Surgical preparation

Animal procedures were in accordance with guidelines provided by the animal committee of the Erasmus MC.
A total of 18 male Wistar rats (postnatal day 19 – 44) and 46 C57/Bl6 mice (postnatal day 21 – 37) were anesthetized with ketamine 60 mg/kg i.p. and medetomidine 0.25 mg/kg s.c. or ketamine/xylazine (65/10 mg/kg) i.p. Additional anesthesia was given when pinching the toes resulted in a withdrawal reflex. Rectal temperature was maintained between 36.5 – 37.5ºC with a homeothermic blanket system (Stoelting ®). The head was immobilized using a metal pedestal fastened to the skull. After a craniotomy directly caudal from the transversal sinus, any cerebellar tissue overlying the colliculi was aspirated and the pia mater was removed. Little or no cerebellar tissue was aspirated in mice. Brain pulsations were reduced by application of agar (agarose 2% in 0.1 M phosphate buffer). All experiments were performed in a single-walled sound-attenuated chamber (Gretch-Ken Industries, attenuation at least 40 dB at 4 – 32 kHz).

Patch-clamp recordings

Thick-walled borosilicate glass micropipettes with filament (4 – 6 MΩ) were filled with (in mM) K-gluconate 125, KCl 20, Na_2phosphocreatine 10, Na_2GTP 0.3, MgATP 4, EGTA 0.5, Hepes 10 (pH 7.2). The IC was approached dorso-caudally at a 30 - 60° angle with the horizontal under high positive pressure, which was lowered to ~30 mbar at ~500 µm below surface in rats and ~200 µm in mice. Giga-ohm seals and whole cell recordings were established using standard techniques (Margrie et al. 2002). Series resistance was on average 63 ± 2 MΩ (n = 99). Data were acquired with a MultiClamp 700A patch-clamp amplifier and pCLAMP 9.2 software (Axon Instruments). Potentials were filtered at 10 kHz (8-pole Bessel filter) and sampled at an interval of 50 µs with a 16-bit A/D converter (Digidata 1322A).

Stimulation protocols

Cells were subjected to constant-current injections with 50 pA steps between -200 pA and +500 pA of different durations (2, 50, 100 and 1000 ms). To test whether the firing patterns change at more negative membrane potentials (Bal et al. 2002), the 1000 ms protocol was repeated, except it was preceded by 1000 ms injection of -200 pA hyperpolarizing current. Many cells were stimulated with tones after completion of the current injection protocols, as described in the accompanying paper (Tan and Borst 2007).

Histology

A subset of cells was filled with biocytin. In these experiments the pipette solution contained 0.5 % biocytin and the K-gluconate concentration was reduced to 115 mM. Biocytin-filled cells were visualized as described by (Horikawa and Armstrong 1988), with minor modifications. Their location within the IC was obtained by comparing the slices with slices from the reconstructed IC of a 25-day old C57/Bl6 mouse, for which the vesicular glutamate transporter 1 (vGLUT1) was used as a marker for the central nucleus (Tan, Theeuwes, Feenstra and Borst, unpublished results).

Electrophysiological data analysis

Data were analyzed using Clampfit 9.2, or using custom-written macros that used the NeuroMatic environment (version 1.91, kindly provided by Dr J. Rothman, University College London) within Igor Pro 5 (Wavemetrics, Lake Oswego, OR).
Membrane potentials were corrected for a –11 mV junction potential.
Cells often showed a slow depolarization during the recording period. Cells were discarded from analysis when resting membrane potential depolarized beyond -45 mV, without spontaneous recovery to initial V_m; current injection protocols were incomplete; action potentials were not observed during current injection; action potentials had <10 mV peak amplitude due to high access resistance; or when localization outside the inferior colliculus was histologically confirmed.

Membrane properties

If the cell fired spontaneously, the action potential threshold (in mV) was estimated from hyperpolarizing current steps, else from depolarizing current injections around the threshold. Input resistance R_m and membrane time constant τ were both calculated by extrapolation of an exponential fit through the average response to hyperpolarizing current steps with durations of 50-100 ms.
The presence of the hyperpolarization-activated current (I_h) was assessed from the response to 100 – 300 pA, 1 s hyperpolarizing current steps. I_h was considered to be present when a depolarizing 'sag' was observed in the averaged response exceeding 10% of the maximal hyperpolarization.
Activation kinetics of I_h were estimated from a fit with a single or a double exponential function to the depolarizing sag (Fig. 3.9B), according to:
$Y = A*\exp(-t/\tau) + C$, and $Y = A_1*\exp(-t/\tau_1) + A_2*\exp(-t/\tau_2) + C$, where τ_1 and τ_2 represent the fast and slow time constants of I_h activation, respectively, and t represents the time relative to the most hyperpolarized point. The data points were weighted with the reciprocal of their standard deviations. A double exponential fit was favored over a single exponential fit when the residuals of the single exponential fit were clearly not randomly distributed, the slow time constant was at least 3 times larger than the fast time constant and the amplitude contribution of both time constants was at least 10%. The amplitude contribution was calculated in the range between the peak depolarization and the end of the 1 s trace.

Firing patterns

Firing patterns were determined at 100 pA above the smallest suprathreshold current injection. Based on their firing patterns, we classified cells largely following criteria established by (Sivaramakrishnan and Oliver 2001), yielding a total of six different firing types: sustained, accommodating, buildup, accelerating and burst (onset and sustained). We first looked whether a cell fired a cluster of 2 or more action potentials. When this occurred only at the onset of depolarization, the cell was classified as burst-onset. If it fired bursts during the entire 1-second depolarization it was classified as burst-sustained. We then looked at the latency of the first spike during depolarization and pre-hyperpolarization. Buildup neurons showed a typical delay in firing the first action potential, which became more pronounced when the depolarizing current was preceded by a hyperpolarization, as described by (Sivaramakrishnan and Oliver 2001). Accelerating neurons showed a clear increase in their firing rate during the depolarizing step. Within this group, either the first inter-spike interval (ISI) was consistently larger than the second, or cells showed a more gradual increase in firing rate, which was followed by accommodation. In contrast to buildup, accelerating, burst-onset or burst-sustained cells, in the remaining cells spike rates decreased exponentially and in these cells the relation between spike rate (calculated from the interspike intervals) and spike interval number was fitted with the equation $S = A \exp(-x/\tau)+B$, where x is spike interval number, S is spike rate, B is spike rate at $x=\infty$ (restricted in the fit to be at least 0) and A+B is the spike rate for the first interval (x=0). From this fit we calculated an accommodation index (AI): $AI = (S_{(x=0)} - S_{(x=1)}) / S_{(x=1)} \times 100\%$, where $S_{(x=0)}$ is the value of the fit at x = 0. Since we used spike rates instead of spike intervals (Sivaramakrishnan and Oliver 2001) a low AI represented a cell with little spike accommodation. The AI is thus an estimate for the percentual increase in the ISI between the first and the second ISI. We use the term accommodation instead of adaptation to avoid confusion with the synaptic adaptation processes studied in the accompanying paper (Tan and Borst 2007). Cells with AI <4% were sustained, else they were classified as accommodating.

Neurons were classified as having rebound spikes when these were observed at least twice following hyperpolarization. In addition, we tested for the presence of afterhyperpolarizations >1 mV below baseline following depolarizing current injections or 'humps' >1 mV above baseline following hyperpolarizing current injections.

Spontaneous postsynaptic potentials

Spontaneous EPSPs were identified using the built-in template method of Clampfit 9.2. The amplitudes and 20-80% rise times of a minimum of 80 spEPSPs occurring in a baseline period of at least 5 s were measured after digital filtering to 1 kHz.
We also tested the relation between the occurrence of spontaneous EPSPs and firing irregularity. As a measure for the fluctuations in the membrane potential due to spontaneous inputs we calculated the average standard deviation of the membrane potential during 3 s, after digital filtering to 1 kHz and after correcting for a linear trend in the average membrane potential. As an estimate for firing irregularity, we used the coefficient of variation (CV) of the deviations from an exponential decrease of the spike rates at 100 pA above threshold. This was calculated by dividing the standard deviation of the residuals of the single exponential fit of the spike rates by the average spike rate. Only accommodating and sustained cells that fired at least 10 spikes during a 1 s depolarizing current step at 100 pA above threshold were included in this analysis.

Statistics

Data are presented as mean ± standard error of the mean (SE). Two-tailed Student's *t*-test, Pearson's χ^2-test or ANOVA with post hoc Tukey HSD test were calculated using SPSS 11. Values of $P < 0.05$ were judged as statistically significant.

RESULTS

Localization of cells within IC

We made in vivo patch-clamp recordings of neurons from the rat or mouse inferior colliculus. The inferior colliculus can be subdivided into a central nucleus, dorsal cortex and external cortex (reviewed in Oliver 2005). To investigate the location within the IC of the cells we recorded from, a subset of 13 cells from 10 different mice were filled with biocytin and histologically retrieved. Figure 3.1 shows an example of a neuron, with its firing pattern in response to current injection (Fig. 3.1A) and a reconstruction of its soma and dendritic tree (Fig. 3.1B).

Because thionine staining alone is insufficient to determine the exact borders of the central nucleus, we used a reconstruction of the mouse IC using vGLUT1 as a marker for the central nucleus (unpublished results) to find the location of the thirteen neurons that were retrieved. The estimated location of the retrieved cells within this reconstruction is displayed in Fig. 3.1C and 3.1D from a caudal and a dorsal view, respectively. About half of the cells (6/13) were localized in the central nucleus, five cells were localized in the dorsal cortex and two in the external cortex of the IC. Their soma size was on average 9 x 16 µm (range 6 – 28 µm). The cells that were localized in the central nucleus obeyed a tonotopic gradient, with low frequencies in dorsolateral regions and high frequencies in ventromedial regions (range 13.9 – 27.8 kHz; *not shown*), in agreement with earlier reports (Stiebler and Ehret 1985; Willott and Urban 1978).

In addition, 86 neurons were acoustically stimulated. One cell did not show any sound-evoked activity in response to pure tones at 80 dB SPL, while two cells fired spontaneously, but did not change their firing rate when a sound stimulus was given. This means that probably less than 5 of the in total 136 neurons (3.5%) were not auditory.

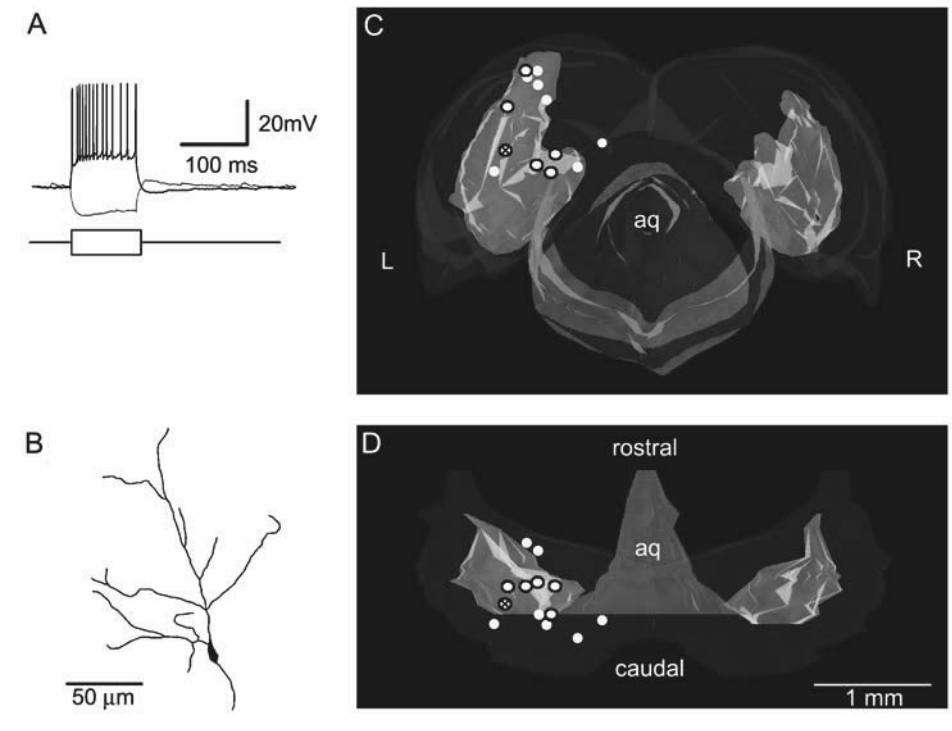

Figure 3.1 Localization of biocytin-filled cells within the mouse inferior colliculus.
A*: response to 100 ms, 200 pA hyperpolarizing and depolarizing constant-current injections of the neuron whose morphology is shown in (*B*).*
B*: Reconstruction of a single neuron (marked in* C *and* D *by a crossed circle).*
C*: Caudal view of a reconstruction of the inferior colliculus. The colliculus inferior is indicated in blue, except for the central nucleus, which is indicated in yellow. Structures outside of the inferior colliculus (peri-aqueductal grey) are indicated in turquoise. Location of biocytin-filled cells is indicated as white circles. Circles with a black outline were localized within the central nucleus. Abbreviations, L: Left, R: Right, aq: cerebral aqueduct.*
D*: as (*C*), except dorsal view.*

Relation between spontaneous synaptic potentials and action potential generation

We investigated to what extent the spontaneous inputs influenced action potential generation. Spontaneous excitatory postsynaptic potentials (spEPSPs) were observed in all cells, whereas spontaneous inhibitory postsynaptic potentials (spIPSPs) were observed much more infrequently and large (>5 mV) spIPSPs were observed in only one cell. An example of spEPSPs is shown in the lower trace of Figure 3.2A. A role for spontaneous inputs in action potential generation was obvious in 14 of the 16 neurons (of a total of 103 neurons) that fired spontaneously in mice, since in these 14 cells spontaneous action potentials were typically triggered on top of spEPSPs. In 7 of these 14 cells, the spontaneous action potentials were triggered by single, relatively large (>5 mV) spEPSPs. In the other 7 cells, the spontaneous action potentials were typically triggered on top of bursts of spEPSPs. In the remaining two spontaneously active cells there was no obvious role for spEPSPs in the timing of action potential generation. One cell had a very negative threshold for action potential generation and the other cell showed an oscillating membrane potential, with action potentials triggered on top of the oscillations. Spontaneously active cells on average had a more depolarized membrane potential (-55.5 ± 1.1 mV, n = 16 vs. -61.7 ± 0.6 mV, n = 87; P < 0.001), whereas their action potential threshold did not differ significantly from the other cells (-49.6 ± 0.5 mV, n = 16 vs. -46.8 ± 0.5 mV, n = 87; P = 0.25). The resting membrane potential is therefore an important factor in determining whether a cell fires spontaneously. In rats, resting membrane potential was also more depolarized in active cells compared with cells that did not fire spontaneously (-57.2 ± 1.2 mV, n = 12 vs. –60.7 ± 1.1 mV, n = 21; P = 0.036). In addition, their action potential threshold was significantly lower (-48.2 ± 1.3 mV, n = 12, vs. –42.9 ± 1.4 mV, n = 21; P = 0.009).

To investigate a possible role for spEPSPs in the cells that were not spontaneously active, we compared the depolarization needed to elicit an action potential with the size of spontaneous inputs. The larger the size of the spontaneous inputs and the closer the action potential threshold is to the resting potential, the larger their effect on action potential generation is expected to be. In 11 cells in which the spEPSPs could be relatively easily distinguished from baseline noise, spEPSPs with an average amplitude of 1.1 ± 0.2 mV and a rise time of 2.0 ± 0.2 ms were observed at an average frequency of around 30 Hz. In these cells, the average ratio between the depolarization needed to reach action potential threshold and the size of the spontaneous EPSPs was 21.3 ± 6.5 (range 3.5-75). Although the relation between the number of active inputs and membrane potential is far from linear and although the amplitudes of spEPSPs were typically variable and skewed towards larger amplitudes (CV 0.78 ± 0.09, skewness 2.0 ± 0.3; n = 11), our results nevertheless suggest that the number of simultaneously active inputs needed to elicit a spike varies considerably between cells.

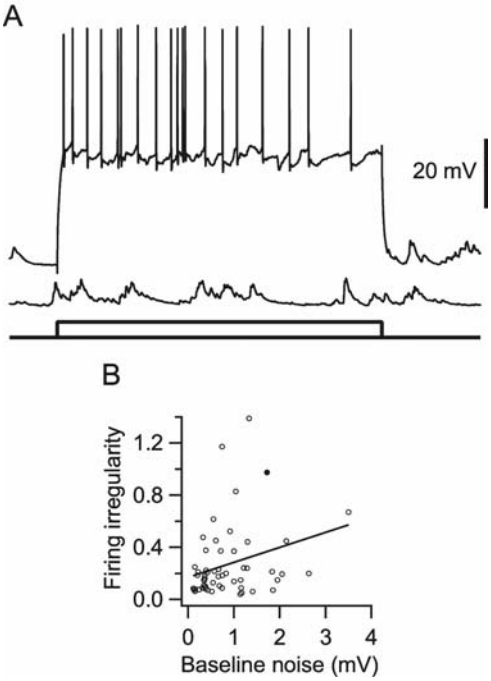

Figure 3.2 Spontaneous inputs affect firing regularity.
A: current clamp recording at resting membrane potential shows spontaneous EPSPs (spEPSPs; lower trace) of variable amplitude. The spEPSPs contribute to irregular firing during 1 s +300 pA depolarizing current step (upper trace). Traces have been offset for display purposes. Current injection protocol is indicated below the two traces.
B: Relation between the irregularity of firing during constant-current injection (calculated as described in the Methods) and the standard deviation of the baseline noise. Filled circle is the experiment displayed in (A). Solid line is the regression line (r = 0.30).

Even if the spontaneous inputs are not sufficiently large to directly trigger action potentials, they could still be large enough to affect firing regularity. For example, in the cell displayed in Figure 3.2A a clear acceleration in the spike rate could be observed (top trace) during a burst of spEPSPs. To quantify the relation between firing regularity and the presence of spEPSPs more systematically, we plotted the relation between the coefficient of variation of the firing rate, which was corrected for accommodation as detailed in the Methods, and the standard deviation of the baseline (Fig. 3.2B). The two were significantly related (r = 0.30; P = 0.026).

Spikelets

A different type of spontaneous potential changes was additionally observed. Spikelets were identified as small (<5 mV), brief, sometimes biphasic potentials (Fig. 3.3). They typically resembled very small action potentials. They were seen both in rats (6 of 33 cells = 18%) and in mice (13 of 103 cells = 13%).

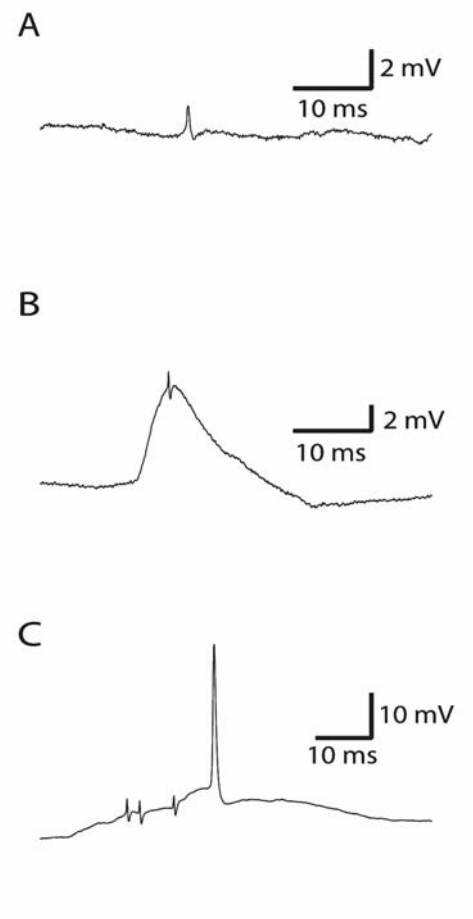

Figure 3.3 Presence of spikelets in the IC.
*Spikelets could occur spontaneously (*A*), on top of a spontaneous EPSP (*B*), or during the rising phase of an action potential (C).*

In the cells in which spikelets were observed, they could occur at rest (Fig. 3.3A), on top of a spontaneous EPSP (Fig. 3.3B), or during the rising phase of a spontaneous action potential (Fig. 3.3C). In mice, cells with spikelets had a significantly lower membrane resistance (82 ± 5 MΩ, n = 13, vs. 110 ± 6 MΩ, n = 90, P < 0.001). Time constant, resting membrane potential, action potential threshold, the presence of I_h or the age of the animal was not significantly different between cells with and without spikelets. In rats, membrane resistance, resting membrane potential and threshold were similar in cells with and without spikelets, although time constant appeared significantly higher in cells with spikelets (15.4 ± 1.7 ms, n = 6, vs. 8.3 ± 0.9 ms, n = 27, P = 0.015). If we assume that the spikelets reflect electrotonic coupling between neurons (Söhl et al. 2005), the lower membrane resistance or the longer time constant may be a consequence of the coupling, although the number of cells with spikelets were small, the differences were not large and they were not consistent across both species.

Classification of spike patterns

All cells responded with spikes to depolarizing current injections of sufficient strength. Based on the intervals between the spikes during a depolarizing step, we classified them into six different groups: sustained, accommodating, burst-onset, burst-sustained, buildup and accelerating. To classify the neurons, we first looked whether they fired in bursts, or showed buildup or accelerating-type firing.

Burst-onset was observed in 5% (5 of 103) of cells (Fig. 3.4AB) and burst-sustained in 10% of cells (10 of 103) in mice. Burst-sustained cells had a typical fast hyperpolarization between the clusters of action potentials, which was not observed in accommodating cells (Fig. 3.4CD). In rats, both burst-onset and burst-sustained were observed in 9% (3 of 33) of cells.

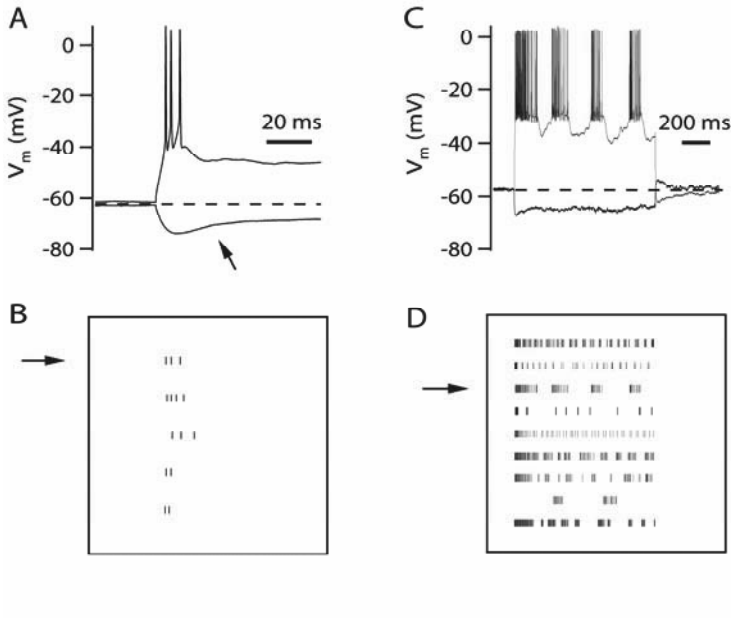

Figure 3.4 Two types of burst firing in mouse IC neurons.
A*: Burst-onset firing pattern was characterized by clustered action potentials at the beginning of depolarizing current injection. The broken line indicates resting membrane potential. Hyperpolarizing current injection showed a depolarizing sag, indicated with arrow.*
B*: Raster plot of all burst-onset cells (n = 5) at 100 pA above threshold, arrow indicates cell shown in (*A*).*
C*: Burst-sustained pattern was observed with clustered action potentials throughout the depolarizing current step.*
D*: Raster plot of all burst-sustained cells (n = 10) at 100 pA above threshold, arrow indicates trace shown in (*C*).*

Eleven neurons (11%) in mice were classified as accelerating. Eight of these neurons showed an acceleration in spike rate followed by a deceleration (Fig. 3.5A-C). In the other three neurons, the first interspike interval was consistently larger than the next interspike interval (Fig. 3.5D-F). These characteristic firing patterns remained present at larger current injections. In contrast to buildup neurons, the firing patterns of accelerating neurons were not affected by a 1 s pre-hyperpolarization. In rats, only one cell (3%) showed an accelerating-type of firing pattern.

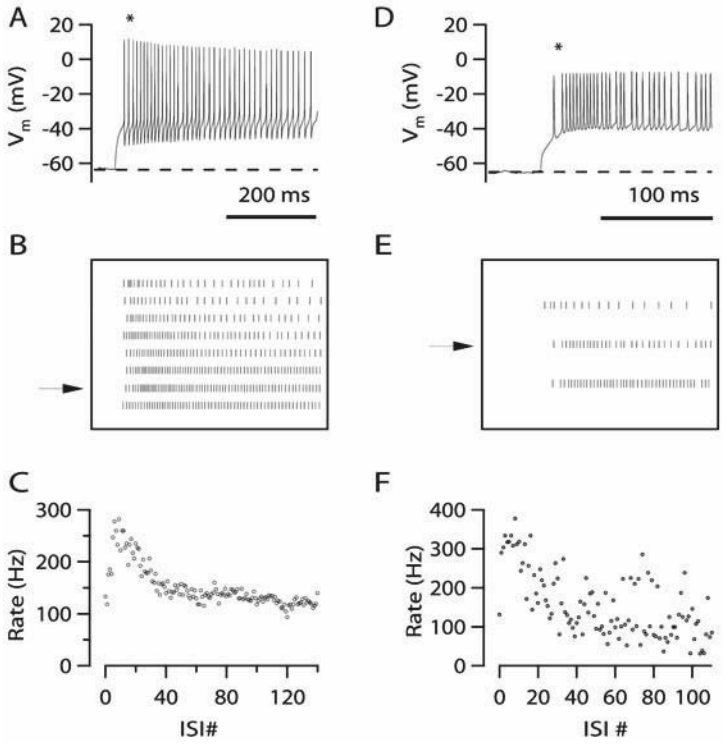

Figure 3.5 Accelerating neurons.
A*: One group of accelerating neurons showed an acceleration (indicated with * in top trace) in spike rate followed by a deceleration (accommodation).*
B*: Raster plot of all accelerating neurons (n = 8) at 100 pA above firing threshold, arrow indicates trace shown in (*A*) and (*C*).*
C*: A plot of the instantaneous spike rate ('Rate') versus interspike interval number ('ISI #') illustrates the initial acceleration followed by a deceleration.*
D*: A second group showed a persisting pause (indicated with * in top trace) between the first and second action potential at more than 3 different current injection levels.*
E*: Raster plot of all 3 pauser neurons at 100 pA above threshold with arrow indicating trace shown in (*D*).*
F*: As (*C*) for instantaneous spike rate versus ISI number from the cell that is shown in (*D*).*

A buildup response during a depolarizing current injection following pre-hyperpolarization was observed in 14 neurons (14%; Fig. 3.6). In these neurons, the delay between the start of the depolarizing current injection and the first spike increased from a value of 64 ± 28 ms (range 6 – 416 ms) for depolarizations from the resting potential of –63 ± 2 mV to a delay of 138 ± 40 ms (range 30 – 476 ms) when the membrane potential was hyperpolarized to –87 ± 3 mV before the depolarizing current injection. Following the pre-hyperpolarization, in all cells the delays remained long, even when the current injection was increased well above the standard level of 100 pA above threshold. In comparison, accelerating, sustained and accommodating cells showed a much smaller delay than buildup neurons, which showed little increase following a pre-hyperpolarization. In these cells, the delay increased from a value of 8 ± 1 ms (range 1 – 24 ms) at the resting membrane potential of –60 ± 1 mV to a delay of 11 ± 1 ms (range 1 – 43 ms) when the membrane potential was hyperpolarized to –75 ± 1 mV. In rats we observed buildup neurons in 12% of cells (4 of 33).

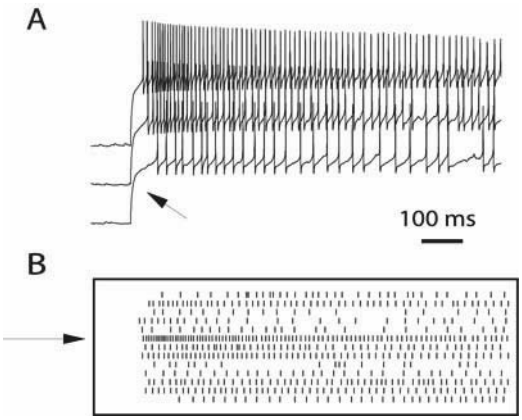

Figure 3.6 Buildup response.
A*: Neuron maintains a delay of the first action potential (indicated with arrow) in response to 150 (threshold) – 250 pA depolarizing current injection following 1 s pre-hyperpolarization. Traces have been vertically offset for display purposes.*
B*: Raster plot of buildup neurons stimulated at 100 pA above threshold. Arrow indicates response from neuron shown in (*A*). (One neuron was not plotted here because it only fired one spike at 100 pA above threshold).*

In the remainder of the cells (61% in mice, 67% in rats) the relation between the firing rates during the current injections and the ISI could be well described by an exponential function (Fig. 3.7A-C). The amount of accommodation differed greatly between cells, but also depended on the amount of current that was injected (Fig. 3.7D). In general, cells that had a low accommodation index (AI) when tested just above firing threshold also had a low AI when tested with larger depolarizing currents. However, cells that showed clear accommodation just above threshold showed a more sustained firing pattern when tested with larger currents (Fig. 3.7).

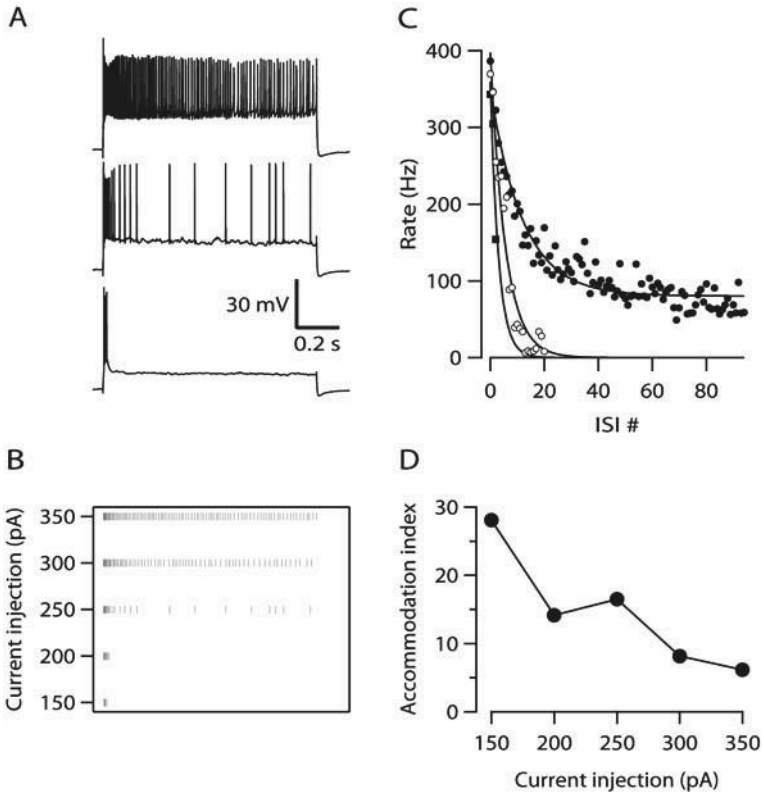

Figure 3.7 Accommodation index changes at different current injection steps.
A*: Response to 1 s depolarizing current injections of (from bottom to top) 150 (threshold), 250 and 350 pA. Traces have been vertically offset.*
B*: Raster plot of responses of the cell shown in (*A*).*
C*: Relation between firing rate and interspike interval number for the responses shown in (*A*), Filled squares response to +150 pA, open circles +250 pA and filled circles +350 pA. Solid lines are exponential fits for each condition.*
D*: Decrease of accommodation index with increasing current injection level.*

At 100 pA above the first level that resulted in one or more spikes, 23% (24 of 103) of cells had an AI <4% and were classified as sustained (Fig. 3.8A-C), the other 38% (39 of 103) as accommodating (Fig. 3.8D-F).

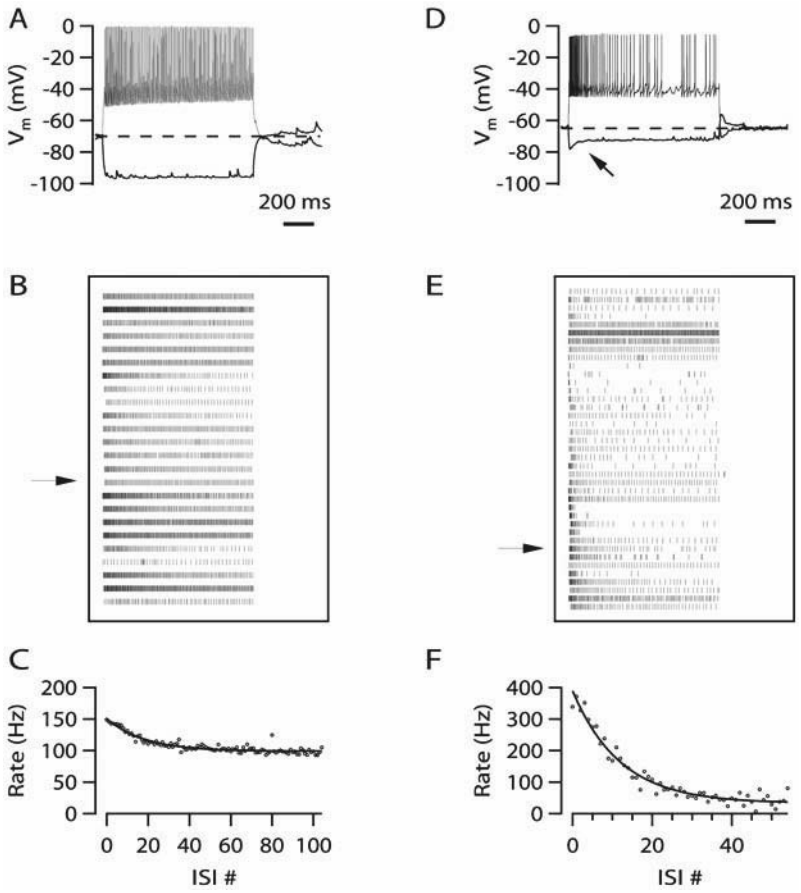

Figure 3.8 Sustained and accommodating firing during depolarizing current injections.
A*: Example of the response of a cell to current injections of -150 and +200 pA. This cell showed a regular pattern, as defined by an accommodation index less than 4%. Dashed line shows mean resting membrane potential.*
B*: Raster plot showing response of all sustained cells in mice (n = 24) at 100pA above firing threshold. Arrow indicates response to depolarizing current injection shown in (*A*).*
C*: Spike rate ('Rate') versus interspike interval number ('ISI #') of cell shown in (*A*). Solid line is a single exponential fit.*
D*: Example of a neuron that showed accommodation during 250 pA depolarizing current injection. Depolarizing sag during hyperpolarization is pointed out with arrow, which is clearly not present in the sustained cell shown in (*A*).*
E*: Raster plot of all accommodating cells (n = 39) analogous to (*B*). Arrow indicates spikes from neuron shown in (*D*).*
F*: Relation between spike rate and interspike interval number for cell shown in (*D*). Solid line is a single exponential fit.*

A subset of these cells (7 sustained, 9 accommodating) showed rebound (anode-break) type firing following hyperpolarizing steps (Fig. 3.9). Rebound spiking was also observed in one buildup and four burst-sustained cells. In rats, 27% (9 of 33) of cells showed sustained firing. An accommodating firing type was observed in 40% of cells (13 of 33 cells). Two accommodating cells fired a rebound spike after hyperpolarization. The presence of spikelets was not associated with a specific firing type.

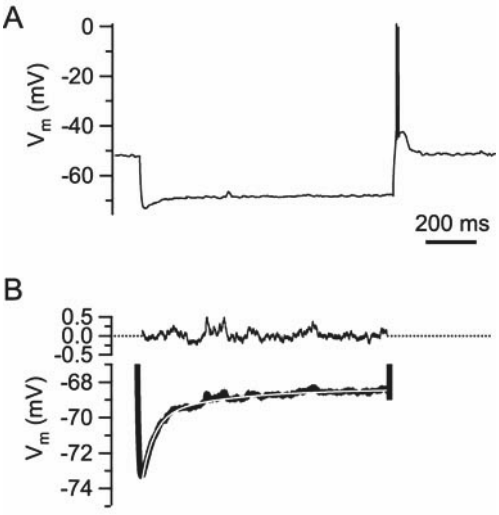

Figure 3.9 Rebound spiking in a cell with a depolarizing sag and a hump.
A*: Response to 1 s, 200 pA hyperpolarizing current injection. This neuron showed a depolarizing 'sag' during hyperpolarization and a 'hump' with rebound spiking after the current injection.*
B*: The average of 20 hyperpolarizing current injections in the same cell (1 s, -200 pA) is shown in the lower trace (thick black line). The thin white line shows the bi-exponential fit (τ_1 = 48 ms, τ_2 = 317 ms, relative contribution of τ_1 72% for the first 1 s). The upper trace shows the residuals of the fit.*

Membrane properties of IC neurons

A summary of the membrane properties of the mouse IC neurons belonging to the six different classes is presented in Table 3.1. Mean input resistance and membrane time constant differed significantly between cell types (ANOVA, $P = 0.001$ resp. $P = 0.025$). Buildup neurons had a significantly larger input resistance compared with accelerating, accommodating, burst-sustained and burst-onset cells ($P < 0.05$; Tukey's HSD test). In addition, buildup neurons had a longer time constant compared with accelerating cells ($P = 0.028$; Tukey's HSD test). Mean resting membrane potential and absolute spike threshold did not differ significantly between groups. Input resistance did not significantly change between 3 and 5 weeks of age and there were no obvious changes in the relative frequency of firing patterns across this age range.
In rat neurons, the average membrane potential was –59 ± 0.8 mV (range –47 to –68 mV; $n = 33$) and spike threshold was 15 ± 1 mV above the resting membrane potential (range 3 – 29 mV; $n = 33$).
No significant differences between cell groups were found in rat IC neurons for resting membrane potential V_m ($P = 0.09$) or threshold ($P = 0.44$). Input resistance, time constant and the presence of a depolarizing sag were not measured due to lack of proper hyperpolarization-protocols.

	buildup	*accelerating*	*sustained*
% of cells (n = total)	14 (14)	11 (11)	23 (24)
R_m (MΩ)	145 ± 18 (14)	81 ± 6 (11)	126 ± 10 (24)
tau (ms)	11.7 ± 1.8 (12)	5.4 ± 0.6 (11)	6.7 ± 1.2 (15)
V_m (mV)	-63.0 ± 2.0 (14)	-64.5 ± 1.6 (11)	-60.6 ± 1.3 (24)
absolute firing threshold (mV)	-44.4 ± 1.4 (14)	-45.4 ± 1.9 (11)	-48.5 ± 1.5 (24)
% of cells with I_h	7 (1)	9 (1)	38 (9)

	accommo dating	*burst-sustained*	*burst-onset*	*average of all cells*
% of cells (n = total)	38 (39)	10 (10)	5 (5)	100 (103)
R_m (MΩ)	98 ± 8 (39)	87 ± 12 (10)	64 ± 9 (5)	106 ± 5 (P = 0.001)*
tau (ms)	7.5 ± 1.3 (17)	3.8 ± 1.1 (2)	no data	7.6 ± 0.7 (P = 0.025)*
V_m (mV)	-59.5 ± 1.1 (39)	-57.8 ± 0.8 (10)	-62.6 ± 1.4 (5)	-60.7 ± 0.6 (P = 0.073)
absolute firing threshold (mV)	-47.7 ± 0.8 (39)	-49.8 ± 1.3 (10)	-44.0 ± 1.4 (5)	-47.2 ± 0.6 (P = 0.089)
% of cells with I_h	72 (28)	80 (8)	100 (5)	50 (52) (P < 0.001)*

Table 3.1 Membrane properties of neurons in the C57/Bl6 mouse inferior colliculus.
Data are given as mean ± SE, with n between parentheses. R_m = input resistance, tau = time constant, V_m = resting membrane potential.

Hyperpolarization-activated current (I_h)

In mice, in 52 of 103 cells a depolarizing sag (of >10%) was observed during hyperpolarizing current injection, suggesting that these cells had the hyperpolarization-activated mixed cation current I_h. These cells had a more depolarized resting membrane potential (-59.4 ± 0.6 mV, n = 52, vs. –62.1 ± 1.0 mV, n = 51, P = 0.03) and a lower action potential threshold (-49.3 ± 0.7 mV, n = 52, vs. –45.1 ± 0.8 mV, n = 51, P < 0.001). Membrane resistance was not significantly different between cells with or without I_h (98 ± 6 MΩ, n = 52, vs. 115 ± 7 MΩ, n = 51, P = 0.11).
We measured the activation of I_h by fitting a single or a double exponential function on the depolarizing sag during hyperpolarizing current injections (Fig. 3.9B). In 14 cells, a single exponential function was sufficient to describe I_h activation. The average time constant was 47 ± 26 ms. In the other 38 cells, a double exponential function was needed with a fast time constant of 42 ± 5 ms, which contributed 68 ± 3% to the total amplitude and a slow time constant, which ranged from 30 ms to more than a few seconds and had a median value of 380 ms.
The fraction of cells with I_h differed greatly between cells with different firing patterns (χ^2-test, P < 0.001). All cells that were highly accommodating, i.e. burst-onset cells or cells with an AI >40%, had I_h and in each case showed a rapid depolarizing sag. Time constant of single exponential or the fast exponential of a bi-exponential fit was in each case <40 ms. The presence of rapidly gating I_h in these cells suggests that the depolarizing sag, which is due to deactivation of I_h during depolarizing current injection, contributes to their firing pattern. An example of a brief depolarizing sag of a burst-onset cell is shown in Fig. 3.5A.
All cells with I_h showed an afterhyperpolarization (AHP) of >1 mV at the end of the depolarizing current injections, whereas only 51% of cells without I_h showed an AHP.
All cells with I I_h h showed a depolarizing overshoot after hyperpolarization ended. This so-called 'hump' is most likely a consequence of the increased activation of I_h during the hyperpolarizing step, reflecting the gradual deactivation of I_h back to the resting open probability (Koch and Grothe 2003). Only 5 of 51 cells without I_h showed a hump, but in these cases the hump had a different time course than the AHP, except in one cell, which did show a marginal presence of I_h (8% depolarizing sag). Presumably, by its contribution to this hump, I_h was important for rebound spiking, since of the 21 cells that showed rebound spiking, 18 had a clear depolarizing sag (>10%) and in 3 it was marginal (4-7%).
We conclude that cells with I_h had a more depolarized resting potential, were more likely to fire bursts (13 of 15 bursting cells had I_h), were more likely to show an afterhyperpolarization following depolarizing current injection, were more likely to fire rebound action potentials and were more likely to accommodate. Cells with strong accommodation showed rapid I_h gating, suggesting that rapid I_h deactivation during depolarizing current injections contributed to the accommodation in these cells.

DISCUSSION

In this chapter we describe basic properties of the neurons in the inferior colliculus (IC) of the rat and the mouse. Although these two species are the most commonly used animals in Neuroscience research, in vivo intracellular recordings from the rodent IC had not yet been reported. In contrast to previous reports in slices, we did not observe single-spike onset firing, whereas we did observe an accelerating firing pattern. Two other new findings that were not apparent in previous slice (or in vivo) recordings were the occurrence of spikelets and the effect that spontaneous EPSPs had on triggering action potentials and thereby on the regularity of firing in many cells.

Spikelets are present in the rodent inferior colliculus

Spikelets resemble very small action potentials. They are widely considered to be the electrophysiological correlate of electrotonic coupling through gap junctions (Söhl et al. 2005). Although they had previously not been reported to be present in the IC, we observed them both in rats and mice, in 13 – 18 % of the cells, respectively. Their location within the IC remains to be investigated. These cells did not show obvious differences in their passive properties and the presence of spikelets was not associated with a specific type of firing pattern. The gap junction proteins Connexin 36 and Pannexin 1 and 2 are expressed in the adult IC, albeit at low levels (Bruzzone et al. 2003; Condorelli et al. 2000; Zappalà et al. 2006). As in other brain regions, a primary role of the gap junctions may be to synchronize cells and as such a possible role in audiogenic seizures (Faingold 2002) deserves further attention.

Spontaneous firing rates were much lower than in extracellular studies

Cells rarely fired spontaneously, in contrast to what has been observed previously using extracellular recordings in rodents (Ehret and Moffat 1985; Palombi and Caspary 1996; Willott and Urban 1978). In other brain areas there is evidence that spike frequencies are overestimated by extracellular recordings (Margrie et al. 2002). Although we cannot exclude that anaesthesia may have contributed to the low observed spike rates (see (Nuding et al. 1999) and refs therein), most previous studies were also done under anaesthesia.

Classification of firing patterns

The neurons of the inferior colliculus are heterogeneous with respect to their firing patterns. We have described six firing patterns in vivo. Their relative frequency was similar between rats and mice. Many of our results correspond to results obtained in slice recordings (Basta and Vater 2003; Koch and Grothe 2003; Li et al. 1998; Peruzzi et al. 2000; Reetz and Ehret 1999; Sivaramakrishnan and Oliver 2001; Wagner 1994), except we did not observe single-spike onset firing, the buildup cells did not have a pauser response and

we observed cells with an accelerating firing type which had previously not been reported in slice recordings from the IC.

We used the changes in the interspike intervals during long depolarizing steps for classifying the cells. In most cells the relation between spike rates and interspike interval number could be adequately described by a single exponential function. Cells in which the fit was poor fired in bursts or showed accelerating responses. Buildup neurons also were distinguished as a separate group. An advantage of the use of the exponential fit over most other methods was that it was more robust against irregular firing, which was observed in many cells, in agreement with extracellular recordings (Rees et al. 1997). Irregularity of firing during current injection was often due to spontaneous EPSPs, which were sufficiently large to cause brief increases in firing rates. Some cells needed summation of only a few spontaneous inputs for a spike to occur, whereas in others many more simultaneously active inputs would be needed to trigger a spike. It would be interesting to test how this difference translates into a difference in auditory function.

In cells in which the exponential fit was adequate, the increase in the spike interval between the first and the second spike was used to classify the cells as sustained or accommodating. This classification was to some extent arbitrary for two reasons. Firstly, all cells showed some degree of accommodation. Secondly, although quantification for accommodation was carried out consequently at the same level above threshold to allow a comparison between cells, at higher current levels accommodating cells became more regular, as was also observed by (Sivaramakrishnan and Oliver 2001). A similar phenomenon can be expected to occur during auditory stimulation, if the excitatory synaptic conductances become larger, an onset response may become more sustained (Rees et al. 1997).

A clear difference between our data and results obtained from slice recordings was the absence of onset neurons that fired only a single spike even with current injections well above the firing threshold. In recordings from rat slices, onset firing has been described in 8 – 24% of neurons (Koch and Grothe 2003; Li et al. 1998; Sivaramakrishnan and Oliver 2001). We may have missed the onset cells, since the Kv1.1 potassium channel, which contributes to onset firing in for example the cochlear nucleus, is mostly expressed in the ventrolateral region of the mouse IC (Grigg et al. 2000), which was underrepresented in our recordings. However, single-spike firing has been observed in all subregions of the adult IC (Li et al. 1998).

We found the classification of buildup and accelerating neurons to be relatively difficult, since both types shared some properties with the buildup-pauser neurons previously described in slice recordings, but both groups also differed in other respects. Cells in both groups typically lacked a depolarizing sag and did not show rebound firing. The buildup neurons had a long delay for the first spike, which increased after prehyperpolarization, as previously reported for buildup-pauser cells in slice recordings (Peruzzi et al. 2000; Sivaramakrishnan and Oliver 2001). However, in contrast to the earlier reports, we did not observe a rapid initial spike at large current injections. In mice, these cells had a relatively large membrane resistance, arguing against a much larger conductance being active at rest. We therefore speculate that the lack of this pauser or 'hump and sag' response could be due to a more rapid activation of the A-type current than in the slice recordings (Fujino et al. 1997; Kanold and Manis 2001).

The cells that we classified as accelerating also shared some properties with the buildup-pauser firing type previously observed in slice recordings. They robustly showed a decrease in interspike intervals, similar to a pauser response. However, the firing was not markedly altered by pre-hyperpolarization, in contrast to earlier reports (Peruzzi et al. 2000; Sivaramakrishnan and Oliver 2001). Neurons with an accelerating firing type have been observed in frog tectum (Gutmaniene et al. 2003) and spinal cord (Jiang et al. 1995; Smith and Perrier 2006; Viana et al. 1995), although in these cases typically no accommodation later during the train was observed. The accelerating firing type may depend on calcium influx (Derjean et al. 2005; Purvis and Butera 2005; Smith and Perrier 2006) or on the presence of a persistent sodium current (Li and Bennett 2003). Voltage clamp studies will be needed to more firmly establish the accelerating and buildup groups and to investigate the ionic mechanisms underlying these firing types.

Burst firing, which we observed in 15-18% of the cells, was seen in slice recordings infrequently in one report (3% of cells; (Bal et al. 2002) and not at all in others (Koch and Grothe 2003; Peruzzi et al. 2000; Sivaramakrishnan and Oliver 2001). This firing type may be more prominent in the dorsal cortex, which was a target in our recordings, and calcium-dependent potassium channels may contribute to the afterhyperpolarizations observed between bursts (Li et al. 1998).

Role of I_h

About half of the neurons in the mouse IC showed a clear depolarizing sag during hyperpolarizing current injections. A similar depolarizing sag has also been observed in in vivo recordings from guinea pig (Pedemonte et al. 1997) and this sag most likely signifies the activation of the cation current I_h, although we cannot exclude contributions from other currents. In slice recordings from rat, this sag was blocked by the specific I_h blocker ZD7288 (Koch and Grothe 2003) and IC neurons are known to express different I_h subunits (Koch et al. 2004; Notomi and Shigemoto 2004). The kinetics of the depolarizing sag we observed largely matched the kinetics of I_h activation observed in slice recordings, although since we estimated I_h activation during current clamp recordings, the precise gating kinetics are somewhat uncertain. In most cells, activation was biphasic, with presumably HCN1 subunits contributing to fast activation and HCN2 homomers responsible for the slowly activating conductance (reviewed in (Robinson and Siegelbaum 2003). I_h seemed to be active already at the resting membrane potential, suggesting that I_h activates at relatively positive potentials in IC neurons, similar to for example octopus cells (Bal and Oertel 2000).

Cells with evidence for the presence of I_h clearly differed from cells without a clear depolarizing sag. They were more likely to fire rebound action potentials, and conversely, all cells with rebound firing had a depolarizing sag. This suggests that activation of I_h during the hyperpolarization contributed to the rebound spikes (Koch and Grothe 2003). We did not investigate the role of calcium channels and calcium-dependent potassium channels in rebound firing (Sivaramakrishnan and Oliver 2001; Smith 1992). In addition, cells with I_h had a more depolarized resting potential, were more likely to fire bursts (13 of 15 bursting cells had I_h) and generally showed more rapid accommodation. Cells with strong accommodation showed rapid I_h gating, suggesting that rapid I_h deactivation during depolarizing current injections contributed to the accommodation in these cells (Koch and Grothe 2003).

In addition, all cells with I_h showed an afterhyperpolarization following long depolarizations (vs. 51% in cells without I_h), as previously observed in slice recordings (Koch and Grothe 2003). In vivo application of specific I_h blockers would be helpful in testing the effect on auditory processing of the contribution of I_h to the resting membrane potential, rebound firing, spike accommodation or the afterhyperpolarization. In the accompanying paper (Tan and Borst 2007) we provide further evidence for a special role of I_h in auditory processing.

Chapter 4

Comparison of responses of neurons in the mouse inferior colliculus to current injections, tones of different durations and sinusoidal amplitude-modulated tones

M.L. Tan, J.G.G. Borst

J Neurophysiol 98:454-466, 2007

ABSTRACT

We made in vivo whole-cell patch-clamp recordings from the inferior colliculus of young-adult, anaesthetized C57/Bl6 mice to compare the responses to constant-current injections with the responses to tones of different duration or to sinusoidal amplitude modulated (SAM) tones. We observed that voltage-dependent ion channels contributed in several ways to the response to tones. A sustained response to long tones was only observed in cells showing little accommodation during current injection. Cells showing burst-onset firing during current injection showed a small response to SAM tones, whereas burst-sustained cells showed a good response to SAM tones.

The hyperpolarization-activated non-selective cation channel I_h had a special role in shaping the responses: I_h was associated with an increased excitability, with chopper and pauser responses and with an afterhyperpolarization following tones. Synaptic properties were more important in determining the responses to tones of different durations. A short-latency inhibitory response appeared to contribute to the long-pass response in some cells and short-pass and band-pass neurons were characterized by their slow recovery from synaptic adaptation. Cells that recovered slowly from synaptic adaptation showed a relatively small response to SAM tones.

Our results show an important role for both intrinsic membrane properties, most notably the presence of I_h and the extent of accommodation, and synaptic adaptation in shaping the response to tones in the inferior colliculus.

INTRODUCTION

The inferior colliculus (IC) receives ascending afferent information from almost all of the major auditory nuclei in the lower brain stem. Auditory information from these nuclei is analyzed and transformed by the cells in the IC and relayed to the thalamus and the cortex. The relation between the specific complement of ion channels and the auditory role of IC neurons is still largely unexplored (Oliver 2005). In response to direct current injections in intracellular or whole-cell recordings, the cells in the IC can respond with a number of distinct firing patterns (Bal et al. 2002; Koch and Grothe 2003; Peruzzi et al. 2000; Sivaramakrishnan and Oliver 2001; Tan et al. 2007). Four important features in their response to current injection are the extent of accommodation during current injection, the presence of burst firing, the presence of an A-type potassium current leading to buildup-pauser firing and the presence of the hyperpolarization-activated cation channel I_h. The significance of these features for auditory processing in the IC is not yet known, but, for example, I_h has been predicted to be involved in the afterhyperpolarization following bursts of action potentials, in generating onset responses, and in synaptic integration (Koch and Grothe 2003).

IC neurons vary not only in their response to current injection, but sound-evoked responses, as measured in extracellular recordings, also vary widely between cells (Chen 1997; Ehrlich et al. 1997; Le Beau et al. 1996; Palombi and Caspary 1996; Rees et al. 1997; Willott and Urban 1978; Xia et al. 2000). It is not yet known whether the situation in the IC is similar to the cochlear nucleus, where the relation between the firing patterns during current injection, the specific inputs and output projections and the auditory role is relatively stereotypical (Cant 1992; Rhode and Greenberg 1992). To explore this relation, we compared the response to tones of different durations and to sinusoidal amplitude modulated (SAM) tones with the response to current injection during in vivo patch-clamp recordings from the IC (Casseday et al. 1994) of young-adult mice. We chose tones of different durations and SAM tones as a stimulus since they have been extensively studied using extracellular recordings (Brand et al. 2000; Casseday et al. 1994; Chen 1998; Pérez-González et al. 2006; Pinheiro et al. 1991; Potter 1965; Xia et al. 2000), but the cellular mechanisms that allow cells to respond specifically to the duration of a sound and the mechanisms that allow synchronization of neural responses to the envelope of SAM tones (Krishna and Semple 2000; Langner 1983; Langner and Schreiner 1988; Rees and Møller 1983) are largely unknown.

MATERIALS AND METHODS

Animal procedures were in accordance with guidelines provided by the animal committee of the Erasmus MC. Patch-clamp recordings from the IC of young-adult, anesthetized C57/Bl6 mice were made exactly as described in our accompanying paper (Tan et al. 2007). Average ABR thresholds for 1- to 2-month old C57/Bl6 mice range from 15 – 25 dB SPL in the 6 – 32 kHz range (Hunter and Willott 1987) .

Auditory stimulation

Sound stimuli were presented in closed field: speaker probes were inserted into both ear canals and stabilized with silicone elastomere (World Precision Instruments). Auditory stimuli were generated with Tucker Davis Technologies hardware (TDT, System 3, RP2.1 processor, PA5.1 attenuator, ED1 electrostatic driver, EC1 electrostatic speaker). Stimulus generation was controlled by a custom-made program written in MATLAB (version 7.0.4; The MathWorks, Natick, MA). All experiments were performed in a single-walled sound-attenuated chamber (Gretch-Ken Industries; attenuation at least 40 dB at 4 – 32 kHz).

Determination of the characteristic frequency

Pure tones (1 – 64 kHz in 5 steps between octaves) were presented at the contralateral ear starting at 80 dB SPL with decreasing steps of intensity (5 dB per step). Tones had durations of 50 ms and a 2 ms rise time, repeated at least 20 times at an interval of at least 150 ms. The frequency with the lowest intensity that elicited an EPSP of at least 1 mV was identified as the characteristic frequency (CF_{EPSP}). This definition is different from that used in extracellular recordings, where CF is the frequency with the lowest intensity for eliciting an action potential.

Duration tuning

Tones of different durations at the characteristic frequency were presented in a fixed order. Durations increased from 1, 2, 4, …to 512 ms with 0.5 ms rise time and an interval of 150 ms between the end of a tone and beginning of the next tone. This set of tones of different durations was repeated at least 20 times with 250 ms between sets. Their amplitude was typically 40 dB above the EPSP threshold.

Amplitude modulation

To study amplitude modulation, 200 ms tones at the characteristic frequency were 70% sinusoidally modulated in amplitude according to:

$$s(t) = [1 + 0.7\sin(2\pi f_m t)]\sin(2\pi f_c t) \qquad (1)$$

where s(t) is the waveform of a tone at the characteristic frequency f_c that was modulated at a lower frequency f_m, which ranged between 10-640 Hz. The tone included a 2 ms rise time, independent of modulation frequency. These sinusoidal amplitude-modulated (SAM) tones were repeated 20 times at an interval of 150 ms.

Calibration

Sound intensities were calibrated between 0.5 and 65 kHz with a condenser microphone (ACO pacific type 7017, MA3 stereo microphone amplifier, TDT SigCal software). During calibration we used a 3 mm diameter PVC heat shrinking tube to mimic a rodent external auditory ear canal. Its diameter and shape were based on the reconstruction of four young-adult rat external auditory ear canals. The speaker probe was inserted at one end of the tube at a distance of 4 mm to the diaphragm of the microphone, resembling the distance from tragus to ear drum.

Analysis

General

Analysis was done with custom written programs that used the NeuroMatic environment (version 1.91, kindly provided by Dr J. Rothman, University College London) within Igor Pro 5 (Wavemetrics, Lake Oswego, OR). Amplitudes, 20-80% rise times and delays were measured after spike truncation. Spikes were truncated by interpolating between the membrane potential 1-2 ms before and after the peak of the action potential. Unless noted otherwise, rise times and delays refer to the EPSP evoked by the last tone in the duration protocol. At least 20 traces were averaged. Peak amplitudes were corrected for noise by subtraction of the standard deviation of the resting membrane potential, measured for a period of at least 10 ms before sound onset. Delays were measured as the delay between sound onset and the intersection between a (horizontal) line through the average baseline and a line through the points of the rising phase at which the EPSP was 20% and 80% of maximal.

Data on the activation of I_h, the classification of different firing types, the accommodation index and membrane properties (such as input-resistance, membrane time constant, resting membrane potential and spike threshold) were taken from the accompanying paper (Tan et al. 2007). Afterhyperpolarizations had to be at least 1 mV. For IPSP amplitudes the maximal value following any of the 10 different durations was used.

Duration tuning

Neurons were classified for duration tuning according to (Brand et al. 2000). For neurons that regularly responded with spikes to tones, it was tested whether the spike count dropped to below 50% of the maximum spike count for any duration. If the drop was for long durations, the neuron was classified as short-pass; conversely, it was classified as long-pass. If the spike count was less than 50% of the maximum count both for short and for long durations, the neuron was classified as band-pass. For neurons that infrequently or never responded with spikes, the size of the EPSPs (after truncation of spikes if present) was used for the classification. Analogously to the spike count criterion, a 50% reduction of EPSP size was used to classify neurons as short-pass, long-pass or band-pass. Neurons that did not match the criteria for either short-pass, long-pass or band-pass were classified as untuned. The responses to 512 ms auditory stimulation were further analyzed. Cells that fired action potentials in response to tones were identified as onset when they fired at most a few action potentials at the onset, sustained when they fired throughout the tone, or pauser when a distinct firing pause could be recognized after the onset of the stimulus (Le Beau et al. 1996; Rees et al. 1997; Willott and Urban 1978).

SAM tones

The modulation amplitude was calculated in two different ways. Firstly by fitting a sine wave to the EPSP amplitudes with a period identical to the period of the sound modulation. Secondly, by averaging every period of the membrane potential and calculating the peak-to-peak amplitude. To avoid the spurious effects of an onset response, the same time period was used for both approaches, which was typically the last 100 ms of the tone. Occasionally, shorter time periods were used when the average membrane potential did not reach a plateau value. Both methods are compared in Figure 4.7A. Unless stated otherwise, the amplitude method has been used in the presentation of the results.

Vector strength

The vector strength R, sometimes called the synchronization index, was calculated as follows (Goldberg and Brown 1969):

$$R = \frac{\sqrt{\left(\sum_i^n \cos\theta_i\right)^2 + \left(\sum_i^n \sin\theta_i\right)^2}}{n} \qquad (2)$$

where θ_i is the phase (between 0 and 2π) of the spike time *i* modulo the modulation period. Since this vector is normalized to the total number of spikes *n*, it takes on values between 0 and 1, with a value of 0 indicating no phase-locking and 1 perfect phase locking. Only spikes that occurred >100 ms after the tone onset were included, to avoid that cells with an onset response had high vector strengths. Our definition thereby deviates from other studies, in which the onset response was partially or fully included (e.g. (Walton et al. 2002), but in which case the rise time of the tones were dependent on the modulation frequency. It was not necessary to correct for spontaneous firing, since this was generally quite infrequent.

Statistics

Data are presented as mean ± standard error of the mean (SE). A difference in the mean of two groups was assessed by Student's *t*-test. Differences in the mean of more than two groups were assessed by ANOVA, followed by a Tukey's HSD test. Statistical significance of R was evaluated using the Rayleigh test (Mardia and Jupp 2000). Values of $P < 0.05$ were judged as statistically significant, unless noted otherwise.

RESULTS

A total of 45 cells from the mouse inferior colliculus (IC) were recorded in whole-cell current clamp. These cells are a subset of a larger number of cells whose passive properties and response to current injection have been described in the accompanying paper (Tan et al. 2007). They had a characteristic frequency (CF_{EPSP}) of 22.0 ± 1.4 kHz (mean ± SE; range 5 - 49 kHz) at a threshold of 29 ± 2.7 dB (range 0 - 80 dB).

Spiking vs. non-spiking

We tested the response to tones of increasing duration at CF_{EPSP}, using tones ranging from 1 to 512 ms, which were given at an inter-tone interval of 150 ms. In all cells an EPSP was evoked in response to a long tone. The EPSP started 10.3 ± 0.7 ms after the onset of the tone and its 20-80% rise time was 8.3 ± 1.5 ms. In 30 of 45 cells the EPSPs were sufficiently large to trigger spikes, in the other cases, only subthreshold responses were observed. In the cells in which action potentials were triggered reliably (i.e., in more than half of the tone presentations) in response to the 512 ms tone, the median spike delay was 10.3 ms after tone onset (n = 17; range 7.9 - 181 ms). The median delay between the onset of the EPSP and the first spike was 1.8 ms (range 0.9 - 172 ms) in these cells. In addition, 6 of the 45 cells showed spikelets. In two of these, the spikelets could be triggered by sound.

Tone-evoked spikes vs. spikes evoked by constant-current injection

Of the 30 cells in which the tones triggered spikes, 17 cells showed an onset response, 3 a pauser response and 10 fired in a sustained manner during long tones. This response depends on both the synaptic input and on the membrane properties of the cell. To partly assess the contribution of the latter, we compared the responses to tones with the responses to constant-current injection. During constant-current injection, 9 of the 45 cells responded as sustained, 15 as accommodating, 7 as buildup-pauser, 6 as accelerating, 3 as burst-onset and 5 as burst-sustained. As described in our accompanying paper (Tan et al. 2007) we use the term accommodation instead of adaptation for current injections to avoid confusion with synaptic adaptation. The responses to current injection could be used to predict some aspects of the response to tones. For example, all burst-sustained cells responded both to depolarizing constant-current injections and to tones with bursts of action potentials. However, the relation was not always that straightforward. Figure 4.1 shows two different accelerating cells, which both showed a non-accommodating response to constant-current injection (Fig. 4.1, A and C). Their response to tones, however, was very different. One cell showed an onset response (Fig. 4.1B), whereas the other fired in a burst-sustained manner during the tone (Fig. 4.1D). Apparently, a non-accommodating response during constant-current injection is not sufficient to yield a sustained response during long tones.

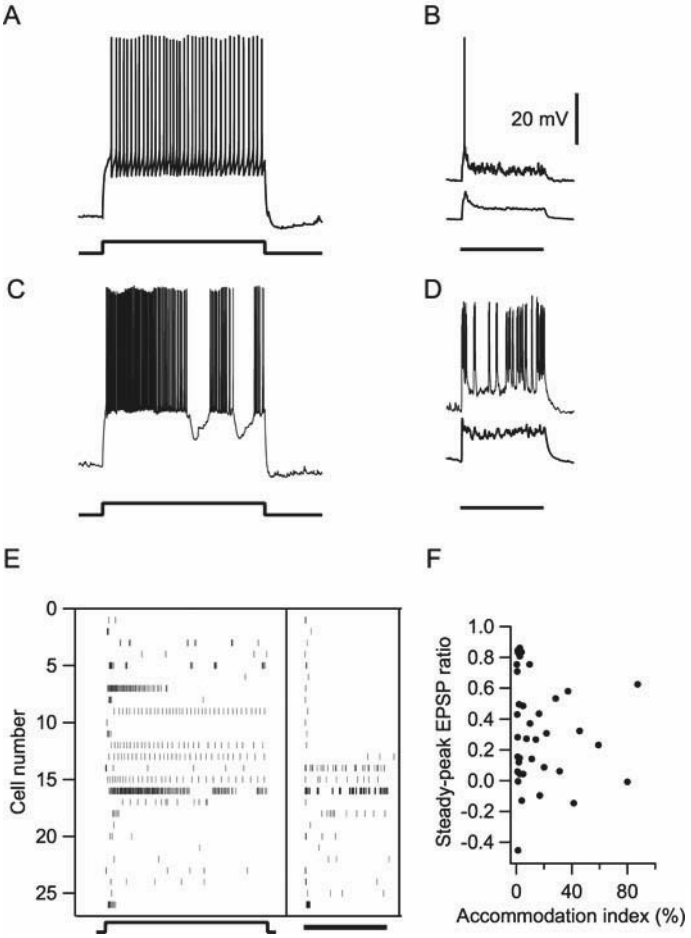

Figure 4.1 Relation between extent of accommodation during current injection and the response to tones.

A*: Whole-cell patch clamp recording from a neuron in the mouse IC. A 1 s, 150 pA current injection (indicated below the traces) results in a non-accommodating firing pattern. The neuron was classified as accelerating.*
B*: A 70 dB, 512 ms tone (indicated below the trace) at the characteristic frequency (24.3 kHz) resulted in an onset response (top trace) in the same neuron as displayed in (*A*). The middle trace, which has been vertically offset, is the average of 20 responses, which were averaged after spike truncation. Resting membrane potential was -67 mV.*
C*: In a different cell, a 150 pA constant-current injection also resulted in a non-accommodating response. This cell was also classified as accelerating.*

D*: A 70 dB, 512 ms tone at* CF_{EPSP} *(27.9 kHz) resulted in a sustained, bursting response. Same neuron as displayed in (*C*). Middle trace is again the average response (after spike truncation). Resting membrane potential was -59 mV.*
E*: Summary of comparison of responses to a tone (left) and to current injection (right). Sound stimulus (horizontal bar below raster plot) was a 512 ms tone at* CF_{EPSP}*, typically 40 dB above threshold. The first response that elicited a spike was selected; therefore responses are not always representative of the response to the tone. Depolarizing current injection was the response to a 1 s depolarizing step (indicated below raster plot) that resulted in the response whose amplitude best matched the maximal EPSP amplitude elicited by the tone stimulation. Cell 1-12 had an onset-type response to sound, 13-23 a sustained response and 24-26 a pauser response. Traces from cell 9 and 16 are displayed in (*A*) and (*C*), respectively.*
F*: Relation between persistency of the EPSP during long tones and the accommodation index. Steady-peak EPSP ratio is the ratio between the EPSP size at the end of a 512 ms tone and the peak EPSP size. Negative ratios indicate a hyperpolarization at the end of the tone. The accommodation index is a measure for the amount of accommodation during 1 sec constant-current injection at 100 pA above the spike threshold. The plot shows that cells with a sustained response to sound (steady-peak EPSP ratio >0.7) are non-accommodating.*

Figure 4.1E shows in a raster plot a comparison of the response to a 1 s depolarizing current injection and the response to the first (of at least 20) presentation of a 512 ms tone. Four cells are not displayed because they did not spike during the 512 ms tone. Although the first response was not always representative for the overall response to tones, from this plot it is clear that the cells that showed an onset response following tones could show both a non-accommodating and an accommodating response during current injection. To compare the two types of cells, we calculated the ratio of the amplitude of the EPSP at the end of the 512 ms tone and the maximum EPSP amplitude during the same tone ('steady-peak EPSP ratio') as a measure for the persistency of the EPSP during long tones. This ratio was clearly larger in the cells that fired in a sustained manner (0.5 ± 0.09; n = 13) than in the cells that had an onset response (0.16 ± 0.05; n = 17; P < 0.01), in agreement with the two cells that were illustrated in Fig. 4.1B and 4.1D (steady-peak EPSP ratio was 0.43 and 0.76 respectively). Evidently, cells that fired in a sustained manner must have had a sustained excitatory drive during the long tones. We compared the steady-peak EPSP ratio for the longest tone duration and the accommodation index, which is a measure for the amount of accommodation during constant-current injection (Tan et al. 2007). This comparison showed that in addition to a sustained excitatory drive, a non-accommodating response to current injection is also a prerequisite for a sustained response during long tones (Fig. 4.1F). Cells with a sustained response during long tones (steady-peak EPSP ratio > 0.7) had a small accommodation index, which was on average 2.7 ± 1.1% (n = 8). These results indicate that sustained firing during current injection is a necessary but not a sufficient condition for a sustained response during long tones.

Inhibition

Since all models that deal with duration tuning emphasize the role of inhibition, we looked whether there was evidence for synaptic inhibition in the IC neurons during tone stimulation at the CF_{EPSP}. In 15 of the 45 cells a short latency IPSP was observed. An example is shown in Figure 4.5C. Its amplitude ranged from -0.3 to –4.8 mV (mean -1.3 ± 0.4 mV), from a resting membrane potential ranging from –47 to –67 mV. In two of the cells with a fast IPSP, this IPSP was long lasting (>50 ms) and during long tones an IPSP-EPSP-IPSP sequence was present. In the other cells, either a sustained EPSP was present, or the membrane potential returned to the baseline level. The delay of the EPSP in the cells with a fast IPSP was a bit longer (11.7 ± 1.1 ms, n = 15 vs. 9.7 ± 0.8 ms, n = 30), but this difference did not reach significance (P = 0.16). In 7 cells that did not show an IPSP at CF_{EPSP}, short-latency IPSPs were observed at other frequencies (not shown).
In addition, in 17 of the 45 neurons, following long (>8 ms) tones the membrane potential hyperpolarized. The amplitude of this afterhyperpolarization was -2.6 ± 0.2 mV (range -1.5 to -4.7 mV). As detailed below, in 16 of these 17 cells the deactivation of the mixed cation current I_h during the tone contributed to or mediated this response.
Rebound spiking was not observed in response to auditory stimulation in any of the 45 cells.

Off responses

In 10 of 45 cells we observed a depolarizing off-response following the tone. The average amplitude of this EPSP ranged from 0.4-3 mV (mean 1.5 ± 0.3 mV). The off-EPSPs were identified by their constant, short latency following the end of tones of different durations (Fig. 4.2). They were unlikely to be a rebound response from an inhibitory input onto the same cell, since in only two of the ten cells there was clear evidence for a late-IPSP during longer tones and in these cells the amplitude of the off-EPSP did not correlate with the size of the late-IPSP. Two other cells had an IPSP preceding the on-EPSP as well. The size of the off-EPSP was in 9 of 10 cells smaller than the size of the on-EPSP evoked by the same tones. As small as these amplitudes were, in three of the five cells that responded with spikes to long tones, the off-EPSPs were sufficiently large to trigger spikes (Fig. 4.2B). In one of the other two cells, spikelets were observed following long tones. The fifth cell showed a complex response consisting of IPSPs and EPSPs. Cells with an off-response generally had relatively small plateau amplitudes during long tones. The amplitude of the EPSP at the end of the tone was 15 ± 9% (n = 10) of the peak amplitude, as compared to 35 ± 5% in the cells without an off-response (n = 35).

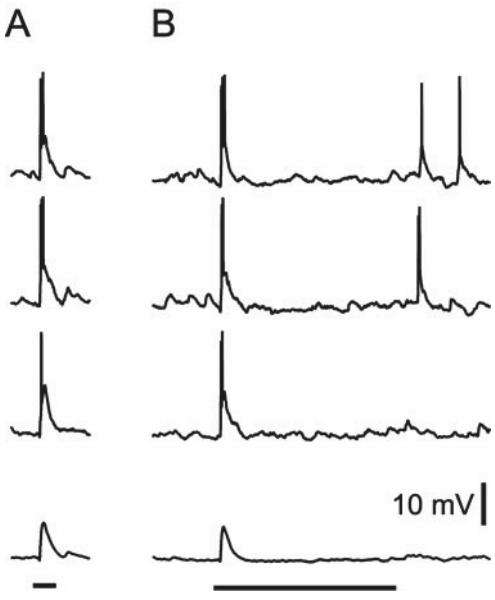

Figure 4.2 Off-EPSP.
Top three traces are consecutive responses to a 32 ms (A) or 256 ms (B), 24.3 kHz (CF_{EPSP}), 60 dB SPL pure tone. In the top two traces the small EPSP was able to trigger a spike at the end of the 256 ms tone. The onset EPSP was preceded by a small IPSP. Bottom trace is the average of 20 responses after spike truncation, showing that the amplitude of the averaged off-EPSP was only 1 mV and that it immediately followed after the tone, both for the 32 ms and the 256 ms tone. Resting membrane potential was -53 mV.

Role of I_h

Based on their response to current injection, 24 of the 45 cells showed evidence for the presence of I_h. These cells had a depolarizing sag following hyperpolarizing current injection. After the current injection, the membrane potential depolarized to values more positive than the resting membrane potential. Upon injection of depolarizing current the opposite was observed, these cells typically showed a hyperpolarizing sag during the current injection followed by an afterhyperpolarization at the end of the depolarizing current injection (Fig 4.3A).

Some differences in the properties of cells with and without I_h are summarized in Table 4.1. On average, cells with I_h had a lower membrane resistance and a more positive membrane potential. Estimated action potential threshold was slightly lower in cells with I_h. In combination with the more depolarized membrane potential, this means that in the cells with evidence for I_h, a much smaller depolarization was needed to trigger an action potential. As a result, although the maximal EPSP size that was reached during sound stimulation was similar, cells with evidence for I_h were more likely to fire spikes in response to the tones.

Properties of cells with and without hyperpolarization-activated current (I_h)

	I_h	**no *I_h***	**Total**
R_m (MΩ)	81 ± 6	99 ± 6	89 ± 5 (P = 0.038) *
V_m (mV)	-54.2 ± 1.0	-60.3 ± 1.5	-57.1 ± 1.0 (P = 0.002) *
Absolute firing threshold (mV)	-48.2 ± 0.8	-45.2 ± 1.2	-46.8 ± 0.7 (P = 0.044) *
threshold – V_m (mV)	6.0 ± 1.1	15.1 ± 1.9	10.3 ± 1.3 (P < 0.001) *
$EPSP_{max}$ (mV)	8.0 ± 0.7	7.7 ± 0.9	7.9 ± 0.5 (P = 0.8)
# cells with sound-evoked spikes	19 of 24	11 of 21	30 of 45 (P = 0.057)

Table 4.1 Differences between neurons with and without I_h.
Data are given as mean ± SE. Abbreviations: R_m, membrane resistance, V_m, resting membrane potential, $EPSP_{max}$, maximal EPSP size reached during sound stimulation. Asterisk (*) indicates differences between cells with and without evidence for the presence of I_h were significant (two-tailed t-test or χ^2-test).

Some cells responded with a short burst of 2 or more action potentials during a tone (Fig. 4.3, B and D). These bursts were often synchronized across trials, resulting in a chopper-like response (Fig. 4.3, C and E). In 12 of the 30 cells that spiked in response to the duration protocol, there was some degree of synchronicity, although the number of spikes was not always sufficient to assess this unambiguously. Of these 12 cells, 11 had evidence for the presence of I_h. In 3 of these cells, the depolarizing sag that was observed during hyperpolarizing current injections could be well described by a single exponential function, with a time constant ranging from 12-18 ms, whereas in the other 8 cells, two exponential functions were necessary. In these 8 cells, a clear fast component was always observed, which averaged 71 ± 4% of the total contribution, with an average time constant of 44 ± 11 ms. The average membrane potential at the peak of the EPSP (after spike truncation) was -45.4 ± 1.6 mV (n = 12) in the cells with a chopper-like response. Since the reversal potential of I_h lies between -29 and -40 mV in auditory neurons (Bal and Oertel 2000; Banks et al. 1993; Cuttle et al. 2001; Rodrigues and Oertel 2006), the deactivation of I_h during tones in these cells is expected to result in a hyperpolarizing sag.

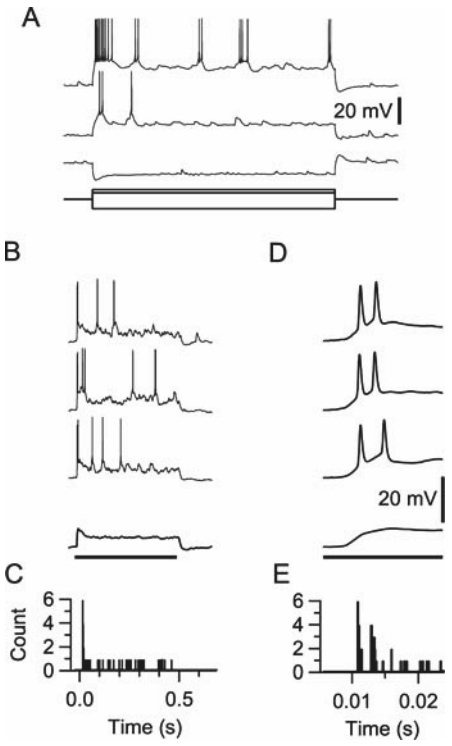

Figure 4.3 Chopper responses are associated with the presence of Ih.
A*: Response to 1 s constant-current injection of -from top to bottom- +150 pA, +100 pA and -150 pA, as indicated below the traces. During hyperpolarizing current injection a depolarizing sag was observed. During depolarizing current injection a hyperpolarizing sag was observed, similar to the responses during tone presentations.*
B*: From top to bottom, responses to three consecutive 16 kHz (CF_{EPSP}), 35 dB, 512 ms tone presentations, average trace (after spike truncation) and tone. Note the similarity of the time course of the hyperpolarizing sag with the sag during current injection (*A*). Vertical calibration bar is shown in (*D*).*
C*: Peristimulus time histogram (PSTH) of spikes. Bin size 0.1 ms.*
D-E*: Same cell except horizontal scale is different to illustrate the chopper-like response to the onset of the last tone. Times in (*C*) and (*E*) are relative to tone onset.*

Three of the chopper-like cells with a sustained component to the EPSP had a pauser response (Fig. 4.4, A and B). In these cells, the hyperpolarizing sag during longer tones was large enough to halt spiking momentarily. Only one of these three cells showed a fast IPSP. In addition, a similar hyperpolarizing sag was observed during constant-current injection (Fig. 4.4C), arguing against a role for an inhibitory input in the pause.

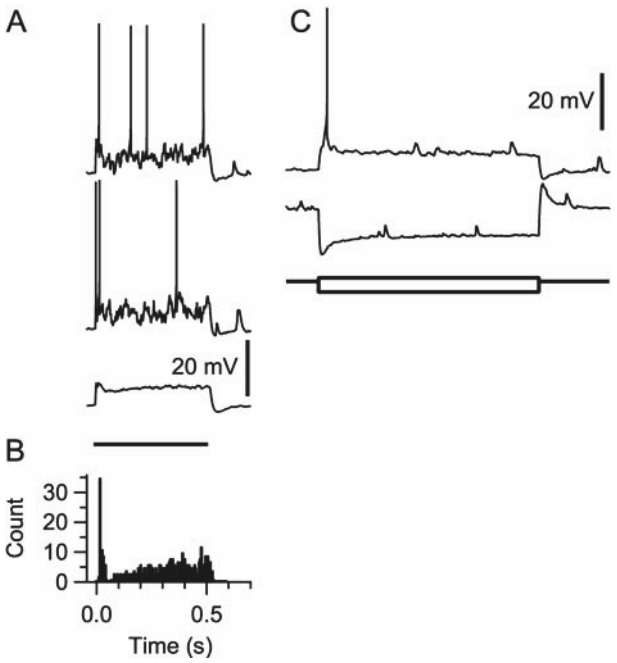

Figure 4.4 Pauser response and afterhyperpolarization in a cell that has I_h.
A*: From top to bottom: two consecutive responses, average trace (after spike truncation) and 55 dB tone stimulus (CF_{EPSP} 16 kHz). Only the response to the last tone is shown. Traces were vertically offset for display purposes. Membrane potential was -51 mV.*
B*: Peristimulus time histogram of spikes evoked by the last sound stimulus. Bin size 5 ms.*
C*: Response to 1 s constant-current injection of +50 pA (top trace) or -150 pA (lower trace), as indicated below the traces. Traces are offset for display purposes. Note the similarity in the time course of the sags and the afterhyperpolarization with the hyperpolarizing sag and the afterhyperpolarization during tones (*A*).*

I_h was associated with an afterhyperpolarization immediately following tones. Sixteen of the 17 cells that showed an afterhyperpolarization after tones longer than 8 ms had clear evidence for the presence of I_h. In the cells with evidence for I_h, the amplitude and the time course of the afterhyperpolarization generally matched the afterhyperpolarization observed following a similar depolarization due to current injection. Conversely, all cells that had both I_h and a sustained EPSP showed an afterhyperpolarization (Fig. 4.3B and 4.4A). In the 8 cells that had I_h, but lacked an afterhyperpolarization, the sustained EPSPs were on average only 0.5 mV (range 0-1.9 mV), which was substantially lower than the sustained EPSPs in cells with I_h that did have an afterhyperpolarization (mean 7.4 mV, range 3 – 12.6 mV).

Summary of the comparison between current injections and tones

From the comparison between the response to sound-evoked stimuli and the response to constant-current injection we were able to show that the two were similar in many respects. Sustained spiking during tones was only observed when the neurons also showed sustained spiking during current injection. I_h was associated with chopper responses and pauser response and played an important role in the afterhyperpolarization following tones.
Next we investigated the type of duration tuning of the cells.

Duration tuning

Based on the criteria described in the Methods section, 19 of the 45 cells showed some form of duration tuning in response to the standard protocol in which tones of increasing duration were given in fixed order (Fig. 4.5; Table 4.2). The remaining 26 cells were classified as untuned.

Short-pass

Three cells showed a short-pass response, since the response to brief tones was clearly larger than the response to longer tones (Fig. 4.5A). In all three cells a clear onset response was observed, in two of three cells the responses were suprathreshold. In one of the three cells a small, rapid IPSP preceded the EPSP and a small afterhyperpolarization followed the spikes. In the non-spiking cell a small excitatory off-response was observed. The response to current injection was very different from the response to tones, since two of the three cells had a sustained response (accelerating and sustained).

Band-pass

In 9 of the 45 cells, a band-pass response was observed. These cells preferentially responded to tones of certain durations and were less responsive to tones that were either briefer or longer in duration. As with the short-pass response, in all cases the responses were onset-type. In 7 of the 9 cells spikes were evoked, in the other two the responses were subthreshold. One of these two cells is illustrated in Fig. 4.5B. In this cell, 1 ms tones evoked an EPSP with an average size of only 1 mV, which increased to around 10 mV at a duration of 32 ms. At longer durations, the EPSPs decreased again to <5 mV. Although the response at the end of the long tones was small, there was no direct evidence for a contribution of inhibitory conductances. EPSPs with similar sizes as spontaneous EPSPs were still observed at the end of long tones (e.g. top trace response to 512 ms, Fig. 4.5B). The other cell with subthreshold responses showed a similar response. In the other 7 cells with a band-pass response, responses were suprathreshold. In two cells there was clear evidence for synaptic inhibition. In both cells a fast IPSP preceded the EPSP. This IPSP outlasted the EPSP in one of these cells and as a result, long tones resulted in a sustained hyperpolarization. In 3 of the 5 remaining band-pass cells, spikes were followed by an afterhyperpolarization. These cells all had evidence for the presence of I_h, since they showed a depolarizing sag during hyperpolarizing current injection. None of the band-pass neurons showed an off-EPSP. The responses to current injection did not elicit a common response pattern in the band-pass cells. One cell had a buildup response, two accelerating, three accommodating, two burst-sustained and one was sustained.

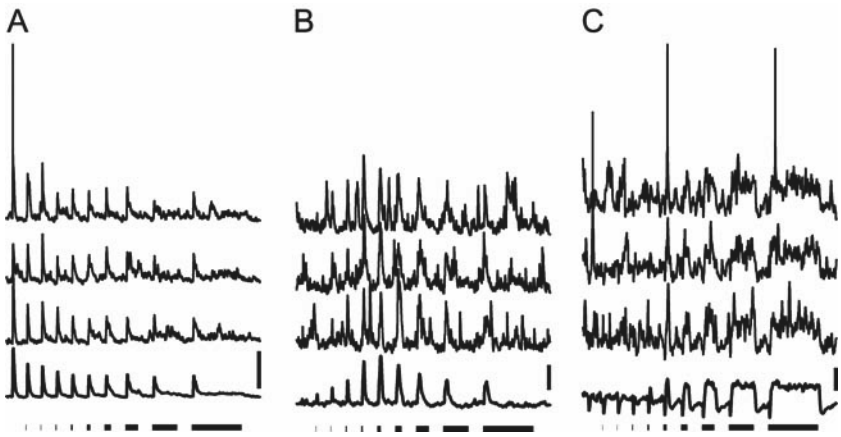

Figure 4.5 Duration tuning.
A-C *are the responses of three different cells to tones of increasing duration at the characteristic frequency (shown below traces). In each case the top three traces are consecutive responses and the bottom trace is the average of at least twenty stimuli. If action potentials were present, they were truncated before averaging. Traces have been vertically offset for display purposes. Vertical calibration bar is 5 mV.*
A*: Short-pass response: EPSPs of decreasing size in response to 32 kHz, 80 dB tones. Resting membrane potential was -56 mV.*
B*: Band-pass response: first an increase, followed by a decrease in the EPSP size in response to 8 kHz, 40 dB tones. Resting membrane potential was -63 mV.*
C*: Long-pass response. First only an IPSP, but at longer durations, an EPSP was observed, which occasionally triggered an action potential.* CF_{EPSP} *was 13.9 kHz, intensity 60 dB and resting membrane potential was -52 mV.*

Long-pass

In 7 of the 45 cells we observed a long-pass response. In these cells the response increased with increasing sound duration. In 6 of the 7 cells the EPSPs were sufficiently large to trigger spikes. Four of the long-pass cells had clear evidence for a fast IPSP, which was already observed at the shortest duration that was tested (1 ms). In three of these cells no EPSP could be observed for durations as long as 4-16 ms in the different experiments. In the fourth cell an EPSP preceded the IPSP already at short durations, and in addition an off-EPSP was observed at longer durations. In these four cells it seems likely that the IPSPs contributed to the long-pass behavior of the cell. In the other three cells there was no evidence for the presence of a short-latency IPSP. In these cells, increasing tones evoked EPSPs of increasing size (Fig. 4.5C). Only one of the long-pass neurons showed an off-EPSP.
Both the rise times and the delays of the excitatory response to the longest tone differed significantly between the groups (Table 4.2).

Properties of excitatory sound-evoked responses					
tuning type	**short-pass** (*n* = 3)	**band-pass** (*n* = 9)	**long-pass** (*n* = 7)	**untuned** (*n* = 26)	**Total** (*n* = 45)
rise time (ms)	3.2 ± 0.5	7.0 ± 1.5	21.7 ± 6.0	5.4 ± 1.3	8.3 ± 1.5
delay (ms)	10.2 ± 0.6	11.8 ± 2.6	14.2 ± 1.9	8.8 ± 0.3	10.3 ± 0.7

Table 4.2 Kinetics of sound-evoked EPSPs for neurons with different duration tuning.
Tones of 512 ms at CF_{EPSP} were given typically at 40 dB above threshold. Data are given as mean ± SE. Both rise time ($P < 0.001$; ANOVA) and delay ($P = 0.02$) differed significantly between the groups. The average rise time of the long-pass group differed significantly from each of the other groups ($P < 0.01$; Tukey's HSD). In addition, long-pass neurons had a significantly longer delay than untuned neurons ($P = 0.02$; Tukey's HSD).

The clearest difference was that the rise times of the long-pass neurons were longer than of the other neurons. This difference was mostly due to the cells with a fast IPSP, which had relatively large rise times (31.2 ± 7.1 ms, $n = 4$ vs. 9.0 ± 2.7 ms, $n = 3$).
Of the 7 long-pass cells, based on their responses to constant-current injection, two were classified as sustained, two as accommodating, two as buildup and one as burst-sustained.
Resting membrane potential, action potential threshold, input resistance, membrane time constant, presence of I_h and kinetics of I_h did not differ significantly between long-pass, short-pass, band-pass and untuned neurons.

Summary duration tuning

In summary, we observed four types of responses to tones of different durations, short-pass, band-pass, long-pass and untuned. All four classes contained various types of firing patterns in response to current injection. In some, but not all of the band-pass and the long-pass neurons, a contribution of a rapid-onset IPSP was apparent. The cells that showed a decrease in EPSP amplitude with the successive tones in the duration protocol in each case had an onset-type response, therefore preceding tones had to be responsible for this decrease. This means that for both the short-pass and the band-pass neurons synaptic adaptation played a crucial role.

Response to SAM tones

To further investigate the role of both membrane properties and short-term synaptic plasticity, we investigated the responses to sinusoidal amplitude-modulated (SAM) tones in a subset of 33 of the 45 cells. In these cells, 200 ms stimuli were given at the same carrier frequency as for the duration stimuli, which was the characteristic frequency (CF_{EPSP}). The amplitude of these tones was 70% modulated at frequencies ranging from 10-640 Hz (Fig. 4.6). In many respects the response to the different SAM tones was similar to the response to the long, non-modulated tones that were given in the duration protocol (Fig. 4.5). The large majority of cells responded with a short-latency EPSP, whose rise time and delay was generally independent of modulation frequency. The lack of a dependence of the initial EPSP of modulation frequency was due to the design of the tones, since the rise time of the SAM tones was always 2 ms, independent of modulation frequency. This onset-EPSP was followed by a plateau with average amplitude that generally matched the amplitude of the plateau reached at the end of the last tone in the duration protocol. In addition, in many cells the membrane potential varied at the same frequency as the modulation frequency (Fig. 4.6). This modulation was not due to cross talk with the stimulation since it was not in phase with the SAM tone. The modulation was especially apparent for the lower frequencies. In most cells the rise time of EPSPs evoked later during the tone became faster as the modulation frequency increased. As a result, the fit with a sine wave with the same period as the modulation sine wave was often quite reasonable (Figs. 4.6, E and F, 4.7A). On average the modulation amplitude decreased with increasing modulation frequency (Fig. 4.7B). None of the cells showed measurable modulation at a modulation frequency of 640 Hz.

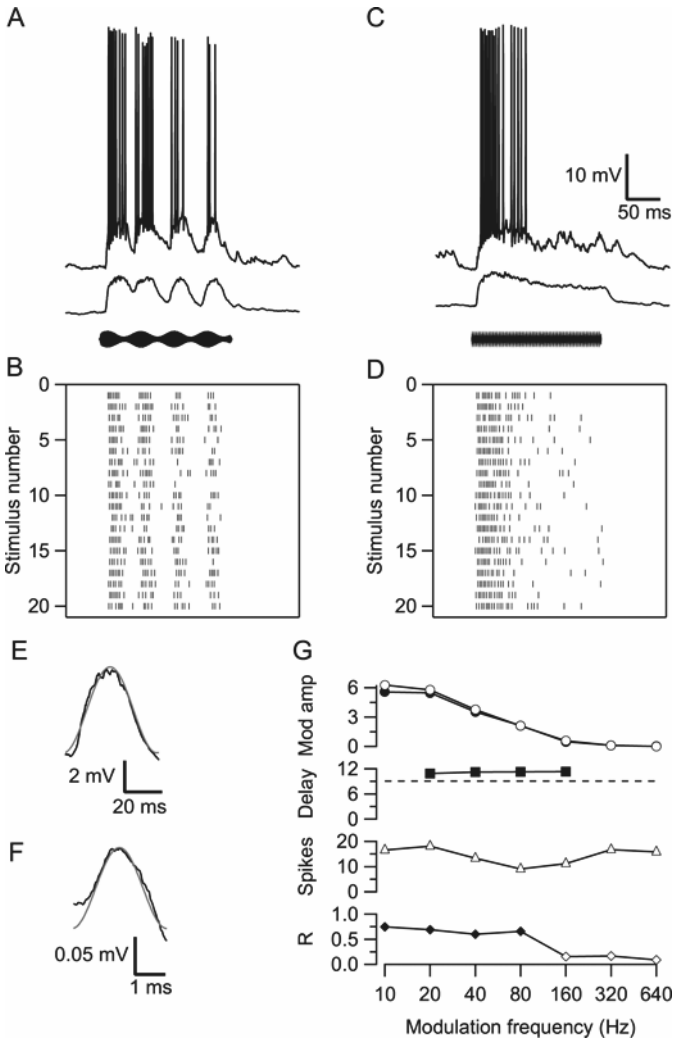

Figure 4.6 Response to SAM tones.

A*: From top to bottom, example trace of membrane potential, average response (after spike truncation) of 20 stimuli and SAM tone, which consisted of a 200 ms, 70 dB, 24.3 kHz tone that was 70% modulated at 20 Hz. Resting membrane potential was -67 mV. Same cell as displayed in Figure 4.1*A, B.

B*: raster plot of spikes triggered by the SAM tone at a modulation frequency of 20 Hz.*

C*: same as (*A*) except modulation frequency of SAM tone was 320 Hz. Calibration bars also apply to (*A*).*

D*: raster plot of spikes triggered by the 320 Hz SAM tone.*

E*: average of the response of the last two 20 Hz modulations after spike truncation. The fit with a 20 Hz sine wave is shown in gray.*

F*: Average response to last 125 ms of the 320 Hz tone, with the fit with a 320 Hz sine wave shown in gray. Note the difference in the scale with the traces in (*E*).*

G*: Top panel: open circles show peak-to-peak amplitude of the averaged membrane potential as a function of frequency, closed circles the amplitude of the sine wave fit to the averaged membrane potential. Membrane potential was averaged as described in (*E*) or (*F*). Second panel from above: time delay (in ms) between modulation of tone and of the fit with a sine wave of the same period to the data (filled squares). The broken line gives the average delay between tone onset and the start of the EPSP. Second panel from below: number of evoked spikes per sweep vs. modulation frequency (open triangles). Bottom panel: vector strength R vs. modulation frequency (diamonds). Filled diamonds indicate significant vector strength (Rayleigh test; P < 0.001).*

The EPSPs that were evoked by the sound modulation were sufficiently large to trigger spikes in some cells. As a result, the response of these cells was phase-locked to the stimulus. To test the importance of this modulation for the phase locking as measured during extracellular recordings, we plotted the relation between the average of the vector strengths at modulation frequencies between 20-80 Hz and the average of the EPSP modulation amplitudes at the same frequencies. Figure 4.7C shows that when the EPSP modulation amplitude is high, the cells are more likely to phase-lock their spikes to the SAM. However, the number of cells that showed robust spiking at all frequencies and the number of repetitions were too low to assess the best-modulation frequency with respect to synchronicity reliably.

In the 6 cells with the largest modulation amplitude we looked at the delay between stimulus and response. At 10 Hz, this delay was generally not very meaningful, since the sine fit was often not good. Between 20-160 Hz the time delay between the SAM tone and the membrane potential fluctuations changed little (Fig. 4.6G). In 4 of 6 cells it was a few ms larger than the minimal delay, the delay between tone onset and the start of the EPSP. In the other two cells, the sine wave fits to the membrane potential fluctuations were not very good and the delays were less meaningful, although again there were no obvious changes in the delay between 20 and 160 Hz. For a modulation frequency of 160 Hz the delay was in each case already more than one sine wave period.

Relation with responses during duration protocol

We also investigated to what extent the responses during the duration could predict the responses during the AM protocol. As a general measure for the ability of the cell to respond to SAM tones we used the average modulation amplitude in the range 20-80 Hz. The peak amplitudes of the response to the first tone (1 ms duration) of the duration protocol did not correlate with the SAM tone response (r = 0.01). As shown in Figure 4.8A, cells that were classified as short-pass in the duration protocol had a relatively small SAM response, whereas cells that were classified as band-pass or long-pass in the duration protocol had a relatively large response to the SAM tones, compared to the response to a 1 ms tone. The poor response of the short-pass response to SAM tone could be due to adaptation during the SAM tone, since the short-pass cells all showed clear adaptation in the duration protocol. In contrast, the 1 ms tone is apparently a much less effective stimulus for the cells with a band-pass or a long-pass response in the duration protocol, which responded more effectively to longer tones. The correlation between the response to SAM tones and to the duration protocol became better for increasing tone duration. For the 16 ms tone duration, the linear correlation coefficient r was 0.57. From Figure 4.8B it is clear that the band-pass cells show a relatively poor response to the SAM tone response compared to the response to a 16 ms tone, whereas some of the long-pass cells responded more effectively to the SAM tones than to the 16 ms tone. The correlation coefficient still increased slightly for longer durations. The relation between the peak amplitudes of the response to the longest tone (512 ms) in the duration protocol and the SAM tone amplitudes is shown in Figure 4.8C. At this point r = 0.64. It is again informative to look at the outliers. A band-pass cell responded better to the SAM tones than to the 512 ms tone, presumably because of the effects of adaptation during the duration protocol. The cells that responded relatively poorly to the SAM tone protocol compared to the response to the 512 ms tone included a long-pass cell that responded very slowly with minimal spike delays >30 ms. Another group of cells that responded relatively poorly to the SAM tones (modulation amplitudes < 1 mV) were characterized by low plateau amplitudes (Fig. 4.8D). Several of these cells had off-responses, suggesting that the cells with off-responses were more specialized in detecting brief changes in sound intensity, rather than the more continuous waxing and waning on top of a steady tone that characterized the SAM tone.

Some cells were able to respond to high modulation frequencies much better than others. This could be due to postsynaptic factors such as the relative ability of the cells to follow rapid changes in conductance or due to presynaptic factors, such as the presence of an input that is resistant to fatigue. To illustrate this ability to follow slow and rapid changes in membrane potential we compared the ratio of the modulation amplitude at 160 Hz and at 20 Hz with the persistency of the response to the last tone of the duration protocol, for which the steady-peak EPSP ratio, the ratio between the amplitude at the end of the tone and the peak amplitude, was taken. Figure 4.8E shows that the two are clearly related (r = 0.61). In contrast, the correlation between this modulation ratio and the time constant was much less obvious (r = -0.37; not shown).

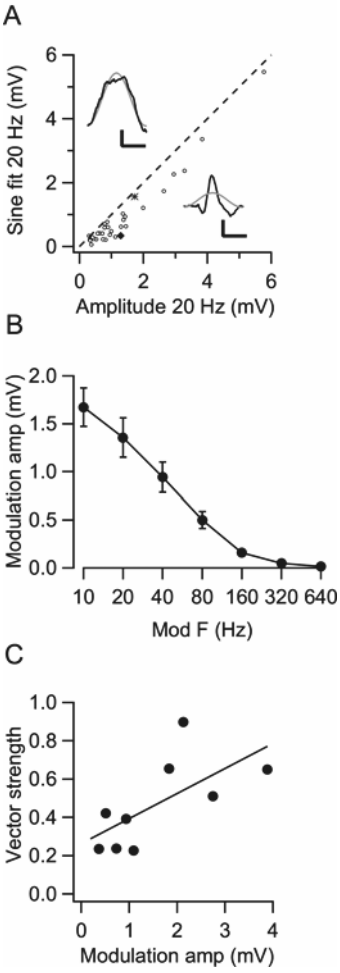

Figure 4.7 Quantification of the response to SAM tones.

A*: Relation between two methods to assess the amount of modulation for a modulation frequency of 20 Hz. The vertical axis gives the amplitude of the sine fit, the horizontal axis the peak-to-peak amplitude of the membrane potential, which had been averaged modulo the SAM tone period. Broken line indicates the identity relation. The insets show two examples. In the top left, the sine wave fit, shown in gray, is very good. This example corresponds to the data point indicated as an asterisk. In the other one, shown in the lower right corner, the fit is poor, due to the presence of an IPSP. This point corresponds to the filled diamond. Vertical calibration bars 0.5 mV, horizontal 20 ms.*

B*: Relation between amplitude of the modulation and the modulation frequency. The amplitude of the modulation was the peak-to-peak amplitude of the averaged response to the SAM tone. For each modulation frequency, responses were averaged both across the traces and across the individual cycles of the last 100 ms of each trace.*

C*: Relation between vector strength and the average amplitude of the AM modulation at frequencies between 20-80 Hz. Vector strength was calculated as detailed in the Methods. Only cells that responded with one or more spikes during the last 150 ms of at least 2 of the 20 SAM tones of 20, 40 and 80 Hz were used. Solid line is the line fit (r = 0.66).*

There was also no obvious correlation of the SAM tone response with age of the animal, its weight, recording depth, membrane resistance, membrane time constant, action potential threshold, characteristic frequency, sound level at threshold, the presence of spikelets, the presence of a fast IPSP or the membrane potential.

Relation between firing pattern and the response to AM modulation

All 4 burst-sustained cells had average modulation amplitudes >1.5 mV (Fig. 4.8F). These 4 cells all showed clear burst firing during current injection, they all had I_h with a prominent rapid component, they all showed a chopper-like response during tones and they all showed a vector strength of at least 0.5. The responses to unmodulated tones or to constant-current injection of one of these cells have been shown in Figure 4.3. Both during current injection and during tones, these cells showed burst firing on top of depolarization typically lasting on average between 30-110 ms in the different cells. These bursts were generally followed by a small afterhyperpolarization, which could be related to changes in the availability of I_h. Apart from the four burst-sustained cells described above, there were also many cells with evidence for the presence of I_h that did not respond well to SAM tones. Of the other two cells with modulation amplitudes >1.5 mV, one was a buildup cell and the other one an accelerating cell, both with no evidence for I_h. These results indicate that the presence of I_h is both not a necessary and not a sufficient condition for a good phase-locking response.

Summary AM tuning

Cells with band-pass or long-pass duration tuning had a relatively large response to SAM tones, whereas short-pass cells did relatively poorly. Burst-sustained cells showed a relatively large response to SAM tones.

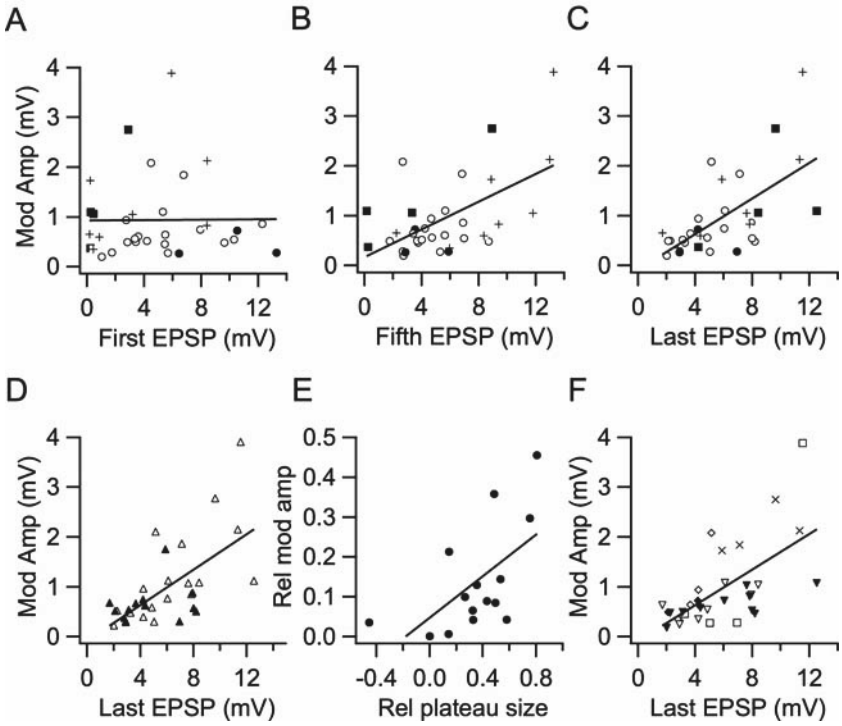

Figure 4.8 Relation between EPSPs evoked by SAM tones and by tones of different durations.

*The symbols in (*A*)-(*C*) indicate the type of tuning. Open circles are untuned neurons, filled circles short pass, crosses band-pass and filled squares long-pass neurons.*

A*: Relation between the average modulation amplitude in the range 20-80 Hz ('Mod Amp') and the amplitude of the response to a 1 ms tone, which was the first EPSP in the duration protocol. Solid line is the regression line (r = 0.01).*

B*: As (*A*), except horizontal axis show the amplitude of the response to a 16 ms tone, the fifth tone in the duration protocol. Solid line is again the line fit (r = 0.57).*

C*: As (*A*) and (*B*), except horizontal axis shows response to 512 ms tone, the last tone in the duration protocol. Solid line is the line fit (r = 0.64).*

D*: As (*C*), except closed triangles show cells with a relative plateau size at the end of the 512 ms tone that was <0.2 of the peak amplitude and open triangles show the other cells in the duration protocol.*

E*: Scatter plot of the ratio between the modulation amplitude at 160 Hz and the modulation amplitude at 20 Hz ('Rel mod amp') against the ratio between the amplitude of the plateau membrane potential and the peak amplitude ('Rel plateau size'). Negative values indicate a hyperpolarization. Only cells with modulation amplitude at 20 Hz of at least 1 mV were taken into account. Solid line is the regression line (r = 0.60).*

F*: As (*C*)-(*D*), but symbols indicate firing type, where open inverted triangles indicate sustained, closed inverted triangles indicate accommodating, open diamonds indicate buildup-pauser, closed diamonds burst-onset, open squares indicate accelerating, and crosses indicate burst-sustained.*

DISCUSSION

Although the response of IC neurons to current injections has been extensively characterized in slice recordings (Bal et al. 2002; Koch and Grothe 2003; Peruzzi et al. 2000; Sivaramakrishnan and Oliver 2001), the significance of the different firing patterns for auditory transduction had not yet been studied. In this paper we therefore compared the changes in the membrane potential of neurons in the mouse IC during constant-current injections with the responses to tones of different durations and to tones whose amplitudes were sinusoidally modulated. We observed that voltage-dependent ion channels contributed in several ways to the response to tones. For example, a sustained response to long tones was only observed in non-accommodating cells. Moreover, the hyperpolarization-activated non-selective cation channel I_h had a special role in shaping the responses: I_h was associated with an increased excitability, with chopper and pauser responses, with an afterhyperpolarization following tones and with a large response to SAM tones. Synaptic properties were more important in determining the responses to tones of different durations. A short-latency inhibitory response appeared to contribute to the long-pass response in some cells and short-pass and band-pass neurons were characterized by their slow recovery from synaptic adaptation. Cells that recovered slowly from synaptic adaptation showed a relatively small response to SAM tones.

Synaptic mechanisms in the response to SAM tones or tones of different duration

Our experiments provide the first characterization of the intracellular response of mouse IC neurons to tones of different duration and of SAM tones. Based on their response to tones of different duration, we classified the cells as short-pass, band-pass, long-pass or untuned. Although the relative frequency of these four groups was similar to results obtained in extracellular recordings in mice and rats (Brand et al. 2000; Pérez-González et al. 2006; Xia et al. 2000), in our experiments both short-pass and band-pass experiments showed onset responses. It therefore seems inevitable that these cells would have been classified differently if we had used a long interval between tones. The cells we tentatively classified as short-pass most likely were cells with an onset response that recovered from synaptic adaptation more slowly than untuned cells with an onset response, rather than cells that were preferentially activated by brief tones. Similarly, the band-pass neurons most likely should be viewed as long-pass neurons that were more sensitive to the effects of adaptation. A special role for inhibition was not apparent in most band-pass neurons; the afterhyperpolarization that was observed in some of the cells appeared to be due to the effects of the deactivation of I_h, as discussed below. For the long-pass category, 4 of 7 cells had a fast IPSP and these cells were characterized by an EPSP with a slow rise time. In these cells, inhibition therefore appears to be important in shaping the long-pass response (Klug et al. 2000; Pérez-González et al. 2006). In the other three cells, a role of inhibition was not apparent. We also did not observe evidence for a special role of inhibition in AM processing (Sinex et al. 2005; Walton et al. 2002), in agreement with the lack of effect of a pharmacological block of

inhibition on phase locking (Burger and Pollak 1998; Caspary et al. 2002; Zhang and Kelly 2001).
The whole-cell recordings allowed us to monitor the underlying membrane fluctuations that determine the firing responses to SAM tones of neurons in the IC. Our data are in agreement with the results of the two cells for which the responses to SAM tones were reported in (Casseday and Covey 1992), who observed a cyclical input pattern, phase-locked to the envelope of the stimulus. Most cells showed a gradual decrease in the size of the evoked responses with increasing modulation frequency, which is in agreement with the observation that the temporal modulation transfer function is already low-pass at the level of the auditory nerve (reviewed by Joris et al. 2004). The observed cut-off frequencies were similar to phase-locked responses in extracellular recordings (e.g., (Burger and Pollak 1998; Gooler and Feng 1992; Langner and Schreiner 1988; Rees and Møller 1983).
We compared the responses to tones of different duration and to SAM tones and found that the responses during the duration protocol, especially the persistency of the response to the last tone, were a good predictor for the size of the phase-locked response in the AM protocol. Cells that showed a relatively large, long-lasting response to the last tone in the duration protocol showed a relatively large response to the SAM tones as well. Therefore, long-pass or band-pass cells did relatively well. In contrast, we observed that neurons that were classified as short-pass, i.e. cells with an onset response showing clear adaptation in the duration protocol, had a small phase-locked response to SAM tones. Cells with low plateau amplitude also responded poorly. We conclude that the ability to have a sustained response to tones is a key factor in determining the ability to respond to SAM tones with a phase-locked response. Our findings agree well with earlier studies, where it was also observed that onset neurons respond poorly to tones with relatively slow rise times, such as SAM tones (Condon et al. 1996; Gooler and Feng 1992; Sinex et al. 2002; Sinex et al. 2005). Onset neurons will be excited more effectively by more rapidly changing tones, such as trains of brief tone bursts (Gooler and Feng 1992; Sinex et al. 2002).

Accommodation and response to tones

The relation between firing patterns during constant-current injection and the response to tones was less clear-cut than in the cochlear nucleus (Feng et al. 1994). We did find, however, that some general membrane properties of the cells, most notably the extent of accommodation during current injection, the presence or absence of bursts and the presence or absence of I_h were important in predicting the responses to tones. The major discrepancy between tone and current-injection responses was that about two thirds of IC neurons showed a sustained response to current injection, but only about one third responded in a sustained manner to tones, which is similar to what has been observed during extracellular recordings (Brand et al. 2000; Walton et al. 2002; Xia et al. 2000). Since the cells of the IC are at least one synapse further downstream, the input to the cells in the IC is subject to additional transformations in between the auditory nerve fibers and the IC, which are presumably responsible for the transient nature of the inputs. Nevertheless, we did observe that cells that fired in a sustained manner during tones, or whose EPSPs decreased only little during long tones, invariably showed little

accommodation during current injection, indicating that little accommodation is a necessary, but not a sufficient condition for a sustained response to long tones. Interestingly, none of the sustained or accommodating cells showed a good response to SAM tones. Although the sample was limited, we did observe that burst-sustained cells showed a good response to SAM tones, similar to stellate cells in the ventral cochlear nucleus, which also have an onset-chopper response to tones and a good phase-locked response to SAM tones (Frisina et al. 1990; Rhode and Greenberg 1994), whereas burst-onset cells did not show a good phase-locked response to SAM tones, suggesting that little accommodation is a necessary, but not a sufficient condition for a good response to SAM tones.
We observed several other examples for a correlation between specific membrane properties and a role in sound transduction in the IC, foremost the presence or absence of I_h.

Cells with I_h were more excitable

About half of the cells in the IC showed evidence for the presence of I_h. These cells showed a depolarizing sag in response to hyperpolarizing current injection and a hyperpolarizing sag during depolarizing current injection. We did not pharmacologically confirm that the sag was due to I_h, but this seems quite likely, since frequency of occurrence and time course matched results in earlier slice studies in the rat, where pharmacology was more easily performed (Koch and Grothe 2003). Nevertheless, we cannot exclude a contribution of additional channels to the observed sag. I_h appeared to play an important role in setting the excitability, since cells with I_h were more likely to respond with spikes to the tones. These cells had a more positive membrane potential and a somewhat lower action potential threshold than cells without I_h, whereas their EPSP sizes did not differ significantly, suggesting that the effect of I_h on excitability was mostly via its effect on the membrane potential. Modulation of I_h is therefore expected to have profound effects on sound transduction in the IC. At the superior olivary complex, in vivo injection of an antagonist to I_h markedly reduces excitability of neurons in the superior olivary complex (Shaikh and Finlayson 2003), suggesting a similar role for I_h at earlier stages of auditory processing.

Cells with I_h were associated with pauser and chopper responses

Both chopper (Brand et al. 2000; Willott and Urban 1978; Xia et al. 2000) and pauser (Kuwada et al. 1997; Rees et al. 1997; Semple and Aitkin 1980) responses to tones were associated with the presence of I_h. These responses were characterized by an onset burst of activity in response to tones. The deactivation of I_h seemed to be responsible for the cessation of activity following the onset response, since a similar pattern was also observed during current injection, when synaptic inhibition does not need to be considered. The deactivation of I_h may play a role as long as the spike thresholds are below the reversal potential for I_h, which has been reported to be between -29 and -40 mV in auditory neurons (Bal and Oertel 2000; Banks et al. 1993; Cuttle et al. 2001; Rodrigues and Oertel 2006), and as long as the resting membrane potential is sufficiently negative to allow activation of I_h. Based on the time course of the observed depolarizing or hyperpolarizing sag during

current injection, these cells belong to the subset of IC neurons that show fast gating of I_h (Koch and Grothe 2003). Intracellular recordings from onset-chopper D-stellate cells in the cochlear nucleus also show a clear hyperpolarizing sag during tones (e.g. (Needham and Paolini 2006). Since these cells also have I_h (Fujino and Oertel 2001; Rodrigues and Oertel 2006), a contribution of deactivation of I_h may contribute to the onset-chopper response in these cells as well.
Because of the similarity of the time course of the hyperpolarizing sag during depolarizing current injection with the time course of the membrane potential in response to tones, we consider the deactivation of I_h a more likely cause for the cessation of firing in pauser responses than synaptic inhibition (Banks and Sachs 1991; Needham and Paolini 2006; Rose et al. 1963). The pauser cells may differ from the other chopper cells by having a delayed excitatory input, as was observed in isolation in several long-pass neurons.

Cells with I_h showed an afterhyperpolarization following long tones

In all cells with I_h that showed a significant plateau depolarization during long tones, an afterhyperpolarization was observed. Since the kinetics matched the afterhyperpolarization observed in the same cells following depolarizing constant-current injection (Koch and Grothe 2003) we conclude that the re-activation of I_h must have contributed to the afterhyperpolarization following long tones. Voltage clamp experiments would be needed to assess a possible additional role of synaptic inhibition. We speculate that this afterhyperpolarization may contribute to off-suppression of spontaneous activity (Willott and Urban 1978), or, more generally, to forward masking. The responses in T-stellate cells of the cochlear nucleus, especially the C_{T2}-subtype (Paolini et al. 2005), show an adapting depolarization followed by an afterhyperpolarization after the end of a tone that was very similar to sustained responses in IC cells containing I_h suggesting a similar function for I_h in these cells.

CONCLUSION

Despite the large variability in the responses to both tones and current injections between IC neurons, some clear patterns emerged. By defining a contribution of accommodation, burst firing or the presence of a sag during constant-current injections to the response to tones, our data show for the first time how the different intrinsic firing patterns of IC neurons contribute to auditory processing. The wide availability of genetically modified mice may help to further dissect the relative contribution of membrane and synaptic properties in auditory transduction in the IC.

Chapter 5

Cellular mechanisms of direction-selective FM tuning in the mouse inferior colliculus

M.L. Tan, J.G.G. Borst

To be submitted

ABSTRACT

Some inferior colliculus (IC) neurons respond selectively either to upward or downward frequency modulated (FM) sweeps. Based on extracellular recordings, several mechanisms have been proposed to account for direction selectivity in FM tuning. To explore the contribution of these mechanisms, we made in vivo whole-cell patch-clamp recordings from the IC of anaesthetized C57/Bl6 mice and compared the responses to pure tone stimulation with the responses to up- and downward FM sweeps. Direction-selectivity was seen in 31% of IC neurons. Upward selective cells had a lower best frequency (BF) than downward cells (7 ± 1 kHz, n = 4, vs. 18 ± 4 kHz, n = 7). The mechanisms that were responsible for direction-selectivity were heterogeneous. In some cells direction-selectivity was already present in the inputs. In other cells, differential temporal summation of EPSPs for both sweep directions was important for direction-selectivity. Synaptic inhibition played an important role in shaping direction-selectivity. It was observed more often in direction-selective (10 of 11) than in non-selective cells (9 of 25). In some direction-selective cells, IPSPs were only present at frequencies either above or below BF, whereas in others a difference in time course of IPSPs at different frequencies appeared to contribute to the direction-selectivity. Our results therefore suggest that spectrotemporal integration of synaptic responses largely shapes FM selectivity at the midbrain level, with an important role for inhibitory inputs.

INTRODUCTION

Biologically relevant sounds generally contain prominent frequency modulations (FM). Vocalizations are a good example, and the vocalizations of mice are not an exception, since they contain brief sweeps, both in up- and in downward direction (reviewed in Nyby 2001). At the level of the cochlear nucleus or higher, cells may preferentially respond to the direction or the rate of the FM (reviewed in Eggermont 2001). Especially in the case of bats, whose calls contain frequency sweeps, at the level of the inferior colliculus (IC) cells may be selective for FM, with durations and rate preferences matching the emitted biosonar calls (Suga 1965, 1969). FM selectivity may be different within the different nuclei of the IC. A preference for upward over downward sweeps was observed more often in the external nucleus compared with the central nucleus in bats (Gordon & O'Neill, 2000). Within frequency band laminae of the mouse central nucleus, the map of sweep speed is concentrically arranged with the representation of downward and of slow speeds mainly in the centre of a lamina (Hage and Ehret 2003). In the rat auditory cortex, patch-clamp recordings showed that much of the selectivity for the FM sweeps was already present in the inputs, suggesting that subcortical auditory structures play an essential role in FM tuning (Zhang et al. 2003). In general, selectivity to the rate or direction of FM has been suggested to be a consequence of the relative timing of EPSPs and IPSPs, with a prominent role in bats for asymmetric sideband inhibition in direction selectivity (Rees and Langner 2005; Voytenko and Galazyuk 2007). Since these mechanisms can be studied only indirectly when using extracellular recordings, we studied the cellular mechanisms of FM tuning by making whole-cell recordings of neurons from the mouse inferior colliculus. We explored to what extent membrane characteristics and synaptic integration of inhibition and excitation contribute to FM tuning.

MATERIALS AND METHODS

In vivo patch-clamp recordings from the IC of young-adult, anesthetized C57/Bl6 mice were made as described previously (Tan et al. 2007).

Surgery

Animal procedures were in accordance with guidelines provided by the animal committee of the Erasmus MC. Twenty-eight C57/Bl6 mice (postnatal day 21 – 37) were anesthetized with ketamine/xylazine (65/10 mg/kg) i.p. or ketamine (60 mg/kg i.p.) plus medetomidine (0.25 mg/kg s.c.). Additional anesthesia was given when pinching the toes resulted in a withdrawal-reflex. The dorsal skin of the skull was shaved; eyelids were closed with superglue and tape to prevent dehydration of the eyes and visual input. A median incision of the dorsal skin of the skull was made. The surface of the skull was scraped clean of tissue then swabbed with 100% ethanol. At bregma, a metal pedestal was applied to the skull with superglue and dental acrylic. To immobilize the head, the animal was placed in a stereotactic frame that was mounted on a floating vibration table (Newport). A speaker probe was inserted into both ear canals surrounded with silicone elastomere (WPI). After cleavage of the dorsal neck muscles, a relatively large (5x5mm) craniotomy of the occipital bone was performed with a dental drill, just caudally from the transverse sinus. Any bleeding of the skull was stopped with application of bone wax. After opening the dura, little cerebellar tissue was removed with a vacuum aspiration system including a Pasteur capillary pipette to achieve ample dorso-caudal exposure of both colliculi. Any bleeding of brain tissue was stopped with cotton balls or gel foam (Surgicel®). Overlying pia mater was carefully removed with the tip of a 0.3 x13 Microlance needle. Peroperatively, a few drops of Ringer solution (NaCl 125, KCl 2.5, NaH2PO4 1.25, MgCl2 1, CaCl2.4H2O 2, D-glucose 25, NaHCO3 25, osmolarity $\approx$ 320 mosmol) were applied to the brain to prevent dehydration. A chlorided silver wire was inserted into residual cerebellar tissue as a reference electrode. Finally, warm agar (agarose 2% in 0.1 M phosphate buffer) was applied into the craniotomy that significantly decreased visible brain pulsations and increased both success rate of gigaseal formation and recording time. One must take into account that with this procedure, ventrolaterally localized neurons are more difficult accessible. Constant rectal temperature (36.5 – 37.5ºC) was achieved with a homeothermic blanket system (Stoelting).

Patch-clamp recordings

Thick-walled borosilicate glass micropipettes with filament (1.5 mm outer diameter, 75 mm length, Hilgenberg GmbH) were cleaned with 100% pure ethanol. Endings were held in a flame to smoothen the sharp edges and to burn the remaining ethanol. Electrodes were pulled with a trough filament (FT330B) in a Flaming / Brown micropipette horizontal puller (P-97, Sutter Instrument company) to shape a relatively slim taper and blunt tip (diameter of approximately 2μm), with a final resistance of $\pm$ 4 – 6 MΩ measured in saline. All electrodes were pulled just prior to the experiment to avoid pollution. Electrode holders were conically drilled inside for extra support and

were cleaned every 4-6 months in a sonificator with distilled water to prevent small glass residues from polluting the electrodes.
Internal solution for patch-clamp recordings contained (in mM) Kgluconate 125, KCl 20, Na_2phosphokreatinase 10, Na2GTP 0.3, MgATP 4, EGTA 0.5, Hepes 10, adjusted with KOH to pH7.2, filtered and stored at -20°. On the day of the experiment 0.5% biocytin was added to a similar solution with a lower concentration of K-gluconate 115 mM, resulting in a total osmolarity of approximately 285 –305 mosmol.
The IC was approached dorso-caudally at a 30 - 60° angle with the horizontal under high positive pressure (> 300mbar), which was lowered to ~30 mbar at ~500 µm below surface in rats and ~200 µm in mice. When electrode resistance increased more than 10% of the initial value positive pressure was increased to 300mbar and an additional lowering of 50µm. When resistance persisted too high (>10% from initial resistance), the electrode would be discarded. If not, steps of 2µm were made at 30mbar positive pressure, using a 10 mV - 10 ms test pulse to observe current changes. One more step after a decrease in current more than 20% was followed by release of positive pressure with or without gentle suction to cell-attached mode (Gigaseal formation). Giga-ohm seals and whole cell recordings were established using standard techniques with mall pulses of suction. Margrie and Brecht reported a success rate of 20 – 50% for in vivo patch clamping (Margrie et al. 2002). With a rather exponential learning curve we were able to record from 1 to eventually 4 cells per animal, with an estimated average survival of 2 to 4 hours per animal.
Data were acquired with a MultiClamp 700A patch-clamp amplifier and pCLAMP 9.2 software (Axon Instruments). Potentials were low-pass filtered at 10 kHz (8-pole Bessel filter) and sampled at an interval of 50 µs with a 16-bit A/D converter (Digidata 1322A). A subset of cells was filled with biocytin. These cells were identified as described in (Tan et al. 2007). Six cells were retrieved, of which three cells were localized in the external and three in the central nucleus.

Stimulation protocols

All experiments were performed in a single-walled sound-attenuated chamber (Gretch-Ken Industries, attenuation at least 40 dB at 4 – 32 kHz).
Membrane properties and firing patterns of these cells were obtained from constant-current injections and have been previously published (Tan et al. 2007).
To find the best frequency (BF), seven octaves of pure tones (1 – 64 kHz) were presented in closed field at the contralateral ear at 80 dB sound pressure level (SPL). Tones had durations of 50 ms and a 2 ms rise/fall time. They were repeated 20 times at an interval of 150 ms. Auditory stimuli were generated with Tucker Davis Technologies hardware (TDT, System 3, RP2.1 processor, PA5.1 attenuator, ED 1 electrostatic driver, EC1 electrostatic speaker). Calibration took place as described previously (Tan and Borst 2007). The closed speaker system was flat to within ± 3 dB between 1 and 64 kHz.
Twenty repetitions of upward and downward linear FM sweeps were presented in closed field at the contralateral ear at a fixed intensity of 80 dB. The sweeps ranged from 1-73 kHz (sweep speed 600 kHz/s, duration 120 ms)

with 5 ms rise/fall time and 180 ms inter-stimulus interval. Additionally, all cells were subjected to sweep speeds of 100 and 300 kHz/s (duration 120 ms, range 1-13 and 1-37 kHz, respectively).
Only cells with stable resting membrane potentials (drift < 5 mV) were included in this study. All measurements were done on the average of 20 repetitions. If spikes were present, they were truncated before averaging (Tan et al. 2007).

Analysis

Firing patterns, action potential threshold, membrane properties and presence of hyperpolarization-activated current (I_h) were calculated from depolarizing and hyperpolarizing current injections as described previously (Tan et al. 2007).
The BF was defined as the frequency at which the 50 ms, 80 dB tone elicited the largest number of action potentials or, in the absence of spikes, the largest excitatory postsynaptic potential (EPSP) amplitude. EPSP amplitudes were calculated as the difference between baseline and the local maximum of the averaged response (after spike truncation) minus one standard deviation of the baseline noise (Tan et al. 2007). To find the EPSP delay, two points during the rising phase of the EPSP were identified at which the amplitudes were 20% and 40% of the maximum amplitude. The EPSP onset was defined as the interception point between a line through these two points and the baseline. The EPSP delay was the delay between sound onset and EPSP onset. Additionally the midpoint delay was calculated, which was the delay between sound onset and the time point in the EPSP rise time at which the amplitude was half maximal. This delay is expected to be more relevant for predicting whether potentials will interact during frequency sweeps. The midpoint delay could be estimated more accurately than the point at which the EPSP was maximal, especially when spikes were present. Inhibitory postsynaptic potential (IPSP) amplitudes, 20-80% rise times and delays were calculated analogously. IPSPs were visually identified and had, on average, amplitudes of at least -0.5 mV.
After the best frequency was determined for each cell, the Directional Selectivity Index (DSI) was calculated for all three sweep speeds (100, 300 and 600 kHz/s) as described in (Britt and Starr 1976):
DSI = (U – D) / (U + D)
U represents the total number of spikes during upward sweeps, D during downward sweeps, except in cells that fired very few or no action potentials, for which we used the maximal EPSP amplitude of the averaged response triggered by the up- or downward sweep. Values of 0.33 – 1 indicated upward selectivity, whereas values between –1 and –0.33 indicated downward selectivity.
DSI values of all three sweep speeds were compared both for spikes as for EPSPs. The DSI value for the highest sweep speed was generally used for classification because it contains the largest frequency range. In two cells that marginally matched the criteria for downward selectivity and non-selectivity, the responses to the other sweep speeds indicated that a classification as, respectively, non-selective and downward selective was more appropriate.
To compare the similarity of the response to upward and downward sweeps, we used Pearson's correlation coefficient *r*, which was calculated in the range

between the start of the response and the end of the response. A value of 1 indicates that responses to up- and downward sweeps were identical. The end of the response was defined as the point at which the correlation function between the upward and the time-reversed downward sweep in the range between 0 and 50 ms after the FM sweep was maximal.
Time integrals of the response to the FM sweeps were calculated after subtracting the resting membrane potential. They were calculated over the same period as taken for the correlations.

Statistics

Data are presented as mean ± standard error. A difference in relative proportions was assessed using the (two-tailed) X^2 test. A difference in the mean of two groups was assessed by Student's *t*-test. Differences in the mean of more than two groups were assessed by ANOVA, followed by a Tukey's HSD test. Values of $P < 0.05$ were judged statistically significant.

RESULTS

Responses to tones

We tested the intracellular response to tones of different frequencies (1, 2, 4, 8, 16, 32 and 64 kHz) in a total of 36 neurons in the mouse inferior colliculus (IC) at an intensity of 80 dB SPL. In 17 of the cells (47%) only excitatory responses were observed at any of these frequencies or during the FM sweeps (Fig. 5.1). In one cell, which fired spontaneously, only sound-induced IPSPs were observed. In the remainder of cells (50%) there was evidence for both EPSPs and IPSPs. In 17 of the cells (47%), one or more of the tones triggered a spike. This means that in approximately half of the other cells only a subthreshold response was evoked. Figure 5.1 illustrates the responses of a neuron to pure tones. In general, EPSP responses were largest in amplitude in the 8 – 32 kHz range (not shown), which is the same range as the best frequency for sound-evoked action potentials (Willott et al. 1991). At the best frequency (BF) the average EPSP amplitude, measured after spike truncation, was 7.6 ± 0.7 mV (n = 35). The delays, rise times and midpoint delays of both EPSPs and IPSPs generally differed at different frequencies for most cells. Figure 5.2 illustrates that on average, EPSP onset delay or midpoint delay were shorter for higher frequencies, with less frequency dependence of EPSP rise time compared to the midpoint delay, suggesting that in general, delays to midpoint were longer for lower frequencies. However, within individual cells the results were not very clear and often the response to the BF had the shortest latency (results not shown).
In many cells the IPSPs were not present on both sides of BF, but asymmetrically distributed. In 5 cells they were only observed at BF and higher, in 4 cells only at BF and lower and in 3 cells they were observed both at lower and higher frequencies. One cell showed an IPSP only at BF, another one fired spontaneously and had sound induced IPSPs. The maximum IPSP amplitude observed in 14 cells was on average –2.8 ± 0.9 mV, with an average delay of 12.3 ± 1.6 ms (n = 12) and rise time of 3.9 ± 0.7 ms (n = 12).

Responses to FM sweeps

A possible consequence of both the frequency-dependence of the time course of the synaptic potentials and of the asymmetrical distribution of IPSPs is that the speed and direction of FM sweeps will result in differential summation of the synaptic potentials. To visualize the spectrotemporal interaction of the synaptic potentials, we compared the response to tones (Fig. 5.1A) with the response to FM sweeps at the same intensity level (Fig. 5.1B,C). As stated before, only about half of the cells showed sound evoked action potentials during pure tone stimulation at 80 dB SPL. The FM sweeps were therefore given at the same intensity level as the tones.

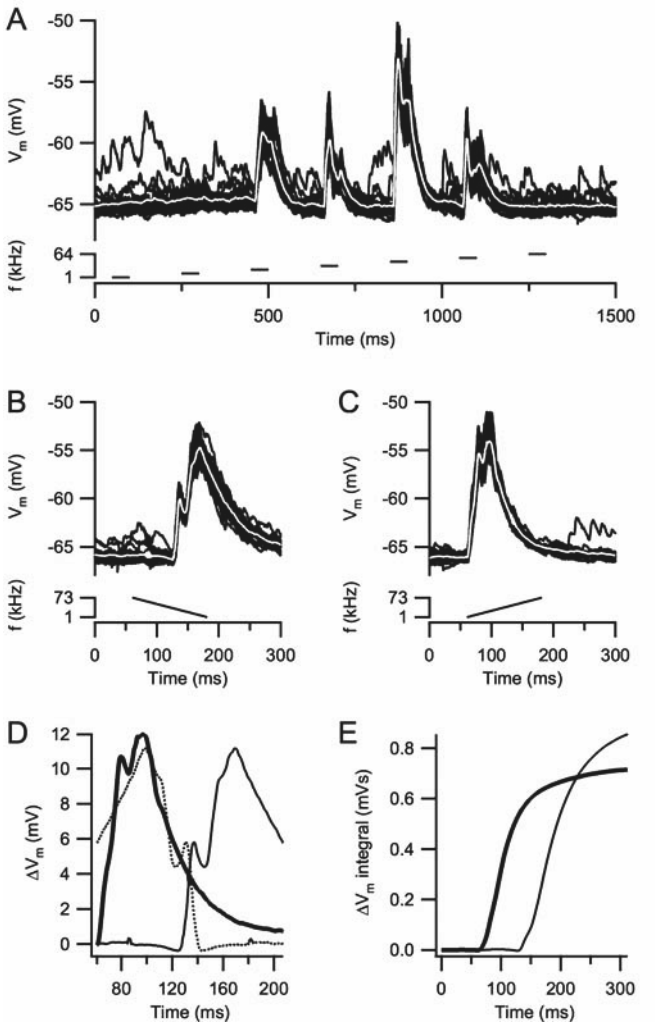

Figure 5.1 EPSP responses to pure tone and FM sweep stimulation in a non-selective cell.
A*: Pure tone stimulation at 4, 8, 16 and 32 kHz (lower panel, logarithmic scale) resulted in an EPSP (upper panel), whereas the cell did not respond to tones of 1, 2, or 64 kHz. Responses to twenty individual tone presentations are overlaid (black traces), the white trace shows the average response. EPSP delays were symmetrically distributed (11 – 12.5 ms), whereas EPSP rise times were larger at lower frequency stimuli (10.7 vs. 4.6 ms). Fluctuations in resting membrane potential are mainly due to spontaneous EPSPs. A very small onset IPSP may be present at 32 kHz and during the downward sweep.*
B*: Downward FM sweep stimulation at 600 kHz/s (lower panel, linear scale) results in EPSP responses (upper panel).*
C*, as in (*B*), except upward sweep direction. Average EPSP size was similar for upward and downward sweeps.*
D*: Response to downward (thick line) and upward sweep are shown together with the time reversed downward response (dashed line). Correlation between the up- and the downward response increased from r = –0.78 to r = 0.92 after time reversal.*
E*: Time integral of voltage responses to downward (thick line) or upward sweep.*

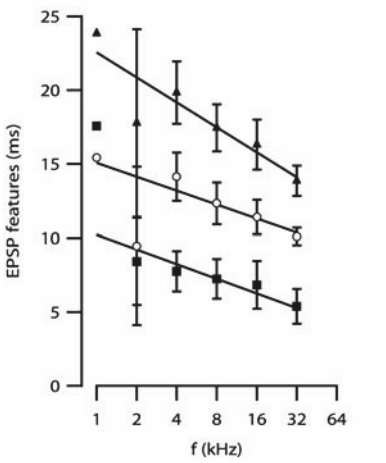

Figure 5.2 EPSP characteristics during pure tone stimulation.
Different properties of the EPSP evoked by pure tone stimulation. Filled triangles represent EPSP delay to midpoint (50% of maximum EPSP amplitude), filled squares EPSP 20-80% rise times and open circles EPSP delay (35 cells; mean ± standard error). Higher frequencies tended to result in shorter delays, rise times and midpoints compared with low frequencies. Solid lines are the regression lines through the data, with r=-0.17, r=-0.18 and r=-0.25 for the relation between rise time, delay and midpoint with frequency, respectively.

A comparison of the maximal amplitude of the response to tones and to FM sweeps showed that they were generally similar (r = 0.81). Although for some cells there were differences, it is likely that the low sampling density for the pure tone responses or the use of only a single FM sweep speed made a large contribution to these apparent differences. In eight cells the maximal EPSP amplitude during the up or down FM sweep was less than half the maximal amplitude evoked by the pure tones. In these cells, the main reason for the relatively small response appeared to be that the time spent in the frequency range eliciting excitatory responses was too brief during the FM sweeps. Most of these cells had a narrow response range (at 80 dB) and most cells responded only to relatively long tones. In most of these cells we could confirm that FM sweeps with lower speeds (100 or 300 kHz/s) elicited clearly larger responses (results not shown). Conversely, in the one cell in which the maximal EPSP amplitude evoked by pure tones was less than half of the amplitude during the FM sweep, we could confirm that this was due to the low sampling density of the pure tone stimuli.
A majority of the cells showed responses to FM sweeps in a more or less predictable way. They showed EPSPs and IPSPs at instantaneous frequencies matching responses observed during simple tone stimulation, after correcting for the appropriate response delays. As a result, typically, the response to the upward FM sweep was more or less the mirror image of the response to the downward FM sweep in these cells. To quantify this, we calculated the maximum of the correlation coefficient *r* between responses to the upward and to the downward sweeps. In most cells there was little or no correlation, or the responses were negatively correlated. On average *r* was –0.28 ± 0.06. However, the correlation of the upward sweep with the mirror image of the downward sweep increased by 1.1 ± 0.08 to a value of *r* = 0.73 ± 0.04 (n = 36; Fig. 5.1D), indicating that in many cells, the upward sweep resembled the mirror image of the downward sweep reasonably well. Another indication that the up and down responses often were mirror images was that the time integrals of the responses to the down and to the up FM sweep were generally similar (0.09 ± 0.045 vs. 0.10 ± 0.051 mVs; P = 0.63; paired t-test; Fig. 5.1E) and that the ratio between the two was not significantly different from 1 (average ratio 1.1 ± 0.14; P = 0.25; n = 35; one outlier not included).

Non-selective cells

In 25 of the 36 cells (69%) there was no obvious direction selectivity. An example is shown in Figure 5.1B,C. In these cells the number of evoked spikes, or in non-spiking cells the maximum amplitude of the responses to upward and downward sweeps, were similar. These cells had a mean BF of 16 ± 2 kHz (range 4 – 32 kHz).
Of the 25 non-selective cells, 14 cells showed clear EPSPs, comparable to the experiment shown in Figure 5.1. Some of them also showed IPSPs, both in response to the tones and the FM sweeps. The mean maximum EPSP amplitude in these cells was 8.8 ± 0.9 mV.
In 10 other cells that were classified as non-selective, the responses to the FM sweeps as well as to pure tones were quite small. On average, the maximum EPSP amplitude during FM stimulation was only 1.7 ± 0.3 mV in these cells, and we cannot exclude that direction selectivity was missed due to the small size of the responses. In one non-selective cell, only IPSPs were evoked both by the tones and by the FM sweeps. Including this cell, only 9 of the 25 non-selective cells had evidence of synaptic inhibition during pure-tone stimulation or the FM sweeps. In contrast, direction selective cells showed inhibition in 10 out of 11 cases. This difference was statistically significant (P = 0.002).

Mechanisms of downward selectivity

Seven of 36 cells (19%) responded better to downward than to upward sweeps. Their best frequencies at 80 dB were in the range of 8 – 32 kHz (mean 18 ± 4 kHz). Six of these cells showed inhibition. An example is shown in Figure 5.3. In this cell, inhibition was present only at low frequencies, which was also observed in 2 other cells.

Two cells showed IPSPs at both lower and higher frequencies, but the IPSPs at the high frequencies were brief, whereas at low frequency tones they were more sustained, suggesting that in these cells the difference in duration of IPSPs was important for direction selectivity (Fig. 5.4). The EPSP was immediately preceded by a clear IPSP in the case of the upward sweep (Fig. 5.4D), but not during the downward sweep (Fig. 5.4C). Another cell showed inhibition over a broad frequency range. In this cell the EPSPs appeared to sum more effectively in the downward direction, leading to a difference between the number of spikes in the upward and the downward direction.

In the last downward-selective cell, there was no sign of inhibition (Fig. 5.5). In this cell the timing of the EPSPs seemed to be responsible for the downward selectivity, with the EPSPs summating more effectively in the downward direction, without a large difference in the time integral in both directions.

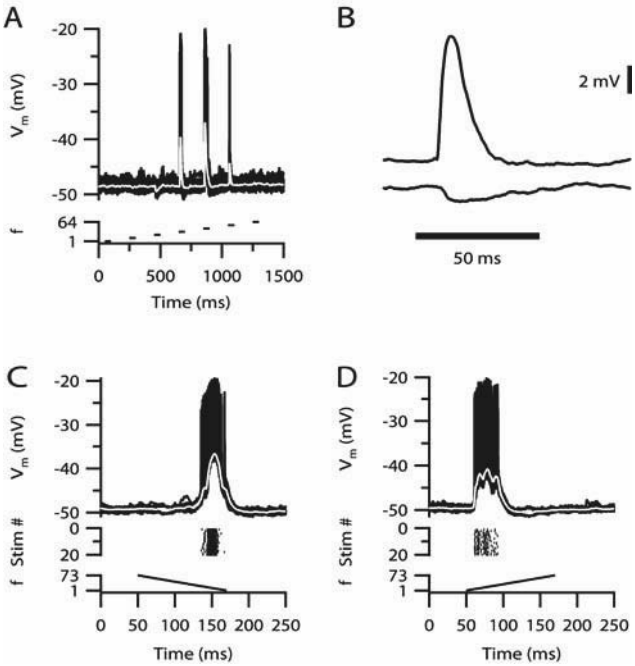

Figure 5.3 Downward selectivity in the presence of sideband inhibition.
A*: Tones of different frequencies (bottom panel) elicited either an IPSP (at 4 kHz, top panel) or an EPSP (at 8, 16, and 32 kHz).*
B*: At higher time resolution different delays are more apparent: EPSP (top trace) in response to 50-ms, 8-kHz tone had a delay of 7.2 ms, IPSP (middle trace) in response to 4 kHz tone had a delay of 10 ms. Traces have been vertically offset for display purposes. Bottom trace shows sound stimulus.*
C*: Top panel shows the response to the downward FM sweep. Middle panel is the raster plot of the evoked spikes during the stimulus presentations (Stim #). Bottom panel shows the FM sweep.*
D*: as (*C*), except sweep direction was upwards. In the upward direction the relatively slow IPSP at low frequencies may have coincided with the EPSP at higher frequencies, resulting in a reduction of its amplitude (9.5 vs. 22.4 mV) and fewer action potentials (135 vs. 207).*

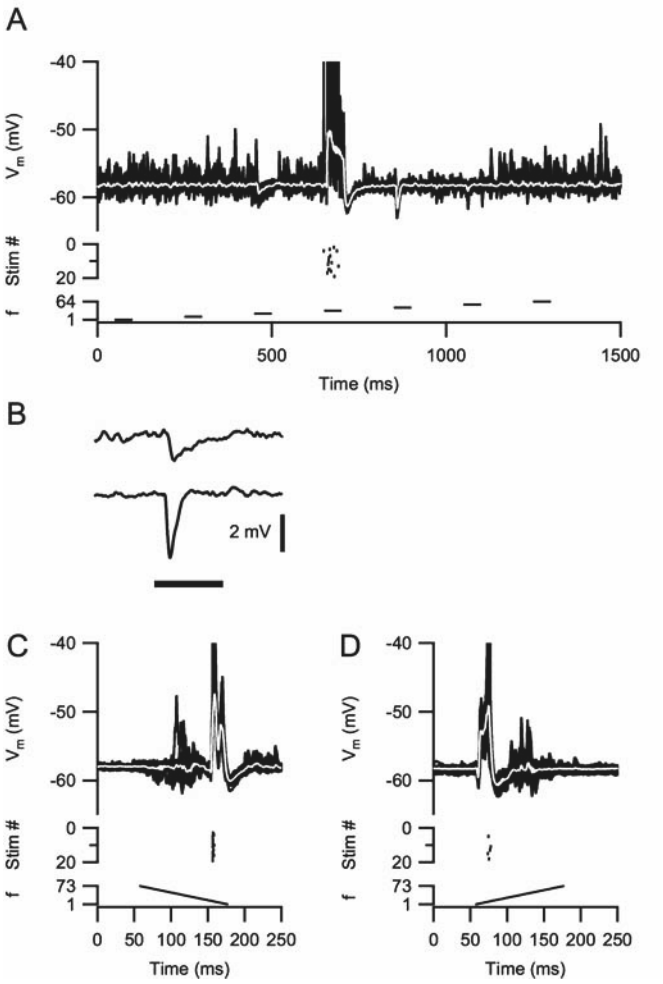

Figure 5.4 Downward selectivity in the presence of bilateral sideband inhibition.
A*: Tones of different frequencies (bottom panel) elicited action potentials (top-panel; spikes were cut-off for display purposes) at 8 kHz. IPSPs with different amplitudes were observed at 4, 16 and 32 kHz (top panel). Middle panel shows raster plot.*
B*: Comparison of time course of IPSPs at 4 (top) and 16 kHz (middle trace). Traces have been vertically offset for display purposes. Bottom trace shows sound stimulus. The IPSP at 4 kHz lasted throughout the tone, whereas the IPSP at 16 kHz was more transient.*
C*: Top panel shows the response to the downward FM sweep. Middle panel is the raster plot of the evoked spikes. Bottom panel shows the FM sweep.*
D*: as (*C*), except sweep direction was upwards. Response to sweeps of both directions contained both EPSPs and IPSPs. However, the relatively slow and prolonged IPSP at low frequencies may have led to a reduction of action potentials in upward direction (DSI = -0.55).*

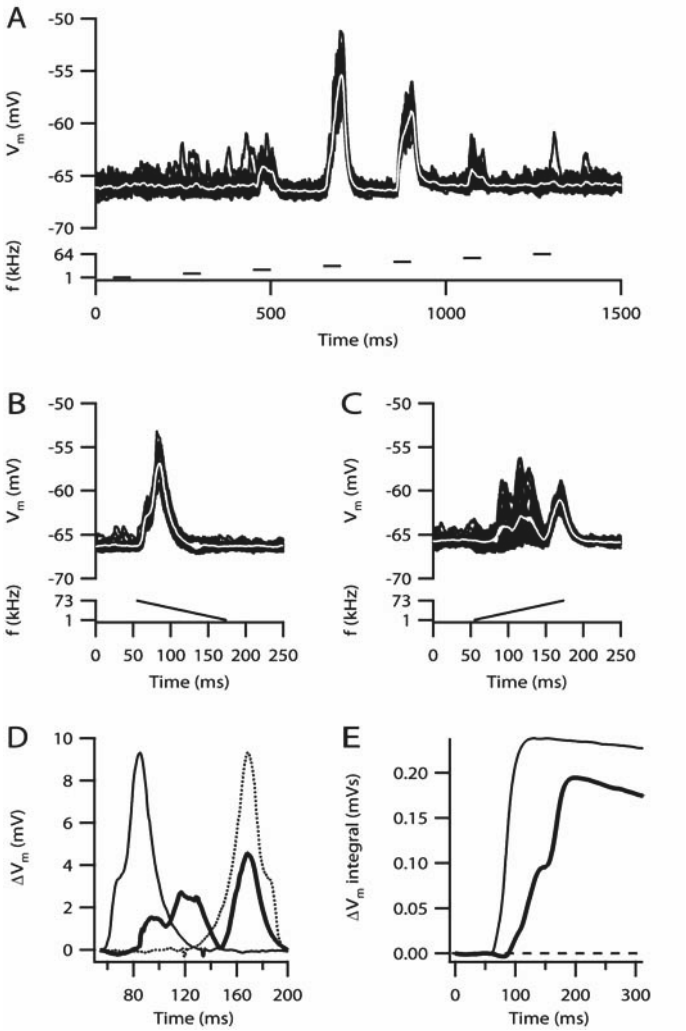

Figure 5.5 Downward selectivity in the absence of inhibition.
A*: Pure tone stimulation (lower panel) resulted in EPSPs (upper panel) at 4, 8, 16 and 32 kHz (white trace). EPSP delay was relatively short for the best frequency (8 kHz) compared with the other frequencies (4.3 vs. 12.6, 9.9 and 12.4 ms respectively), but EPSP rise times were larger at the frequencies with the largest amplitudes (8 and 16 kHz), 23.7 and 23.1 ms vs. 8.1 and 6.5 ms for 4 and 32 kHz, respectively.*
B*: Response to downward FM sweep.*
C*, as in* B*, except upward sweep direction. The direction selectivity index of this cell at 600 kHz/s was –0.35.*
D*: Response to downward (thin line) and upward sweep (thick line) are shown together with the time-reversed downward response (dashed line). The EPSP response to downward sweeps is briefer, but has larger amplitude. In upward direction the response contains separate consecutive EPSPs. Correlation between the up- and the downward response increased from r = –0.35 to r = 0.70 after time reversal.*
E*: Time integral of voltage responses to downward (thin line) or upward sweep, illustrating that despite the much smaller peak amplitude, the integrated EPSP of the upward sweep was not much smaller than of the downward sweep.*

Upward selectivity

The remaining four direction-selective cells had a preference for upward FM sweeps. Their best frequencies at 80 dB were in the range of 4 – 8 kHz (mean 7 ± 1 kHz). This was significantly lower compared with downward selective cells (P = 0.046), in agreement with results obtained in rat IC (Poon and Yu 2000) and auditory cortex (Zhang et al. 2003).
All 4 cells showed an EPSP at the beginning of the upward but not the downward sweep. Figure 5.6 illustrates an upward selective cell with inhibition mainly at frequencies above BF. During the downward sweep, the IPSP could be observed both before and after the EPSP, whereas in the upward direction the IPSP followed the EPSP, suggesting that asymmetric side band inhibition was responsible for direction selectivity in this cell. The other 3 cells also showed evidence for synaptic inhibition during the FM sweeps. In all three cells the correlation between the up and the time-reversed downward sweep was low (r <0.44). In one of the three cells a complex pattern of IPSPs and EPSPs was observed both in response to pure tones and to the FM sweeps (Fig. 5.7) and we presume that the timing of the synaptic potentials played a role in the upward selectivity in this cell. In the other cells inhibition was probably too small to explain the lack of an EPSP during the downward sweep, suggesting that additional upstream processes must have contributed in direction selectivity in these two cells.

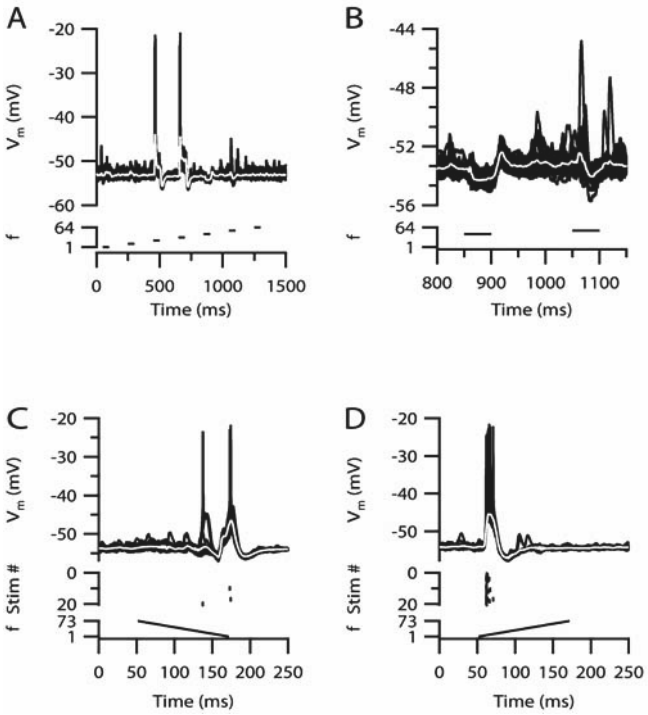

Figure 5.6 Upward selectivity in the presence of sideband inhibition.
A*: Response to tones of different frequencies (top panel), as indicated in the middle panel. The best frequency of this cell was 4 kHz (EPSP delay 9.1 ms).*
B*: On the left: IPSP response to 16 kHz tone followed by an offset hump, shown at higher time resolution (IPSP delay 6.8 ms). On the right: EPSP – IPSP response to 32 kHz tone (IPSP delay 21.5 ms).*
C*: Top panel shows response to the downward FM sweep. Middle panel is the raster plot of the evoked spikes during the stimulus presentations (Stim #). Bottom panel shows the FM sweep.*
D*: as (*C*), except sweep direction was upwards. For spikes, the DSI = 0.76 in favour of upward selectivity, most likely due to inhibition at higher frequencies than BF.*

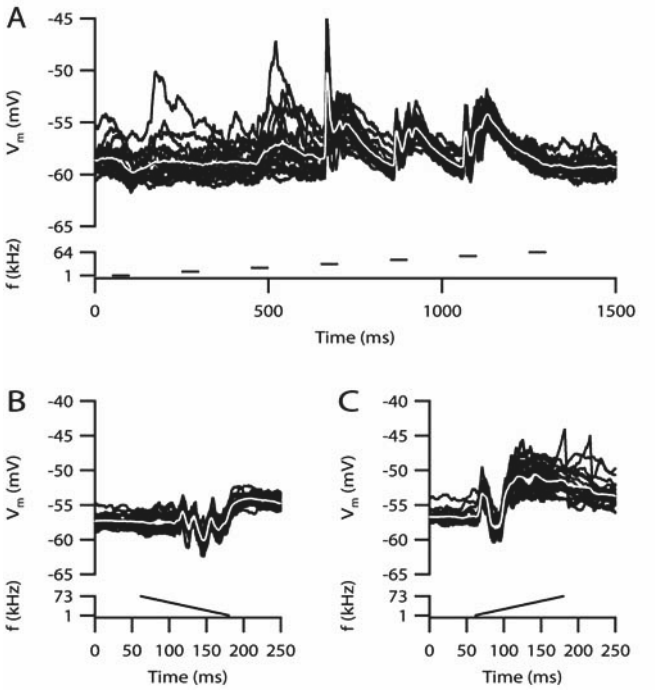

Figure 5.7 Upward selectivity with a complex response to pure tones.
A*: Pure tone stimulation (lower panel) resulted in a slowly rising EPSP at 4 kHz and a complex sequence of EPSPs and IPSPs (upper panel) at 8, 16 and 32 kHz (white trace).*
B*: Downward FM sweep stimulation at 600 kHz/s (lower panel, linear scale) also resulted in a complex response containing both EPSPs and IPSPs (upper panel).*
C*: as in (*B*), except upward sweep direction, resulting in an EPSP-IPSP sequence followed by a delayed EPSP. The DSI of this cell at 600 kHz/s was 0.33.*

Relation with other cellular parameters

In general it was not possible to predict the response to FM sweeps from the membrane properties of the cells, although the mean membrane resistance R_m was significantly higher in upward selective cells (176 ± 43 MΩ), compared with non-selective (103 ± 10 MΩ; P = 0.03, Tukey's HSD) and downward selective cells (85 ± 15 MΩ; P = 0.02, Tukey's HSD). The membrane time constant (τ) was also higher in upward selective cells (19.1 ± 4.9 ms) compared with non-selective (5.9 ± 0.6 ms; P < 0.001) and downward selective cells (4.8 ± 0.2 ms; P < 0.001). Resting membrane potential (range –55 to –74 mV), action potential threshold (range –37 to –76 mV) and presence of hyperpolarization-activated current (I_h) (overall 53% of 36 cells) were not significantly different among groups. Upward or downward selectivity was not associated with a particular firing pattern during constant-current injection.

DISCUSSION

We studied the response to upward and downward FM sweeps in the mouse inferior colliculus and observed that neurons that showed a clear preference for either the upward or downward direction were more likely to show (measurable) synaptic inhibition.

In our study, direction selectivity was seen in 31% of IC neurons of C57/Bl6 mice, similar to what was observed in extracellular recordings when the same sweep speed and frequency range was used (24%; (Hage and Ehret 2003)). A comparison with other studies is hampered by methodological differences, although it seems likely that a higher percentage of cells with selectivity to FM sweep direction would have been obtained if we had varied sweep speeds and range more extensively.

There was little or no evidence for the presence of FM-selective cells, as have been infrequently observed in bats (Suga 1965, 1969; Xie et al. 2007). However, there were several cells that did not spike in response to any of the simple tones or to the FM sweeps and we cannot exclude that a more judicious combination of sweep speed, range and direction would have driven these cells more effectively. Conversely, there were some cells that had a relatively poor response to the FM sweeps, but this appeared to be largely due to the lack of time spent at the excitatory frequencies during the high sweep speed. In three cells we could confirm that lower sweep speeds triggered much larger responses, in agreement with the view that the time course and bandwidth of excitatory responses are important for FM rate tuning (Rees and Langner 2005).

Possible mechanisms that have been proposed to explain the direction selectivity of IC neurons include asymmetric side band inhibition, or more generally the timing of inhibition, the timing of excitation, effects of postsynaptic voltage-dependent ion channels such as the hyperpolarization-activated cation channel I_h, and upstream effects at the level of the cochlear nucleus or the ventral nucleus of the lateral lemniscus (Fuzessery et al. 2006; Rees and Langner 2005; Voytenko and Galazyuk 2007; Xie et al. 2007). To test their contribution we compared the response to FM sweeps with the response to simple tones of different frequencies. Remarkably, in almost half of the cells we did not observe synaptic inhibition, although we cannot exclude that a larger driving force for chloride ions or a more extensive characterization of the pure tone responses would have revealed the presence of inhibitory inputs in more cells (Ehret and Schreiner 2005; Xie et al. 2007). Sharply tuned cells with inhibition within less than an octave may have been missed, although these narrow-band class II type of cells are observed only in a minority of cells in the mouse IC (Egorova et al. 2001; Hage and Ehret 2003). A role for inhibition in direction selectivity became apparent from the observation that the majority of cells that showed evidence for inhibition showed direction selectivity, whereas almost all cells that lacked evidence for synaptic inhibition also lacked direction selectivity. How inhibition contributed to direction selectivity differed between cells. In four cells asymmetric side band inhibition was important, in three other cells the timing of inhibition (onset versus delayed) seemed more relevant. Our results are therefore in line with the mechanisms predicted from extracellular recordings (Brimijoin and O'Neill 2005; Fuzessery and Hall 1996; Fuzessery et al. 2006; Gordon and O'Neill 2000, 1998; Suga 1965; Suga and Schlegel 1973) and an

intracellular study in which only the responses to downward sweeps were tested (Voytenko and Galazyuk 2007), but differ from the interesting observations on FM-selective cells in the bat, in which the response to simple tones was dominated by both onset and offset IPSPs (Xie et al. 2007).
In three cells it was clear that inhibition was not the only contributing mechanism. The timing of EPSPs appeared to be an additional mechanism. The delay and time course of EPSPs varied as a function of frequency. This leads to differential summation depending on sweep direction, as suggested by others (reviewed in (Rees and Langner 2005). We observed that EPSPs tended to start more rapidly at higher frequencies. This increase was similar to the increase in delays observed for first-spike latencies in the mouse (Walton et al. 1998), which probably originates in the cochlea (Ruggero and Temchin 2007), although additional effects downstream from the cochlea likely contribute as well (Walton et al. 1998). The contribution to upward selectivity was not very important, however, since it was not observed consistently in upward selective cells. It may become more important if exponential FM sweeps are used (Felsheim and Ostwald 1996), since the relation between EPSP midpoint and frequency appeared to be exponential rather than linear (Fig. 5.2). EPSP timing did contribute to direction selectivity since in several direction-selective cells the difference in EPSP time courses at different frequencies appeared to lead to differential summation of EPSPs during upward and downward FM sweeps, as suggested by similar EPSP integral but clearly different EPSP peak amplitude.
In two other cells, it seemed unlikely that direction selectivity could be fully explained by the differential summation of IPSPs and/or EPSPs, suggesting a more prominent role for upstream processes in these cells (Fig. 5.7).
We did find that upward selective cells on average had a relatively high membrane resistance and a large membrane time constant, but its significance for direction selectivity at present is unclear.
In conclusion, our results from intracellular recordings confirm the results of extracellular studies showing a prominent but not exclusive role for inhibition in shaping FM direction selectivity (Brimijoin and O'Neill 2005; Fuzessery et al. 2006; Gordon and O'Neill 2000; Heil et al. 1992; Suga and Schlegel 1973). The diversity of synaptic responses of mouse IC neurons is impressive, both within and between cells, with varying latency and time course of IPSPs and EPSPs, inevitably resulting in some degree of direction selectivity for FM sweeps, depending on intensity and sweep range or speed. This effect is fortified by the non-linear relation between spike count and the amplitude of postsynaptic potentials, as in some of the direction selective cells the difference between peak amplitude of EPSPs evoked by the sweeps in both directions were only small. It therefore seems likely that our list of possible mechanisms for FM direction selectivity is not exhaustive. Nevertheless, our results provide direct support for the idea that FM selectivity largely emerges at the level of the midbrain due to spectrotemporal integration of synaptic responses, with an important role for inhibitory inputs in shaping direction selectivity.

Chapter 6

General discussion

The main goal of this study was to gain insight into mechanisms underlying auditory processing at the level of the midbrain. This thesis describes a first inventory of sound-evoked responses of IC neurons and their responses to constant current injection. More specifically, we examined which cell-specific conditions can shape the incoming auditory signal, how inhibitory and excitatory inputs are integrated at the level of the midbrain and how sound-evoked responses can be explained or even predicted from synaptic inputs and cell properties. Figure 6.1 shows a descriptive cellular model for auditory processing in the IC based on the results obtained in our study. As a whole, this figure also implies the connection between chapters three to five. The building blocks for processing by neurons in the IC are: excitatory and inhibitory inputs converge at the level of the midbrain; IC neurons with certain membrane characteristics process these inputs and shape the incoming signal; postsynaptic responses include 6 types of firing patterns after constant current injection and sound-evoked responses to tones of different durations, amplitude-modulated (AM) and frequency-modulated (FM) sound stimuli. In chapters three to five we studied the functional contribution of membrane properties, firing patterns and the presence of I_h on sound processing. In this General Discussion, different mechanisms of auditory processing will be discussed, limitations of the present study will be mentioned and proposals for future research will be given.

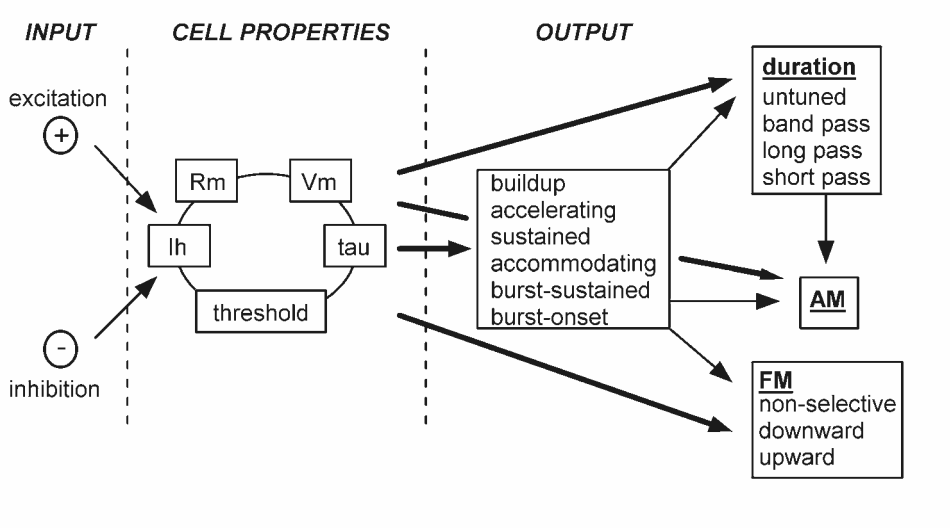

Figure 6.1 A descriptive model for central auditory processing in the IC based on our study results.

We explored to what extent cell properties determine how synaptic integration of excitatory and inhibitory inputs lead to certain firing patterns, duration tuning, AM tuning and FM tuning. Excitation includes depolarizing current injection, spontaneous (spEPSPs) or sound-evoked inputs resulting in excitatory postsynaptic potentials (EPSPs). Inhibition includes hyperpolarizing current injection, or sound evoked inhibitory postsynaptic potentials (IPSPs). Membrane properties of each cell have been determined, also shown in Table 3.1 (Rm = membrane resistance, Vm = resting membrane potential, Ih = hyperpolarization-activated current, tau = membrane time constant, threshold = action potential threshold). Constant current injections reveal 6 types of firing patterns: buildup (n=14), accelerating (n=11), sustained (n=24), accommodating (n=39), burst-sustained (n=10) and burst-onset (n=5). Stimulation with sounds of different durations show that most cells are untuned (n=27). Cells that were duration tuned showed a band pass (n=9), long pass (n=7) or short pass (n=3) response to long tones. AM tuning was mostly seen in burst-sustained, band-pass and long-pass cells. The majority of cells were non-selective to upward and downward FM sweeps (n=25), whereas downward (n=7) and upward (n=4) selective cells mostly showed inhibition compared with non-selective cells.

I. Differences and similarities with previous studies.

The in vivo patch clamp technique brought to light several differences with extracellular studies.
First of all, the number of cells that spontaneously fired action potentials was much lower compared with extracellular studies (Ehret and Moffat 1985; Margrie et al. 2002; Palombi and Caspary 1996; Willott and Urban 1978). In vivo patch clamp studies in other brain areas suggest that spontaneous firing may be overestimated with extracellular recordings (Margrie et al. 2002). The resting membrane potential appeared to be an important factor in determining whether a cell fires spontaneously, because spontaneously firing cells had a significantly more depolarized resting membrane potential compared with cells that did not fire spontaneously, whereas their firing threshold was similar.
Secondly, an interesting new finding in our study is that the irregularity of firing can be influenced by spontaneous EPSPs, as shown in chapter three (Fig. 3.2). In past reports, firing patterns were mainly attributed to the presence of certain ion channels, i.e. potassium, calcium, and calcium-activated potassium channels (Bal and Oertel 2007; Grigg et al. 2000; Rothman and Manis 2003; Sivaramakrishnan and Oliver 2001; Smith 1992; Wu 2005). The influence of spontaneous EPSPs on the irregularity of firing has probably never been described before, simply because subthreshold activity cannot be measured with conventional extracellular recordings (Ehret and Moffat 1985; Palombi and Caspary 1996; Willott and Urban 1978).
The six firing patterns that we observed with our in vivo patch clamp recordings were more or less similar to previous brain slice recordings in the IC (Bal et al. 2002; Peruzzi et al. 2000; Sivaramakrishnan and Oliver 2001), but a clear difference with in vitro reports was the absence of single-spike onset firing (chapter 3). Our recordings were restricted to a dorsocaudal, medial region of the IC due to the overlying transverse sinus. Therefore, a possible explanation could be that ventrolateral cells were underrepresented (due to our dorsocaudal approach), while in this region the Kv1.1 potassium channel – that is involved in onset firing - is mostly expressed (Grigg et al. 2000). Alternatively, some of the reported differences could be developmental, since slice recordings were usually made from animals less than three weeks old (Bal et al. 2002; Peruzzi et al. 2000; Sivaramakrishnan and Oliver 2001). Table 3.1 shows how the six types of cells differed in their membrane properties including input resistance, resting membrane potential, membrane time constant and firing threshold. In general, the basic properties of the neurons in the inferior colliculus of mice and rats during in vivo recordings matched those obtained previously in slice preparations. Any differences with existing literature may be largely due to age and recording method, i.e. use of sharp microelectrodes (Bal et al. 2002; Basta and Vater 2003; Koch and Grothe 2003; Li et al. 1998; Nelson and Erulkar 1963; Pedemonte et al. 1997; Peruzzi et al. 2000; Reetz and Ehret 1999; Sivaramakrishnan and Oliver 2001).
We also found that some cells showed more accommodation than others (considering buildup cells to accommodate the least and burst-onset the most). Table 3.1 shows that the prevalence of I_h increases with the degree of accommodation. The functional relevance of the degree of accommodation seems that cells showing little accommodation are able to show a sustained

response to long sounds (Fig. 4.1). In addition, cells that show a sustained response to long sounds have a relatively large response to AM sounds.
In general, next to recording method and age, a third possible reason for the large diversity in firing patterns and sound-evoked responses could be that we may not have recorded only from cells of the central nucleus, but from cells in the dorsal and lateral cortex as well. We therefore advocate in chapter two that histological confirmation should be performed to determine what region within the IC the recorded cell was located. In addition, immunolocalization of vesicular glutamate transporters (vGLUT) 1 and 2 can be used to define the central nucleus, lateral and dorsal cortex, which is difficult with only conventional cytochrome oxidase staining. Our results are generally similar to a recent study in rat (Altschuler et al. 2008). Both studies show that vGLUT2 staining has higher intensities in dorsal and lateral cortex compared with the central nucleus (Fig. 2.1C) and vGLUT2-positive puncta appear to have a higher density than vGLUT1-positive puncta in most regions of the IC (Fig. 2.1B and C). VGLUT 1 and 2 are largely non-overlapping markers whose inputs and functions are suggested to be different. In the central nucleus, vGLUT1 inputs are most likely derived from the VCN (Friedland et al. 2006), while lateral cortex probably receives vGLUT1 inputs from DCN (Ryugo et al. 1981), cortical (Fremeau et al. 2001), or non-auditory inputs (Oliver 2005). In future experiments it might be helpful to use post-mortem immunohistochemistry to discover functional differences between lateral, dorsal and central nucleus.
With regard to the observed large diversity of sound-evoked responses, our results also showed many similarities with extracellular studies. For instance, chapter four described the distribution of duration tuning: most cells were untuned, followed by band-pass and long-pass. Only a few cells were short-pass, similar to earlier reports (Brand et al. 2000; Perez-Gonzalez et al. 2006). In chapter five we described that direction-selectivity was seen in 31% of IC neurons, this was also similar to extracellular recordings (Hage and Ehret 2003). Upward selective cells had a lower best frequency (BF) than downward cells, which seems logical since the lower frequencies are triggered first in upward direction. This has previously been described in auditory cortex (Zhang et al. 2003). Still, one third of cells we recorded from did not fire action potentials and showed only subthreshold sound-evoked responses, even at 80 dB SPL. With extracellular recordings these cells would have been completely missed.

II. Membrane properties and firing patterns make a small contribution to AM, duration, and FM tuning.

From our data, membrane properties alone cannot be used to predict the type of firing pattern after current injection or the auditory response in duration, AM and FM tuning (thick lines in Fig. 6.1), in contrast to what has been observed in the cochlear nucleus (Feng et al. 1994; Oertel 1991). The role of I_h will be discussed separately below. The functional meaning of buildup neurons having the largest input resistance and a longer time constant remains unclear because this type of firing pattern was not restricted to a certain sound-evoked response (i.e. type of duration-tuning or FM selectivity).
In chapter five we studied the contribution of membrane properties to FM tuning. Compared with non-selective and downward selective cells, upward

selective cells had a higher input resistance and membrane time constant, but other membrane properties and firing patterns during constant current injection were not associated with upward or downward selectivity. Therefore, input resistance and time constant alone are insufficient tools to predict the response to FM sweeps.
In duration tuning all four classes (untuned, long-pass, band-pass and short-pass) contained different types of firing patterns after current injection with membrane properties that did not differ significantly from another. Figure 4.1 shows that cells with a sustained response to sounds with long duration are nonaccommodating. Vice versa, however, sustained firing during current injection is not a sufficient condition for a sustained response during long tones. A small significant finding is shown in Table 4.2: long-pass cells had a longer delay and rise time of the EPSP measured during the longest tone. One would expect that a correlation between long-pass neurons and a buildup pattern after current injection exists, since buildup neurons have a significantly larger input resistance and a longer membrane time constant compared with other firing types, but this observation was not made in our series. Besides, this would only seem logical in case a cell would receive constant excitatory inputs. Apparently long-pass duration tuning includes additional mechanisms, for example the presence of a short-latency IPSP, which was seen in half of our long-pass cells (Fig. 4.5). Similar to duration tuning, membrane properties were not obviously correlated with the response to SAM-tones, but burst-sustained cells had relatively large responses to SAM-tones. These cells were capable to phase-lock to the envelope of the SAM-tones, but did not accommodate as strongly as burst-onset cells which are probably more important for precise temporal coding as in brief consecutive tone bursts (Gooler and Feng 1992; Sinex et al. 2002).
From the above we can conclude that a sustained response to sounds with long duration is seen in nonaccommodating cells and that burst-sustained firing is associated with large responses to AM sounds. Hyperpolarizing and depolarizing current injections were used to mimic inhibitory and excitatory inputs and allowed us to measure the membrane properties and firing patterns of a cell. However, this artificial stimulation is directly on the cell that is recorded from and can never resemble sound stimulation in reality – which is also one of the disadvantages of in vitro recordings. One must realize that during sound stimulation multiple neurons from upstream regions in the brainstem are activated, together they already shape the incoming signal. This suggests that presynaptic inputs or synaptic adaptation must play an additional role.

III. Synaptic inputs and synaptic adaptation affect firing patterns, AM, duration and FM tuning.

One mechanism of sound processing that we found is synaptic adaptation. In the duration series some cells showed an onset EPSP with a decrease in EPSP amplitude with the successive tones. This was especially seen in short-pass cells. It may be possible that if we had stimulated in an interspersed manner with longer interstimulus intervals to avoid synaptic adaptation, short-pass and band-pass cells would have been seen less often. Synaptic adaptation also seemed to play a role in AM tuning. The cells with a short-pass response to long tones (showing clear adaptation in the duration protocol) responded

poorly to SAM tones, whereas band-pass and long-pass cells showed a relatively large response to SAM tones (Fig. 4.8). This suggests that the ability to respond with a sustained response to simple tones is important for AM tuning.

In chapters four and five we conclude that synaptic inputs play an important role in duration and FM tuning. In the duration series, some cells with band-pass or long-pass response were associated with a rapid-onset IPSP (Fig. 4.5). Many studies suggest that sideband inhibition plays an important role in sound processing (Brimijoin and O'Neill 2005; Casseday et al. 1994; Fuzessery et al. 2006; Gordon and O'Neill 1998; Heil et al. 1992; Suga 1965; Suga and Schlegel 1973; Voytenko and Galazyuk 2007), but there are only few literature reports that show direct evidence for this mechanism either by using GABA-blockers (Fuzessery and Hall 1996) or intracellular recordings (Covey et al. 1996; Voytenko and Galazyuk 2007). Our FM series confirms that some direction-selective cells have IPSPs at frequencies either above or below BF. In other cells a difference in time course of IPSPs at different frequencies appeared to contribute to the direction-selectivity. Temporal summation of EPSPs played an additional role in FM tuning (Fig. 5.5). The classical sideband inhibition in the IC is partly comparable with visual cortex. In this brain area, the preference of simple cells for a certain direction can be predicted from a linear sum of the responses to stationary stimuli (Jagadeesh et al. 1993). In the little brown bat, only one third of FM responses in IC neurons can be explained by linear temporal summation of IPSPs and EPSPs (Voytenko and Galazyuk 2007). In these animals, inhibition is observed in 77% of cells. In Mexican free-tailed bats inhibition is seen in 64% (Xie et al. 2008), which is both much higher compared with our duration series (33% of all cells) and FM series (53% of all cells) in mice. Due to the pipette solution that we used, the driving force for chloride was not very large. Therefore, we cannot exclude that the contribution of inhibition was underestimated in our experiments. Inhibition may make a more prominent contribution at higher sound intensities (Casseday and Covey 1992; Covey et al. 1996; Rose et al. 1963), at other frequencies than the CF (Casseday and Covey 1992; Covey et al. 1996), or during ipsilateral stimulation (Casseday and Covey 1992; Covey et al. 1996; Nelson and Erulkar 1963).

We have stated previously that membrane properties only seemed to contribute little to sound processing. Moreover, many duration- and FM-tuned cells did not have evidence for inhibition. It is therefore likely that upstream processes play an additional role, since FM selectivity is already present in the cochlear nucleus (Britt and Starr 1976). Apart from the mechanism of linear summation of inhibition and excitation, non-linear processes such as transformation between membrane potential and firing rate have been shown to play an additional role in visual cortex (Priebe and Ferster 2005). Whether this suggestion can be extrapolated to the entire auditory system needs to be investigated, but a recent study in mouse IC confirms the existence of a supralinear relation between average membrane potential and spike rate (Geis and Borst 2009). Our responses were only measured at resting membrane potential. It is not clear whether the tuning curve of an IC neuron may vary with its membrane potential as seen in auditory cortex neurons. In auditory cortex synaptic excitation and inhibition have the same frequency tuning. This so-called co-tuning for the same tonal receptive fields have been found measured at different membrane potentials (Tan et al. 2004; Wehr and

Zador 2003). Conceivably, a balanced inhibition may sharpen temporal precision (Wehr and Zador 2003). Whether this phenomenon also exists in the IC could be investigated with in vivo whole-cell recordings at different membrane potentials.

IV. I_h is associated with burst firing, chopper and pauser responses, and plays an important role in temporal coding.

In chapter three we described that in half of the cells a depolarizing sag was observed during hyperpolarizing current injection, suggesting that these cells have the hyperpolarization-activated sodium/potassium current I_h. Cells with I_h had a more depolarized resting potential, were more likely to fire bursts, and were more likely to accommodate. In addition, I_h seemed to play an important role in temporal coding, especially in determining the end of tone. Our series confirms that cells with I_h are more likely to show an afterhyperpolarization (AHP) following depolarizing current injection and are more likely to fire rebound action potentials after hyperpolarizing current injection, which is in agreement with brain slice recordings (Bal and Oertel 2000; Koch and Grothe 2003) and other brainstem auditory nuclei (Leao et al. 2006; Shaikh and Finlayson 2003). Cells with strong accommodation showed rapid I_h gating, suggesting that rapid I_h deactivation during depolarizing current injections contributes to the accommodation in these cells (Koch and Grothe 2003).
In chapters four and five we explored the functional meaning of I_h. It turned out that I_h was not important for AM-selectivity, since many cells with I_h that were subjected to SAM-tones did not phase-lock very well. Neither did I_h play a role in FM-selectivity, as suggested by Voytenko and Galazyuk, which may not be surprising since Koch and Grothe already found that I_h current reduces temporal summation of EPSPs and IPSPs (Koch and Grothe 2003; Voytenko and Galazyuk 2007).
In chapter four we observed that at the end of the tone I_h played an important role in the AHP, not only during current injection but following tones as well (shown in Fig. 4.4). This suggests that temporal coding in the IC is the net result of presynaptic inputs and intrinsic properties, which is comparable with MGB neurons (Wenstrup 2005). Rebound spiking has been suggested to be involved in band-pass duration, but our series does not confirm that I_h was significantly seen more often in any type of duration-tuned cell (Casseday et al. 1994). Furthermore, Table 4.1 demonstrates that cells with I_h are more excitable due to a more depolarized membrane potential and have a lower firing threshold. In this series, we also found a lower membrane resistance in cells with I_h, but this is not consistent with the previous chapter, therefore its functional meaning is not yet clear. Finally, Figures 4.3 and 4.4 illustrate that I_h is associated with chopper and pauser responses following tones. All the above demonstrates that cells with I_h are capable of shaping the incoming sound and detecting the end of a tone.
However, technical limitations of our study include that in some cells the hyperpolarizing current injection was rather small. Protocols were designed starting at –200 pA independently of the membrane resistance. This means that cells were not equally hyperpolarized. It may well be that some cells with I_h were missed, simply in case the membrane potential was not enough hyperpolarized to activate I_h channels. In addition, we did not verify that the

depolarizing sag was truly I_h by using for instance pharmacological blocker ZD7288 (Koch and Grothe 2003). Therefore, we cannot exclude the role of other currents.
An alternative method for investigating the functional role of I_h could be, instead of constant current injection, the use of dynamic clamp method (Hughes et al. 1998; Leao et al. 2006; Sharp et al. 1993). With this method it is possible to inject current with kinetics that is similar to I_h. Dynamic current injection should be applied to cells that initially do not show a depolarizing sag during hyperpolarizing current injection. Any sound stimulus of interest can be given. Then, simultaneously inject current with kinetics similar to I_h and present the same sound stimulus. The sound-evoked responses with and without I_h can then be compared to verify the contribution of I_h to shaping the incoming signal.

V. Spikelets are present in the rodent IC.

The presence of spontaneous spikelets in 13 – 18% of mice and rats (Fig.3.2) is an accidental observation of our study; to our knowledge this has never been reported before. These small electrical potentials have been described in other brain regions such as amygdala and hippocampus (Klueva et al. 2003; Valiante et al. 1995). Several hypotheses have been made on the functional origin of spikelets, varying from simultaneously synchronized action potential firing of adjacent local cells (Vigmond et al. 1997) to antidromically conducted ectopic action potentials at axon terminals (Klueva et al. 2003) or conducted via axonal gap junctions (Traub et al. 2002). As described in other brain regions, spikelets may be involved in seizure generation (Klueva et al. 2003; Valiante et al. 1995). Especially in genetically epileptic prone rats and mice these seizures can be audiogenically induced (Faingold 1988; Seyfried et al. 1999). Tonic-clonic limb movements were observed in some of our animals, but unfortunately we did not register in which animals these possible audiogenic seizures were seen and whether these animals had spikelets. The functional meaning of spikelets truly being involved in audiogenic seizures can therefore not be confirmed from our study. Interestingly, audiogenic seizures have also been described to occur more often in animals with hearing loss (Faingold 2005) due to decreased inhibition (less GABA) or increased excitability (more glutamate). The in vivo patch clamp method promises opportunities to further explore possible mechanisms of audiogenic seizures in genetically epileptic prone rodents and/or rodents with hearing loss. For instance, one could observe when a cell with spikelets is stimulated at high intensity of its best frequency an audiogenic seizure is induced. In addition, it is possible to determine whether cells are more excitable in general (i.e. more depolarized resting membrane potential, lower firing threshold, increased prevalence of I_h) and whether inhibitory inputs are diminished.

VI. Next step 1: how can single cell physiology be used to study a neuronal network? Can other stimuli be used to study speech perception?

Our study was focused on single cell physiology and yielded a large intercellular diversity. How several cells are connected to one another and how they respond to sound, as a "system" needs to be investigated. It seems

attractive to believe that some sort of functional organization is present within the IC, analogous to visual and somatosensory cortex where anatomical columns represent functionally organized receptive fields (Kerr et al. 2007; Ohki et al. 2005). To confirm this hypothesis, simultaneous electrophysiological recordings should be made of different neurons. Visual guidance, provided by for instance 2-photon calcium-dye imaging, may further contribute to explore networks within the IC. Unfortunately, this technique has a limited recording depth (<400 μm) (Kerr et al. 2007; Ohki et al. 2005), which means that measurements in the IC are probably restricted to dorsal cortex and low frequency response areas of the CNIC.
In order to comprehend sound processing in the IC, we have dissected sound stimuli to pure tones or tones that are modulated with one factor: frequency-modulated, amplitude-modulated or tones of different durations. Understandably, in daily life, these simple stimuli do not exist. In my opinion, it seems that complex sounds, such as vocalizations or dynamic ripples containing multimodulated sounds (Eggermont 2001; Holmstrom et al. 2007), will not further clarify how the IC works as a network in this stage of current knowledge. As discussed above, the responses to simple stimuli are already quite diverse and can be complicated.

VII. Next step 2: the in vivo patch clamp method can be used to explore mechanisms of hearing loss.

This thesis has focused on the basic mechanisms of sound processing in the inferior colliculus. How do our results relate to hearing disorders? A few suggestions for future research are given in this paragraph.
During our experiments we have used rodents because, next to cat, the rodent is the smallest mammal with an auditory system that is similar to the human auditory system (Ehret and Riecke 2002). An additional argument to use rodents for this study includes the presence of a large number of mouse and rat models with different types of hearing loss, i.e. noise-induced, age-related, hereditary and syndromic hearing loss (Kremer and Cremers 2009; Petit 2006; Shaddock Palombi et al. 2001; Willott 2005). Of course, mouse models cannot be directly extrapolated to human disease, among others because mice have ultrasonic hearing. However, as stated before, objective psychophysiological tests are limited in humans and post-mortem temporal bone studies usually involve older patients. This means that the first steps of pathophysiological mechanisms behind hearing loss are missed. To this date we extensively rely on animal models, simply because they are the best we have. I believe that with relatively simple experiments a few questions can be answered concerning mechanisms underlying hearing loss.
In terms of sensorineural hearing loss (i.e. age-related or noise-induced), many studies suggest that loss of inhibition in the IC results in broader tuning curves and diminished temporal coding, which already originates in the cochlea or central auditory nuclei as well (Willott 2005). Age-related hearing loss can be studied by performing in vivo patch clamp recordings in the same species as our study. C57/Bl6 mice have an adult auditory system at one month and show a decrease in number and size of neurons in the CNIC in the second year of life. This implicates that changes at a cellular level contribute to hearing loss and are not only due to a decrease in afferent inputs (Kazee et al. 1995). With the in vivo patch clamp technique it is possible to examine

whether membrane characteristics are robust at older age, whether all firing patterns continue to exist, whether the same distribution of I_h is found, whether inhibitory inputs diminish, etc. Sound-evoked responses in older animals can be compared with the results of our study. Does temporal coding indeed decrease with older age? Do the cellular responses to FM and AM sounds deteriorate at older age? What parts of our cellular model (Fig. 6.1) are important for these changes? Is it just an altered balance between excitatory/inhibitory neurotransmitter efficacy (Shaddock Palombi et al. 2001) or do cell specific changes or perhaps adaptation processes contribute as well? There is evidence that acquired hearing loss results in a shift of high tot low BF's in the IC, which does not occur in the VCN (Willott 2005). What are the mechanisms behind this phenomenon?
The same questions arise for noise-induced hearing loss, which may also reflect changes in the IC. In vivo patch clamp recordings can be compared before and after noise exposure. Several reports suggest that increased excitability is a consequence of decreases in inhibitory inputs (Salvi et al. 2000; Syka 2002). Cui et al. showed that expression of potassium channels is altered already a few days after cochlear ablation lasting up to several months (Cui et al. 2007). Loss of these two-pore potassium channels leads to increased excitability. What are possible homeostatic mechanisms to maintain the same level of excitability? Perhaps these homeostatic mechanisms also contribute to the presence of tinnitus?
To answer all these questions, the in vivo patch clamp method is somewhat limited due to restricted maximal stable recording time and survival of the animal, but I have great confidence that experimental procedures will continue to evolve to overcome this limitation. In any case, a large advantage of this technique is that subtreshold activity and voltage-dependent potassium channels can still be studied, while non-spiking cells are missed with extracellular recordings.

In conclusion:

The IC is characterized by its heterogeneity. It is likely that cells within the IC are not programmed to have one response to one specific stimulus only. Cell specific characteristics and intrinsic mechanisms of adaptation are subjected to inputs from adjacent and upstream neurons and ultimately shape the incoming signal. The in vivo patch clamp method is a promising tool to explore central auditory processing in an intact auditory system and can be used to further explore the mechanisms behind hearing loss. Hopefully, eventually it may help to optimize treatment options for hearing loss (i.e. pharmacology, electrical implantology) in the future.

Summary

In this thesis, different aspects of central auditory processing in the inferior colliculus (IC) of young-adult mice and rats are described. The IC is an auditory nucleus in the midbrain, which is an important relay station between lower (upstream) brainstem nuclei and higher (downstream) structures such as thalamus and auditory cortex. How central auditory processing takes place at the cellular level within the IC in response to different sound stimuli has hardly been studied. The purpose of the research described in this thesis was to investigate the contribution of membrane properties and synaptic integration of excitatory and inhibitory inputs to sound processing in an intact auditory system. As the experimental approach the "in vivo patch-clamp" technique was used, which enables to measure both membrane properties and sound-evoked activity of a single cell.

Macroscopically, it is difficult to make a clear distinction between dorsal cortex and central nucleus. **Chapter 2** describes how a combination of biocytin cell injections and vesicular glutamate transporter -1 and -2 (vGlut1/vGlut2) stainings can be used to investigate in which part of the IC the recorded cells were located. VGlut1 and vGlut2 seemed to have a complementary expression pattern and together they can help to identify the central nucleus more properly.

In **chapter 3** the firing patterns and basic membrane properties of cells in the IC were characterized. Six different firing patterns were discriminated. To a large extent our results agree with previous slice recordings. The absence of onset firing, the absence of a classic pause in buildup neurons and a description of accelerating cells were the most distinct differences with earlier experiments performed in slice recordings. Basal membrane properties such as resting membrane potential, firing threshold, membrane resistance, membrane time constant and the presence of the so-called hyperpolarization-activated voltage-dependent sodium/potassium channel I_h were analyzed to examine whether these membrane properties could be used to predict which type of firing pattern will occur after constant current injection. Approximately half of the cells showed evidence for the presence of I_h. These cells had a more depolarized resting membrane potential than cells without I_h, they showed more often an afterhyperpolarization after depolarizing current injection, they fired more often rebound spikes after the end of hyperpolarizing current injection, and more often showed an accommodating or burst-type firing pattern. Buildup cells had a significantly higher input resistance and a larger time constant. In addition, spontaneous excitatory synaptic potentials (spEPSPs) seemed to make a large contribution to the irregularity of spike patterns. Finally, the first evidence for the presence of electrical synapses in the IC was observed as some cells showed spikelets. These spikelets may play a role in sound-induced epilepsy.

In **chapter 4** membrane properties, inhibition (IPSP), firing patterns (after constant current injection) and I_h were further explored in order to learn to what extent they contribute to processing sound stimuli of different durations (duration tuning) or to the processing of amplitude-modulated sounds (AM tuning). There were four types of responses of duration tuning: short-pass, band-pass, long-pass and untuned. The distribution of these classes was similar to those observed in extracellular recordings. Each class of duration tuning contained all types of firing patterns without any significant contribution of membrane properties. Fast onset inhibition was mainly seen in band-pass and long-pass cells. Short-pass cells showed a sound-induced onset excitatory response; it is likely that synaptic adaptation occurred in these cells. Sinusoidal amplitude modulated sound stimuli (SAM-tones) were used to study AM tuning. Burst-sustained cells showed a relatively large response, as well as cells that were classified as band-pass and long-pass. Membrane properties alone were insufficient to predict the response to SAM-tones. However, a separate role seems to be reserved for I_h. Cells with I_h were more excitable, probably due to their more depolarized resting membrane potential and relatively low firing threshold. These cells more often showed a chopper and pauser response and they always showed an afterhyperpolarization at the end of the stimulus. This chapter shows that the clearest mechanism in duration tuning seems to be synaptic integration of excitatory and inhibitory inputs and synaptic adaptation, while AM tuning seems to be more influenced by the presence of calcium-dependent potassium channels and the absence of adaptation. The presence of I_h can additionally shape the incoming auditory signal.

Finally, **chapter 5** describes that spectrotemporal integration of synaptic responses plays an important role in FM tuning. In literature, inhibition is hypothesized to be a prominent factor in this mechanism, although the evidence is largely indirect. We compared the responses of pure tones to up- and downward FM-sweeps. Almost one third of the cells had a preference for up- or downward sweeps. Direction-selective cells more often showed inhibition than non-selective cells. Summation of EPSPs with different delays and timing played an additional role. This study confirms with direct evidence that FM tuning is largely determined by the synaptic integration of excitatory and inhibitory inputs, while membrane properties and ion-channels seem to play a lesser role.

In conclusion, the auditory responses and membrane properties of IC neurons are very diverse. By showing how the diversity in membrane properties and synaptic inputs can lead to specific tuning for complex sounds, we provide a cellular explanation for the contribution of the IC to central auditory processing.

Samenvatting

In dit proefschrift worden verschillende aspecten van centraal auditieve verwerking in de colliculus inferior (IC) beschreven bij jong volwassen muizen en ratten. De IC is een auditieve hersenkern in het mesencephalon en wordt beschouwd als een belangrijk schakelstation tussen lager gelegen hersenkernen van de hersenstam enerzijds en hoger gelegen thalamus / cortex anderzijds. Over hoe centraal auditieve verwerking op celniveau plaats vindt in de IC bij verschillende geluidsstimuli was tot op heden weinig bekend. Het doel van dit onderzoek is met behulp van de "in vivo patch-clamp" techniek de bijdrage van celeigenschappen en synaptische integratie van excitatie en inhibitie te bestuderen bij de transmissie van geluid in een intact auditief systeem. Hierbij werd gebruik gemaakt van de "in vivo patch-clamp" techniek waarbij het mogelijk was om zowel membraan eigenschappen van een cel te meten als diens reactie op geluid.

Gedurende de fysiologische experimenten werd de identificatie van de centrale kern visueel beperkt vanwege de dorsocaudale benadering. Macroscopisch is het niet mogelijk om onderscheid te maken tussen dorsale cortex en centrale nucleus. **Hoofdstuk 2** beschrijft hoe immunohistochemie, waaronder biocytine celinjectie en vesiculaire glutamaat transporter (vGlut) kleuringen, gebruikt kan worden om de localisatie van de gemeten cellen te bevestigen. vGlut1 en vGlut2 leken complementair aan elkaar en juist deze combinatie maakte het mogelijk om de centrale kern beter identificeren.

In **hoofdstuk 3** werden 6 vuurpatronen en basale membraan eigenschappen van IC neuronen uitvoerig beschreven. Deze serie toont veel overeenkomsten met in vitro metingen. De afwezigheid van een onset vuurpatroon (met 1 actiepotentiaal), de afwezigheid van een klassieke pauze bij de buildup cellen en een beschrijving van "accelerating" cellen zijn de belangrijkste verschillen met bestaande literatuur. Basale membraan eigenschappen werden nauwkeurig in kaart gebracht, zoals rustmembraanpotentiaal, vuurdrempel, membraan weerstand, membraan tijdsconstante en de aanwezigheid van een spannings-afhankelijk natrium / kalium kanaal I_h, geactiveerd door hyperpolarisatie. Dit heeft het doel te inventariseren of deze membraaneigenschappen kunnen voorspellen welk vuurpatroon een cel zal vertonen na stroominjectie. Ongeveer de helft van alle cellen hadden I_h. Deze cellen waren in rust meer gedepolariseerd dan cellen zonder I_h, zij toonden vaker een nahyperpolarisatie na depolariserende stroom injectie en vuurden vaker rebound actiepotentialen. Het I_h kanaal was vaker aanwezig bij accommoderende en burst-type cellen. Voorts hadden buildup cellen een significant hogere input weerstand en een langere tijdsconstante. Bovengenoemde gegevens bleken echter onvoldoende om te voorspellen met welke membraaneigenschappen er een bepaald vuurpatroon tot stand komt. Daarnaast werd gezien dat spontane excitatoire post-synaptische potentialen (spEPSP) een grote invloed hadden op het onregelmatig vuren van actiepotentialen. Tot slot toonde onze studie aan dat er electrische synapsen bestaan in de IC; dit werd gezien in de vorm van spikelets. Deze relatief kleine potentialen zouden wellicht een rol kunnen spelen bij auditieve epileptische insulten.

Hoofdstuk 4 beschrijft het onderzoek naar de rol van inhibitie (IPSP), de membraaneigenschappen, de vuurpatronen (na stroominjectie) en I_h bij het verwerken van geluid met een verschillende duur (duration-tuning) of een bepaalde amplitude-modulatie (AM-tuning). Bij duration-tuning waren vier verschillende klassen onder te verdelen: short-pass, band-pass, long-pass en untuned type cellen. De verdeling van deze klassen was vergelijkbaar met extracellulaire metingen. In elk van deze klassen werden vrijwel alle verschillende soorten vuurpatronen gezien zonder significante bijdrage van membraaneigenschappen. Snelle onset inhibitie werd voornamelijk, maar niet bij alle, band-pass en long-pass cellen gezien. Daarnaast toonden short-pass cellen vooral een geluidsgeïnduceerde onset respons, waarbij synaptische adaptatie waarschijnlijk een belangrijke rol speelde. AM-tuning werd onderzocht met behulp van sinusoïde gemoduleerde geluidsstimuli (SAM-tonen). Vooral burst-sustained cellen toonden een relatief grote respons hierop, evenals cellen die geclassificeerd waren als band-pass en long-pass. Op zich staande membraaneigenschappen konden niet gebruikt worden om de reactie op SAM-tonen te voorspellen. Een speciale rol leek echter weggelegd voor I_h. Cellen met I_h bleken namelijk makkelijker in staat te zijn tot het vuren van actiepotentialen, mede dankzij een meer gedepolariseerde rustmembraanpotentiaal en een relatief lagere vuurdrempel. Zij toonden vaker een geluidsgeïnduceerde chopper en pauser respons met daarbij ook altijd een nahyperpolarisatie aan het einde van de stimulus. Dit hoofdstuk laat zien dat het belangrijkste mechanisme bij duration-tuning de synaptische integratie van excitatoire en inhibitoire inputs lijkt te zijn samen met synaptische adaptie, terwijl AM-tuning met name beïnvloed wordt door de aanwezigheid van calcium-afhankelijke kalium kanalen en de afwezigheid van adaptatie. De aanwezigheid van I_h kan daarbij het inkomend geluid nog verder vormen.

In **hoofdstuk 5** tenslotte wordt beschreven dat spectro-temporele integratie van synaptische responsen een belangrijke rol speelt in FM-tuning. In de literatuur wordt verondersteld, maar is tot nu toe nog onvoldoende bewezen, dat inhibitie een prominente factor is. Wij vergeleken de reacties op pure tonen met de responsen op op- en neerwaartse FM-sweeps. Bijna een derde van de cellen had een voorkeur voor op- of neerwaartse FM-sweeps. Cellen die selectief waren voor een bepaalde opwaartse of neerwaartse richting toonden vaker inhibitie dan niet-selectieve cellen. Daarnaast speelde de delay en timing van EPSPs een rol, hetgeen voor elke frequentie verschillend was. Deze studie bevestigt direct dat FM-tuning vooral bepaald wordt door synaptische integratie van excitatoire en inhibitoire inputs, terwijl er een kleinere rol is weggelegd voor membraaneigenschappen en ion-kanalen.

Concluderend zijn de auditieve responsen en membraaneigenschappen van cellen in de colliculus inferior zeer uiteenlopend. Met dit proefschrift hebben wij enkele cellulaire verklaringen gegeven voor de bijdrage van de IC aan centraal auditieve verwerking. Hopelijk zal deze eerste inventarisatie in de toekomst kunnen leiden tot een duidelijker inzicht in de fysiologie binnen de colliculus inferior en uiteindelijk het gehele centraal auditieve systeem.

Dankwoord

Prof. dr. J.G.G. Borst, beste Gerard. Tijdens je eerste introductie over wat dit promotietraject zou inhouden kende ik waarschijnlijk minder dan de helft van je vocabulaire. Eén jaar nadat ik mijn lege kamer had omgetoverd tot De Auditieve In Vivo Patch Clamp Opstelling (die op dat moment echter nog steeds niet werkte) kwamen van jou de cryptische woorden: "na die ene paper uit 1996 is er nooit meer in vivo gepatch-clampt in de colliculus, daar zal wel een reden voor zijn". Dankzij wat duitse voodoo en aanwezigheid van in jouw ogen triviale factoren was het met een race tegen de klok nog maar nauwelijks gelukt om voldoende data bij elkaar te verzamelen voordat ik de kliniek in zou verdwijnen. Met je grenzeloze geduld en 1-op-1 monster-sessies van soms wel 5 uur achtereen bracht je mij alle fijne kneepjes van de electrofysiologie bij en begon ik langzaam aan te begrijpen waar ik al die tijd mee bezig was geweest. Ik besef dat het een groot voorrecht is geweest om direct met je te hebben samengewerkt. Ik ken geen wetenschapper die eerlijker, kritischer, en volhardender is dan jij. Kwaliteit gaat boven kwantiteit. Onze gezamenlijke pietepeuterigheid heeft de snelheid waarmee de eerste mammoet-artikelen zijn gepubliceerd niet bepaald bevorderd, waarschijnlijk zelfs exponentieel vertraagd. Heel veel dank voor je intensieve begeleiding, ik heb veel geleerd van je analyserend vermogen. Zonder jou was dit proefschrift nooit gebaard.

Prof. dr. L. Feenstra, na hora est voor mij nog steeds geen Louw. Wat jullie destijds aan capaciteiten in mij zagen blijft voor mij een groot raadsel. Ondanks mijn ingeleverde cijferlijst was het jullie niet opgevallen dat neurologie en fysiologie beide mijn zwakste punten waren tijdens geneeskunde. Hoe ironisch is dan dat deze aanstaande KNO-arts uiteindelijk promoveert op een electrofysiologisch onderwerp bij de afdeling neurowetenschappen. Ik dank u voor de mogelijkheden die u mij heeft gegeven om dit promotie-onderzoek gecombineerd te doen met een opleidingsplaats tot KNO-arts, alsmede voor uw grenzeloze vertrouwen en bemoedigende schouderklopjes, toen ik het bij tijd en wijle even niet meer zag zitten.

Prof.dr. R.J. Baatenburg de Jong, dank voor de ruimte die u mij heeft gegeven om dit promotie-onderzoek af te ronden tijdens mijn klinische deel van de KNO-opleiding.

Drs. H.P. Theeuwes, beste Hilco. Jouw optimisme en vrolijke noot hebben bijgedragen om dit abstracte project wat leven in te blazen. Ook al was jouw mobiele telefoon van tijd tot tijd hoogst irritant! De uren die je hebt geïnvesteerd in het perfusie-hok, in het histologie-lab, achter de microscoop en met Photoshop hebben geleid tot een aantal prachtige figuren. Hartelijk dank voor je inzet en gezelligheid, zelfs op koninginnedag 2009. Ik wens je veel succes toe met je ontelbare projectjes, je komt er wel, mits je niet alles tegelijkertijd probeert uit te voeren (en je telefoon op "stil" zet).

Drs. C. Donkersloot, beste Kees. Naast mijn BINAS-lijstje was jij voor mij de wikipedia van "alles wat maar met computers, boutjes, of insecten" te maken had. Dank voor alles wat je voor mij uitgeKeest hebt. Je hebt mij zeer terecht herhaaldelijk doen herinneren aan het feit dat levende wezens niet te versimpelen zijn tot het samenvatten in 1 wiskundige formule.

Dr. R. Habets, beste Ron. Het Alcien-blue incident zal ik nooit vergeten. Dank voor de basisingrediënten die je mij geleerd hebt om te patchen. Ik wens je veel succes toe in je verdere carrière.

J. van der Burg, beste Hans. Ik dacht dat de woorden nooit zouden komen, maar hier zijn ze dan: Dank je wel, voor alles wat je verHanst hebt. Het wordt tijd dat je je post-it-memo-behang gaat vervangen.

Elize, Mandy en Erika. Eenieder die langdurig met jullie gewerkt heeft zal zich waarschijnlijk over een paar jaar met een lawaadip rond 4 kHz op mijn poli melden. Bedankt voor alles wat jullie mij aan histologie geleerd hebben, het was vooral erg gezellig!

Programmeurs Teun van Immerzeel en Wim Holland, dankzij jullie hulp kon ik na hoeveel keer wel niet gecalibreerd te hebben eindelijk mijn proefdieren wat laten horen. Schaarse handleidingen, bugs en nog meer tekortkomingen zorgden voor een grote uitdaging om de verschillende software compatibel met elkaar te maken. Hartelijk dank voor jullie uitleg, programmeerwerk en bezoekjes aan mijn opstelling.

Van alle andere medewerkers van "de 12^{e}" met wie ik heb samengewerkt, wil ik in het bijzonder Jeanette Lorteije, Marcel van der Heijden, Adrian Rodriguez-Contreras, Samantha Spangler, Dick Jaarsma, Silviu Rusu en Tom Ruigrok bedanken voor hun technische adviezen, discussies en commentaar op manuscripten. Loes Nijs en Edith Klink wil ik bedanken voor hun snoepwinkel aan bureau-artikelen uit de kast met de flaporen. Loes, heel erg bedankt voor je hulp met alle formulieren in de laatste fase van dit proefschrift.

Prof. dr. P.X. Joris, beste Philip. Hartelijk dank voor de gastvrijheid op het lab en bij u thuis tijdens mijn eerste kennismaking met electrofysiologische metingen in vivo. Dankzij de Leuvense katten kreeg ik inzicht in welke microchirurgische vaardigheden er benodigd waren om dit project werkend te krijgen. Deze vaardigheden blijken uiteindelijk ook bijzonder handig op OK.

Prof. dr. M. Brecht and dr. S. Komai, dear Michael and Shoji. Thank you very much for teaching me the basic principles of in vivo patch-clamping and for showing me that it can be fun too! A mysterious mix of German and Japanese voodoo at least proved that my experimental set up had the potential to become a powerful tool.

Paranimf drs. A.P. Nagtegaal, beste Paulus. Kom je nog een kopje thee halen met een stukje fruit? Gedeelde smart is halve smart! Met geen andere KNO-arts kan ik doormijmeren over de invloed van "I_h" op het algemeen welbevinden. Ik wens je veel sterkte toe met de rest van je promotie. Als ik je ergens nog ongevraagd advies over kan geven of een overdosis chocolademousse mag voorschotelen dan kun je altijd bij me aankloppen!

Paranimf dr. M.A.J. van Looij, lieve Mar. Klaar met die boekjes, nu geen excuses meer! Vanaf heden alleen nog maar geflambeerde basilicum, do-it-yourself-dinners en shop-'til-we-drop! New York, here we come!

Overige Leden van het Tuttenclubje, Veer en Caro, uiteindelijk krijgen we dan toch een gemeenschappelijke functie: moederen! Ik kijk altijd uit naar onze afspraakjes, de Randstad is toch niet zo heel groot.

(Oud-) assistenten van de KNO: Luuk en Nien jullie zijn de volgende aan de beurt; de Haagsche clan Nadjah, Franky Boy, Charlotte, Stijn en Floris: voor de vele car-pool ritjes is altijd wel een bob te vinden (soms wel 9 maanden lang), "oude garde" Willem, Q, Laura, Schroeffie, Marc en Jeroen: "vroeger was alles anders", en voor de huidige groep geldt: Claire, Katja, Thijs, Gulnez, Tom, Marieke en Saskia dank voor jullie gezelligheid!

Drs. A. Halim, lieve Angel. Dank voor alle dagen dat je ons uit de brand hebt geholpen als we last-minute een oppas nodig hadden, voor je culinaire adviezen en je heerlijke uitprobeersels. Ik gun je van harte een opleidingsplaats bij de KNO, en dan het liefst één bij ons in de buurt!

Ons vast financieel-gastronomisch-adviesbureau van der Wal-Wedekind, Jochem en Elisabeth. Geld, gezondheid, geluk, gegraaf-in-de-achtertuin, geboor-in-de-muur. Wat is het toch altijd heerlijk om onder het genot van een Omelette Siberienne bij jullie te onthaasten.

Lieve VU-dames, T, Phlip, Els, Fleura, en Margriet: "two down one to go", straks kunnen de gesprekken tijdens onze etentjes "onderzoeksvrij" verklaard worden! Wat hebben we veel ellende gedeeld met elkaar. Gelukkig zijn de ups net zo groots als de downs geweest. Vrij baan voor luiers, paprika-plantjes, en onbenullige huiselijke frustraties! Slechts nog één huwelijk te gaan....

Drs. A.C.W. Reus. Reusje, jij hebt mij altijd gesteund en geadviseerd in alles wat er in mijn drukke leven zich afspeelt. Je talrijke kaartjes zijn inmiddels een behoorlijke placemat op mijn bureau geworden. Als we voor elke minuut die we afgekletst hebben een eurocent hadden gekregen waren we nu multimiljonair geweest. Ik heb groot respect voor hoe jij en Ewout in het leven staan. Jullie optimisme na de geboorte van Lotte is inspirerend. En wat heerlijk dat Floor ons leven heeft verrijkt!! Op naar de volgende vakantie met nóg meer kleintjes.

Drs. I.L. Marsidi, lieve Ien. Van abon-balletjes tot vogelhapjes, praktische cadeaus en bungalow-for-rent: je staat altijd voor ons klaar. Dank je wel voor je hulp oma Ina!

Mijn ouders, lieve Pa en Ma. Je best doen, iets speciaals maken van wat je doet en vooral datgene afmaken waar je aan begonnen bent, zijn 3 belangrijke bouwstenen die jullie meegegeven hebben in mijn leven. Maar ook dankbaar zijn voor wat je hebt en genieten van het hier en nu spelen een grote rol in geluk en welzijn. Aan jullie is dit boekje opgedragen, jullie zijn mijn steun en toeverlaat. Bedankt voor jullie oneindige vertrouwen en liefde.

Drs. H.L. Tan, beste Hwan. Zo'n ambitieus zusje lijkt me vreselijk om mee opgegroeid te zijn, desalniettemin is onze band onbreekbaar. Jouw adviezen zijn voor mij altijd zeer waardevol. Ik ben trots dat je mijn broer bent.

Lieve Thijs, mijn P.M. Naast rots in de branding ben jij mijn "diamond in the rough". Vanaf nu is het over met die 1-dag-géén-werk-weken. Ons compromis is gehaald, 7 jaar buffelen. Bedankt voor je eindeloze geduld met al die dagen dat ik in het ziekenhuis of op het lab was. Ik wil nu alleen maar genieten, heel erg veel zelfs! Met jou tot in de eeuwigheid. Op naar de Pan op dinsdagmiddag!

Hugo-Max, mijn manneke man, jij bent voor mij "the greatest spirit".

Curriculum vitae

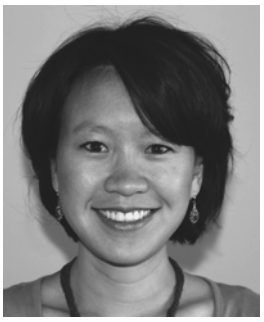

De auteur van dit proefschrift werd geboren op 4 april 1976 te Utrecht. Na het doorlopen van de Montessori School te Zeist, de Anne Frank School te Bunnik en het behalen van het gymnasium diploma op het Christelijk Lyceum te Zeist, werd een jaar High School in Schaumburg (Illinois), Verenigde Staten voltooid. In 1994 begon zij aan de studie Geneeskunde aan de Vrije Universiteit te Amsterdam. Het wetenschappelijk onderzoek werd bij de afdeling Kindergeneeskunde uitgevoerd en afgerond in 1999 met een posterpublicatie op een kinderoncologisch congres in Montreal, Canada (SIOP/ASPHO). Het arts-examen werd behaald in juli 2001 met o.a. keuze-coschappen Spoedeisende Hulp in het West-Fries Gasthuis te Hoorn en KNO/Hoofd-Halschirurgie in het Antoni van Leeuwenhoekziekenhuis /Nederlands Kanker Instituut. De eerste schreden als basis-arts werden gezet op de Spoedeisende Hulp in het Waterlandziekenhuis te Purmerend, gevolgd door een arts-assistentschap op de afdeling KNO/Hoofd-Halschirurgie in het AvL/NKI te Amsterdam. In december 2002 begon zij in het Erasmus MC te Rotterdam als arts-assistent op de afdeling KNO onder Prof.dr. L. Feenstra, later onder leiding van Prof. dr. R.J. Baatenburg de Jong en als arts-onderzoeker op de afdeling Neurowetenschappen onder begeleiding van Prof.dr. J.G.G. Borst. Naar verwachting zal de opleiding tot KNO-arts afgerond worden in 2010. De auteur is gehuwd met Thijs Overbeek. Samen hebben zij een zoon Hugo-Max (2007) en wonen in Den Haag.

List of publications

Tan ML and Feenstra L. Ingezonden brief: Diagnose in beeld (156). Een man met een hematoom achter het oor. *Ned Tijdschr Geneeskd* 147: 2500-2501, 2003.

Tan ML and Feenstra L. Recidiverend gehoorverlies bij de ziekte van Crohn. *Ned Tijdschr KNO-heelkunde* 10: 229-232, 2004.

Tan ML, Lohuis PJFM, Besnard APE, and Balm AJM. Mediastinaal abces als gevolg van laryngoscopie na chemo-irradiatie voor hypopharynxcarcinoom. *Ned Tijdschr KNO-heelkunde* 11: 139-141, 2005.

Tan ML, Theeuwes HP, Feenstra L, and Borst JG. Membrane properties and firing patterns of inferior colliculus neurons: an in vivo patch-clamp study in rodents. *J Neurophysiol* 98: 443-453, 2007.

Tan ML and Borst JG. Comparison of responses of neurons in the mouse inferior colliculus to current injections, tones of different durations, and sinusoidal amplitude-modulated tones. *J Neurophysiol* 98: 454-466, 2007.

Tan ML and Blom HM. Inspiratoire stridor door paroxysmale paradoxale stemband dysfunctie. *Ned Tijdschr KNO-heelkunde* (accepted for publication), 2009.

Lohuis PJFM, **Tan ML**, Bonte K, van den Brekel MWM, Balm AJM, and Vermeersch HB. Superficial parotidectomy via modified facelift incision. *Ann Otol Rhinol Laryngol* 118: 276-280, 2009.

den Bakker MA, Beverloo HB, van den Heuvel-Eibrink MM, Meeuwis CA, **Tan ML**, Johnson LA, French CA, and van Leenders GJLH. NUT midline carcinoma of the parotid gland with mesenchymal differentiation. *Am J Surg Pathol* (accepted for publication), 2009.

List of abbreviations

ABR	auditory brainstem response
AC	auditory cortex
AM	amplitude modulated
APD	auditory processing disorder
AVCN	anteroventral cochlear nucleus
BF	best frequency
CF	characteristic frequency
CN	cochlear nucleus
CNIC	central nucleus of inferior colliculus
DC	dorsal cortex (of inferior colliculus)
DCN	dorsal cochlear nucleus
DNLL	dorsal nucleus of lateral lemniscus
EPSP	excitatory postsynaptic potential
FM	frequency modulated
GB	globular bushy cell
GABA	gamma –amino butyric acid
IC	inferior colliculus
ICC	inferior colliculus commissure
I_h	hyperpolarization-activated current
IHC	inner hair cell
ILD	interaural level difference
INLL	intermediate nucleus of lateral lemniscus
i.p.	intraperitoneally
IPSP	inhibitory postsynaptic potential
ITD	interaural time difference
LC	lateral cortex (of inferior colliculus)
LL	lateral lemniscus
LNTB	lateral nucleus of trapezoid body
LSO	lateral superior olive
MGB	medial geniculate body (of thalamus)
MOC	medial olivocochlear system
MNTB	medial nucleus of trapezoid body
MSO	medial superior olive
NADPH-d	nicotinamide adenine dinucleotide phosphate-diaphorase
OAE	oto-acoustic emissions
OHC	outer hair cell
PC	pillar cell
PVCN	posteroventral cochlear nucleus
R_m	membrane resistance
SB	spherical bushy cell
s.c.	subcutaneously
SC	superior colliculus
SOC	superior olivary complex
SPL	sound pressure level
tau	membrane time constant
TEA	tetraethylammonium
TM	tectorial membrane
VCN	ventral cochlear nucleus
vGlut	vesicular glutamate transporter

V_m	resting membrane potential
VNLL	ventral nucleus of lateral lemniscus

References

Ahuja TK and Wu SH. Intrinsic membrane properties and synaptic response characteristics of neurons in the rat's external cortex of the inferior colliculus. *Neuroscience* 145: 851-865, 2007.

Aitkin LM, Webster WR, Veale JL, and Crosby DC. Inferior colliculus. I. Comparison of response properties of neurons in central, pericentral, and external nuclei of adult cat. *J Neurophysiol* 38: 1196-1207, 1975.

Altschuler RA, Tong L, Holt AG, and Oliver DL. Immunolocalization of vesicular glutamate transporters 1 and 2 in the rat inferior colliculus. *Neuroscience* 154: 226-232, 2008.

ASHA. Central Auditory Processing: Current Status of Research and Implications for Clinical Practice [Technical Report]. Available from www.asha.org/policy: American Speech-Language-Hearing Association, 1996.

Atlas AB. Allen Institute for Brain Science, 2004-2006.

Bal R, Green GG, Rees A, and Sanders DJ. Firing patterns of inferior colliculus neurons-histology and mechanism to change firing patterns in rat brain slices. *Neurosci Lett* 317: 42-46, 2002.

Bal R and Oertel D. Hyperpolarization-activated, mixed-cation current (I(h)) in octopus cells of the mammalian cochlear nucleus. *J Neurophysiol* 84: 806-817, 2000.

Bal R and Oertel D. Voltage-activated calcium currents in octopus cells of the mouse cochlear nucleus. *J Assoc Res Otolaryngol* 8: 509-521, 2007.

Bamiou DE, Musiek FE, and Luxon LM. Aetiology and clinical presentations of auditory processing disorders - a review. *Arch Dis Child* 85: 361-365, 2001.

Banks MI, Pearce RA, and Smith PH. Hyperpolarization-activated cation current (I_h) in neurons of the medial nucleus of the trapezoid body: voltage-clamp analysis and enhancement by norepinephrine and cAMP suggest a modulatory mechanism in the auditory brain stem. *Journal of Neurophysiology* 70: 1420-1432, 1993.

Banks MI and Sachs MB. Regularity analysis in a compartmental model of chopper units in the anteroventral cochlear nucleus. *J Neurophysiol* 65: 606-629, 1991.

Basta D and Vater M. Membrane-based gating mechanism for auditory information in the mouse inferior colliculus. *Brain Res* 968: 171-178, 2003.

Bauer CA and Jenkings HA. Otologic Symptoms and Syndromes. In: *Otolaryngology Head & Neck Surgery* (4th ed.), edited by Cummings CW. Philadelphia: Elsevier Mosby, 2005, p. 2867-2880.

Brand A, Urban R, and Grothe B. Duration tuning in the mouse auditory midbrain. *J Neurophysiol* 84: 1790-1799, 2000.

Brimijoin WO and O'Neill WE. On the prediction of sweep rate and directional selectivity for FM sounds from two-tone interactions in the inferior colliculus. *Hear Res* 210: 63-79, 2005.

Britt R and Starr A. Synaptic events and discharge patterns of cochlear nucleus cells. II. Frequency-modulated tones. *J Neurophysiol* 39: 179-194, 1976.

Brown CJ. Electrophysiologic Assessment of Hearing. In: *Otolaryngology Head & Neck Surgery* (4th ed.), edited by Cummings CW. Philadelphia: Elsevier Mosby, 2005, p. 3466-3502.

Bruzzone R, Hormuzdi SG, Barbe MT, Herb A, and Monyer H. Pannexins, a family of gap junction proteins expressed in brain. *Proc Natl Acad Sci U S A* 100: 13644-13649, 2003.

Burger RM and Pollak GD. Analysis of the role of inhibition in shaping responses to sinusoidally amplitude-modulated signals in the inferior colliculus. *J Neurophysiol* 80: 1686-1701, 1998.

Calford MB. The parcellation of the medial geniculate body of the cat defined by the auditory response properties of single units. *J Neurosci* 3: 2350-2364, 1983.

Cant NB. The Cochlear Nucleus: Neuronal Types and Their Synaptic Organization. In: *Springer Handbook of Auditory Research*, edited by Webster DB, Popper AN and Fay RR. New York: Springer-Verlag, 1992, p. 66-116.

Cant NB. Projections from the Cochlear Nuclear Complex to the Inferior Colliculus. In: *The inferior colliculus*, edited by Winer JA and Schreiner CE. New York: Springer, 2005, p. 115-131.

Cant NB and Benson CG. An atlas of the inferior colliculus of the gerbil in three dimensions. *Hear Res* 206: 12-27, 2005.

Cant NB and Benson CG. Organization of the inferior colliculus of the gerbil (*Meriones unguiculatus*): differences in distribution of projections from the cochlear nuclei and the superior olivary complex. *J Comp Neurol* 495: 511-528, 2006.

Caspary DM, Milbrandt JC, and Helfert RH. Central auditory aging: GABA changes in the inferior colliculus. *Exp Gerontol* 30: 349-360, 1995.

Caspary DM, Palombi PS, and Hughes LF. GABAergic inputs shape responses to amplitude modulated stimuli in the inferior colliculus. *Hear Res* 168: 163-173, 2002.

Casseday JH and Covey E. Frequency tuning properties of neurons in the inferior colliculus of an FM bat. *J Comp Neurol* 319: 34-50, 1992.

Casseday JH and Covey E. A neuroethological theory of the operation of the inferior colliculus. *Brain Behav Evol* 47: 311-346, 1996.

Casseday JH, Ehrlich D, and Covey E. Neural tuning for sound duration: role of inhibitory mechanisms in the inferior colliculus. *Science* 264: 847-850, 1994.

Chen C. Hyperpolarization-activated current (I_h) in primary auditory neurons. *Hear Res* 110: 179-190, 1997.

Chen GD. Effects of stimulus duration on responses of neurons in the chinchilla inferior colliculus. *Hear Res* 122: 142-150, 1998.

Chernock ML, Larue DT, and Winer JA. A periodic network of neurochemical modules in the inferior colliculus. *Hear Res* 188: 12-20, 2004.

Coleman JR and Clerici WJ. Sources of projections to subdivisions of the inferior colliculus in the rat. *J Comp Neurol* 262: 215-226, 1987.

Condon CJ, White KR, and Feng AS. Neurons with different temporal firing patterns in the inferior colliculus of the little brown bat differentially process sinusoidal amplitude-modulated signals. *J Comp Physiol [A]* 178: 147-157, 1996.

Condorelli DF, Belluardo N, Trovato-Salinaro A, and Mudo G. Expression of Cx36 in mammalian neurons. *Brain Res Rev* 32: 72-85, 2000.

Covey E, Kauer JA, and Casseday JH. Whole-cell patch-clamp recording reveals subthreshold sound-evoked postsynaptic currents in the inferior colliculus of awake bats. *J Neurosci* 16: 3009-3018, 1996.

Cui YL, Holt AG, Lomax CA, and Altschuler RA. Deafness associated changes in two-pore domain potassium channels in the rat inferior colliculus. *Neurosci* 149: 421-433, 2007.

Cuttle MF, Rusznak Z, Wong AY, Owens S, and Forsythe ID. Modulation of a presynaptic hyperpolarization-activated cationic current (I(h)) at an excitatory synaptic terminal in the rat auditory brainstem. *J Physiol* 534: 733-744, 2001.

Derjean D, Bertrand S, Nagy F, and Shefchyk SJ. Plateau potentials and membrane oscillations in parasympathetic preganglionic neurones and intermediolateral neurones in the rat lumbosacral spinal cord. *J Physiol* 563: 583-596, 2005.

Deweese MR and Zador AM. Shared and private variability in the auditory cortex. *J Neurophysiol* 92: 1840-1855, 2004.

Edeline JM, Manunta Y, Nodal FR, and Bajo VM. Do auditory responses recorded from awake animals reflect the anatomical parcellation of the auditory thalamus? *Hear Res* 131: 135-152, 1999.

Eggermont JJ. Between sound and perception: reviewing the search for a neural code. *Hear Res* 157: 1-42, 2001.

Egorova M, Ehret G, Vartanian I, and Esser K-H. Frequency response areas of neurons in the mouse inferior colliculus. I. Threshold and tuning characteristics. *Exp Brain Res* 140: 145-161, 2001.

Ehret G and Moffat AJM. Inferior colliculus of the house mouse II. Single unit responses to tones, noise and tone-noise combiantions as a function of sound intensity. *J Comp Physiol [A]* 156: 619-635, 1985.

Ehret G and Riecke S. Mice and humans perceive multiharmonic communication sounds in the same way. *PNAS* 99: 479-482, 2002.

Ehret G and Schreiner CE. Spectral and Intensity Coding in the Auditory Midbrain. In: *The Inferior Colliculus*, edited by Winer J and Schreiner CE. New York: Springer, 2005, p. 312-345.

Ehrlich D, Casseday JH, and Covey E. Neural tuning to sound duration in the inferior colliculus of the big brown bat, Eptesicus fuscus. *J Neurophysiol* 77: 2360-2372, 1997.

Eisenberg LS, Maltan AA, Portillo F, Mobley JP, and House WF. Electrical stimulation of the auditory brain stem structure in deafened adults. *J Rehabil Res Dev* 24: 9-22, 1987.

Faingold CL. The genetically epilepsy-prone rat. *Gen Pharmacol* 19: 331-338, 1988.

Faingold CL. The Midbrain and Audiogenic Seizures. In: *The Inferior Colliculus*, edited by Faingold CL. New York: Springer, 2005, p. 603-625.

Faingold CL. Role of GABA abnormalities in the inferior colliculus pathophysiology - audiogenic seizures. *Hear Res* 168: 223-237, 2002.

Felsheim C and Ostwald J. Responses to exponential frequency modulations in the rat inferior colliculus. *Hear Res* 98: 137-151, 1996.

Feng JJ, Kuwada S, Ostapoff EM, Batra R, and Morest DK. A physiological and structural study of neuron types in the cochlear nucleus. I. Intracellular responses to acoustic stimulation and current injection. *J Comp Neurol* 346: 1-18, 1994.

Fremeau RT, Jr., Troyer MD, Pahner I, Nygaard GO, Tran CH, Reimer RJ, Bellocchio EE, Fortin D, Storm-Mathisen J, and Edwards RH. The expression of vesicular glutamate transporters defines two classes of excitatory synapse. *Neuron* 31: 247-260, 2001.

Fremeau RT, Jr., Voglmaier S, Seal RP, and Edwards RH. VGLUTs define subsets of excitatory neurons and suggest novel roles for glutamate. *Trends Neurosci* 27: 98-103, 2004.

Friauf E. Tonotopic order in the adult and developing auditory system of the rat as shown by c-fos immunocytochemistry. *Eur J Neurosci* 4: 798-812, 1992.

Friedland DR, Popper P, Eernisse R, and Cioffi JA. Differentially expressed genes in the rat cochlear nucleus. *Neuroscience* 142: 753-768, 2006.

Frisina RD, Smith RL, and Chamberlain SC. Encoding of amplitude modulation in the gerbil cochlear nucleus: I. A hierarchy of enhancement. *Hear Res* 44: 99-122, 1990.

Frisina RD and Walton JP. Neuroanatomy of the Central Auditory System. In: *Handbook of Mouse Auditory Research: from Behavior to Molecular Biology.* (1st ed.), edited by Willott JF: CRC Press, 2001, p. 243-277.

Fujino K, Koyano K, and Ohmori H. Lateral and medial olivocochlear neurons have distinct electrophysiological properties in the rat brain slice. *J Neurophysiol* 77: 2788-2804, 1997.

Fujino K and Oertel D. Cholinergic modulation of stellate cells in the mammalian ventral cochlear nucleus. *J Neurosci* 21: 7372-7383, 2001.

Fuzessery ZM and Hall JC. Role of GABA in shaping frequency tuning and creating FM sweep selectivity in the inferior colliculus. *J Neurophysiol* 76: 1059-1073, 1996.

Fuzessery ZM, Richardson MD, and Coburn MS. Neural mechanisms underlying selectivity for the rate and direction of frequency-modulated sweeps in the inferior colliculus of the pallid bat. *J Neurophysiol* 96: 1320-1336, 2006.

Geis HR and Borst JGG. Intracellular responses of neurons in the mouse inferior colliculus to sinusoidal amplitude-modulated tones. *J Neurophysiol* 101: 2002-2016, 2009.

Goldberg JM and Brown PB. Response of binaural neurons of dog superior olivary complex to dichotic tonal stimuli: some physiological mechanisms of sound localization. *J Neurophysiol* 32: 613-636, 1969.

Gonzalez-Lima F and Cada A. Cytochrome oxidase activity in the auditory system of the mouse: a qualitative and quantitative histochemical study. *Neuroscience* 63: 559-578, 1994.

Gooler DM and Feng AS. Temporal coding in the frog auditory midbrain: the influence of duration and rise-fall time on the processing of complex amplitude-modulated stimuli. *J Neurophysiol* 67: 1-22, 1992.

Gordon M and O'Neill WE. An extralemniscal component of the mustached bat inferior colliculus selective for direction and rate of linear frequency modulations. *J Comp Neurol* 426: 165-181, 2000.

Gordon M and O'Neill WE. Temporal processing across frequency channels by FM selective auditory neurons can account for FM rate selectivity. *Hear Res* 122: 97-108, 1998.

Grigg JJ, Brew HM, and Tempel BL. Differential expression of voltage-gated potassium channel genes in auditory nuclei of the mouse brainstem. *Hear Res* 140: 77-90, 2000.

Gutmaniene N, Svirskiene N, and Svirskis G. Firing properties of frog tectal neurons in vitro. *Brain Res* 981: 213-216, 2003.

Hage SR and Ehret G. Mapping responses to frequency sweeps and tones in the inferior colliculus of house mice. *Eur J Neurosci* 18: 2301-2312, 2003.

Hamill OP, Marty A, Neher E, Sakmann B, and Sigworth FJ. Improved patch-clamp techniques for high-resolution current recording from cells and cell-free membrane patches. *Pflugers Arch* 391: 85-100, 1981.

Heil P, Langner G, and Scheich H. Processing of frequency-modulated stimuli in the chick auditory cortex analogue: evidence for topographic representations and possible mechanisms of rate and directional sensitivity. *J Comp Physiol [A]* 171: 583-600, 1992.

Herzog E, Bellenchi GC, Gras C, Bernard V, Ravassard P, Bedet C, Gasnier B, Giros B, and El Mestikawy S. The existence of a second vesicular glutamate transporter specifies subpopulations of glutamatergic neurons. *J Neurosci* 21: RC181, 2001.

Hilbig H, Beil B, Hilbig H, Call J, and Bidmon HJ. Superior olivary complex organization and cytoarchitecture may be correlated with function and catarrhine primate phylogeny. *Brain Struct Funct*: (Epub ahead of print), 2009.

Holmstrom L, Roberts PD, and Portfors CV. Responses to social vocalizations in the inferior colliculus of the mustached bat are influenced by secondary tuning curves. *J Neurophysiol* 98: 3461-3472, 2007.

Horikawa K and Armstrong WE. A versatile means of intracellular labeling: injection of biocytin and its detection with avidin conjugates. *J Neurosci Methods* 25: 1-11, 1988.

House WF, Berliner KI, and Eisenberg LS. Present status and future directions of the Ear Research Institute cochlear implant program. *Acta Otolaryngol* 87: 176-184, 1979.

Hudspeth AJ. Hearing. In: *Principles of Neural Science* (4th ed.), edited by Kandel ER, Schwartz JH and Jessell TM: McGraw-Hill, 2000, p. 590-613.

Hughes SW, Cope DW, and Crunelli V. Dynamic clamp study of I_h modulation of burst firing and delta oscillations in thalamocortical neurons in vitro. *Neuroscience* 87: 541-550, 1998.

Hunter KP and Willott JF. Aging and the auditory brainstem response in mice with severe or minimal presbycusis. *Hear Res* 30: 207-218, 1987.

Ito M, van Adel B, and Kelly JB. Sound localization after transection of the commissure of Probst in the albino rat. *J Neurophysiol* 76: 3493-3502, 1996.

Jaarsma D, Haasdijk ED, Grashorn JAC, Hawkins R, van Duijn W, Verspaget HW, London J, and Holstege JC. Human Cu/Zn superoxide dismutase (SOD1) overexpression in mice causes mitochondrial vacuolization, axonal degeneration, and premature motoneuron death and accelerates motoneuron disease in mice expressing a familial amyotrophic lateral sclerosis mutant SOD1. *Neurobiol Dis* 7: 623-643, 2000.

Jagadeesh B, Wheat HS, and Ferster D. Linearity of summation of synaptic potentials underlying direction selectivity in simple cells of the cat visual cortex. *Science* 262: 1901-1904, 1993.

Jiang MC, Cleland CL, and Gebhart GF. Intrinsic properties of deep dorsal horn neurons in the L6-S1 spinal cord of the intact rat. *J Neurophysiol* 74: 1819-1827, 1995.

Joris PX, Schreiner CE, and Rees A. Neural processing of amplitude-modulated sounds. *Physiol Rev* 84: 541-577, 2004.

Kaneko T, Fujiyama F, and Hioki H. Immunohistochemical localization of candidates for vesicular glutamate transporters in the rat brain. *J Comp Neurol* 444: 39-62, 2002.

Kanold PO and Manis PB. A physiologically based model of discharge pattern regulation by transient K^+ currents in cochlear nucleus pyramidal cells. *J Neurophysiol* 85: 523-538, 2001.

Kashima ML, Goodwin WJ, Balkany T, and Casiano RR. Special Considerations in Managing Geriatric Patients. In: *Otolaryngology Head & Neck Sugery* (4th ed.), edited by Cummings CW. Philadelphia:
Elsevier Mosby, 2005, p. 351-366.

Kazee AM, Han LY, Spongr VP, Walton JP, Salvi RJ, and Flood DG. Synaptic loss in the central nucleus of the inferior colliculus correlates with sensorineural hearing loss in the C57Bl/6 mouse model of presbycusis. *Hear Res* 89: 109-120, 1995.

Kelly JB and Caspary DM. Pharmacology of the Inferior Colliculus. In: *The Inferior Colliculus*, edited by Winer JA and Schreiner CE. New York: Springer, 2005, p. 248-281.

Kerr JND, de Kock CPJ, Greenberg DS, Bruno RM, Sakmann B, and Helmchen F. Spatial organization of neuronal population responses in layer 2/3 of rat barrel cortex. *J Neurosci* 27: 13316-13328, 2007.

Klueva J, Munsch T, Albrecht D, and Pape HC. Synaptic and non-synaptic mechanisms of amygdala recruitment into temporolimbic epileptiform activities. *Eur J Neurosci* 18: 2779-2791, 2003.

Klug A, Khan A, Burger RM, Bauer EE, Hurley LM, Yang L, Grothe B, Halvorsen MB, and Park TJ. Latency as a function of intensity in auditory neurons: influences of central processing. *Hear Res* 148: 107-123, 2000.

Koch U, Braun M, Kapfer C, and Grothe B. Distribution of HCN1 and HCN2 in rat auditory brainstem nuclei. *Eur J Neurosci* 20: 79-91, 2004.

Koch U and Grothe B. Hyperpolarization-activated current (I_h) in the inferior colliculus: distribution and contribution to temporal processing. *J Neurophysiol* 90: 3679-3687, 2003.

Kramer S, Smits J, Goverts S, and Festen J. Gehoorstoornissen samengevat. In: Volksgezondheid Toekomst Verkenning, Nationaal Kompas Volksgezondheid. <http://www.nationaalkompas.nl> Gezondheid en ziekte\ Ziekten en aandoeningen\ Zenuwstelsel en zintuigen\ Gehoorstoornissen. Bilthoven: RIVM, 2006.

Kremer H and Cremers FP. Positional cloning of deafness genes. *Methods Mol Biol* 493: 215-238, 2009.

Krishna BS and Semple MN. Auditory temporal processing: responses to sinusoidally amplitude-modulated tones in the inferior colliculus. *J Neurophysiol* 84: 255-273, 2000.

Kulesza RJ, Jr. Cytoarchitecture of the human superior olivary complex: nuclei of the trapezoid body and posterior tier. *Hear Res* 241: 52-63, 2008.

Kulesza RJ, Vinuela A, Saldana E, and Berrebi AS. Unbiased stereological estimates of neuron number in subcortical auditory nuclei of the rat. *Hear Res* 168: 12-24, 2002.

Kuwada S, Batra R, Yin TC, Oliver DL, Haberly LB, and Stanford TR. Intracellular recordings in response to monaural and binaural stimulation of neurons in the inferior colliculus of the cat. *J Neurosci* 17: 7565-7581, 1997.

Langner G. Evidence for neuronal periodicity detection in the auditory system of the Guinea fowl: implications for pitch analysis in the time domain. *Exp Brain Res* 52: 333-355, 1983.

Langner G and Schreiner CE. Periodicity coding in the inferior colliculus of the cat. I. Neuronal mechanisms. *J Neurophysiol* 60: 1799-1822, 1988.

Le Beau FE, Rees A, and Malmierca MS. Contribution of GABA- and glycine-mediated inhibition to the monaural temporal response properties of neurons in the inferior colliculus. *J Neurophysiol* 75: 902-919, 1996.

Leao KE, Leao RN, Sun H, Fyffe REW, and Walmsley B. Hyperpolarization-activated currents are differentially expressed in mice brainstem auditory nuclei. *J Physiol* 576: 849-864, 2006.

Li Y and Bennett DJ. Persistent sodium and calcium currents cause plateau potentials in motoneurons of chronic spinal rats. *J Neurophysiol* 90: 857-869, 2003.

Li Y, Evans MS, and Faingold CL. In vitro electrophysiology of neurons in subnuclei of rat inferior colliculus. *Hear Res* 121: 1-10, 1998.

Lim HH, Lenarz T, Joseph G, Battmer RD, Patrick JF, and Lenarz M. Effects of phase duration and pulse rate on loudness and pitch percepts in the first auditory midbrain implant patients: Comparison to cochlear implant and auditory brainstem implant results. *Neuroscience* 154: 370-380, 2008.

Liu BH, Wu GK, Arbuckle R, Tao HW, and Zhang LI. Defining cortical frequency tuning with recurrent excitatory circuitry. *Nat Neurosci* 10: 1594-1600, 2007.

Liu X-B, Low LK, Jones EG, and Cheng H-J. Stereotyped axon pruning via plexin signaling is associated with synaptic complex elimination in the hippocampus. *J Neurosci* 25: 9124-9134, 2005.

Loftus WC, Malmierca MS, Bishop DC, and Oliver DL. The cytoarchitecture of the inferior colliculus revisited: a common organization of the lateral cortex in rat and cat. *Neuroscience* 154: 196-205, 2008.

Malmierca MS, Le Beau FE, and Rees A. The topographical organization of descending projections from the central nucleus of the inferior colliculus in guinea pig. *Hear Res* 93: 167-180, 1996.

Mardia KV and Jupp PE. *Directional statistics*. Chichester, UK: Wiley, 2000.

Margrie TW, Brecht M, and Sakmann B. In vivo, low-resistance, whole-cell recordings from neurons in the anaesthetized and awake mammalian brain. *Pflügers Arch* 444: 491-498, 2002.

Meininger V, Pol D, and Derer P. The inferior colliculus of the mouse. A Nissl and Golgi study. *Neuroscience* 17: 1159-1179, 1986.

Merchán M, Aguilar LA, Lopez-Poveda EA, and Malmierca MS. The inferior colliculus of the rat: quantitative immunocytochemical study of GABA and glycine. *Neuroscience* 136: 907-925, 2005.

Metherate R and Ashe JH. Facilitation of an NMDA receptor-mediated EPSP by paired-pulse stimulation in rat neocortex via depression of GABAergic IPSPs. *J Physiol* 481 (Pt 2): 331-348, 1994.

Needham K and Paolini AG. Neural timing, inhibition and the nature of stellate cell interaction in the ventral cochlear nucleus. *Hear Res* 216-217: 31-42, 2006.

Neher E and Sakmann B. Single-channel currents recorded from membrane of denervated frog muscle fibres. *Nature* 260: 799-802, 1976.

Nelson PG and Erulkar SD. Synaptic mechanisms of excitation and inhibition in the central auditory pathway. *J Neurophysiol* 26: 908-923, 1963.

Notomi T and Shigemoto R. Immunohistochemical localization of I_h channel subunits, HCN1-4, in the rat brain. *J Comp Neurol* 471: 241-276, 2004.

Nuding SC, Chen GD, and Sinex DG. Monaural response properties of single neurons in the chinchilla inferior colliculus. *Hear Res* 131: 89-106, 1999.

Nudo RJ and Masterton RB. Stimulation-induced [14C]2-deoxyglucose labeling of synaptic activity in the central auditory system. *J Comp Neurol* 245: 553-565, 1986.

Nyby JG. Auditory Communication Among Adults. In: *Handbook of mouse auditory research: from behavior to molecular biology*, edited by Willott JF. Boca Raton: CRC Press, 2001, p. 3-18.

Oertel D. The role of intrinsic neuronal properties in the encoding of auditory information in the cochlear nuclei. *Curr Opin Neurobiol* 1: 221-228, 1991.

Ohki K, Chung S, Ch'ng YH, Kara P, and Reid RC. Functional imaging with cellular resolution reveals precise micro-architecture in visual cortex. *Nature* 433: 597-603, 2005.

Oliver DL. Neuronal Organization in the Inferior Colliculus. In: *The inferior colliculus*, edited by Winer JA and Schreiner CE. New York: Springer, 2005, p. 69-114.

Otsu N. A threshold selection method from gray level histograms. *{IEEE} Trans Systems, Man and Cybernetics* 9: 62-66, 1979.

Palombi PS and Caspary DM. Physiology of the young adult Fischer 344 rat inferior colliculus: responses to contralateral monaural stimuli. *Hear Res* 100: 41-58, 1996.

Paolini AG, Clarey JC, Needham K, and Clark GM. Balanced inhibition and excitation underlies spike firing regularity in ventral cochlear nucleus chopper neurons. *Eur J Neurosci* 21: 1236-1248, 2005.

Paxinos G and Watson C. *The Rat Brain in Stereotaxic coordinates*. San Diego: Academic Press, 1998.

Pedemonte M, Torterolo P, and Velluti RA. In vivo intracellular characteristics of inferior colliculus neurons in guinea pigs. *Brain Res* 759: 24-31, 1997.

Perez-Gonzalez D, Malmierca MS, Moore JM, Hernandez O, and Covey E. Duration selective neurons in the inferior colliculus of the rat: topographic distribution and relation of duration sensitivity to other response properties. *J Neurophysiol* 95: 823-836, 2006.

Peruzzi D, Sivaramakrishnan S, and Oliver DL. Identification of cell types in brain slices of the inferior colliculus. *Neuroscience* 101: 403-416, 2000.

Petit C. From deafness genes to hearing mechanisms: harmony and counterpoint. *Trends Mol Med* 12: 57-64, 2006.

Pinheiro AD, Wu M, and Jen PHS. Encoding repetition rate and duration in the inferior colliculus of the big brown bat, *Eptesicus fuscus*. *J Comp Physiol A* 169: 69-85, 1991.

Pollak GK, Marsh DS, Bodenhamer R, and Souther A. A single-unit analysis of inferior colliculus in unanesthetized bats: response patterns and spike-count functions generated by constant-frequency and frequency-modulated sounds. *J Neurophysiol* 41: 677-691, 1978.

Poon PWF and Yu PP. Spectro-temporal receptive fields of midbrain auditory neurons in the rat obtained with frequency modulated stimulation. *Neurosci Lett* 289: 9-12, 2000.

Poremba A, Jones D, and Gonzalez-Lima F. Metabolic effects of blocking tone conditioning on the rat auditory system. *Neurobiology of learning and memory* 68: 154-171, 1997.

Potter HD. Patterns of acoustically evoked discharges of neurons in the mesencephalon of the bullfrog. *J Neurophysiol* 28: 1155-1184, 1965.

Priebe NJ and Ferster D. Direction selectivity of excitation and inhibition in simple cells of the cat primary visual cortex. *Neuron* 45: 133-145, 2005.

Purvis LK and Butera RJ. Ionic current model of a hypoglossal motoneuron. *J Neurophysiol* 93: 723-733, 2005.

Ramón y Cajal S. *Histology of the Nervous System of Man and Vertebrates.* New York: Oxford University Press, 1995.

Rapin I and Gravel J. "Auditory neuropathy": physiologic and pathologic evidence calls for more diagnostic specificity. *Int J Pediatr Otorhinolaryngol* 67: 707-728, 2003.

Rees A and Langner G. Temporal Coding in the Auditory Midbrain. In: *The inferior colliculus*, edited by Winer J and Schreiner C. New York: Springer, 2005, p. 316-376.

Rees A and Møller AR. Responses of neurons in the inferior colliculus of the rat to AM and FM tones. *Hear Res* 10: 301-330, 1983.

Rees A, Sarbaz A, Malmierca MS, and Le Beau FE. Regularity of firing of neurons in the inferior colliculus. *J Neurophysiol* 77: 2945-2965, 1997.

Reetz G and Ehret G. Inputs from three brainstem sources to identified neurons of the mouse inferior colliculus slice. *Brain Res* 816: 527-543, 1999.

Rhode WS and Greenberg S. Encoding of amplitude modulation in the cochlear nucleus of the cat. *J Neurophysiol* 71: 1797-1825, 1994.

Rhode WS and Greenberg S. Physiology of the Cochlear Nuclei. In: *The mammalian auditory system: neurophysiology*, edited by Popper AN and Fay RR, 1992, p. 94-152.

Robinson RB and Siegelbaum SA. Hyperpolarization-activated cation currents: from molecules to physiological function. *Annu Rev Physiol* 65: 453-480, 2003.

Rodrigues ARA and Oertel D. Hyperpolarization-activated currents regulate excitability in stellate cells of the mammalian ventral cochlear nucleus. *J Neurophysiol* 95: 76-87, 2006.

Rodriguez-Contreras A, de Lange RPJ, Lucassen PJ, and Borst JGG. Branching of calyceal afferents during postnatal development in the rat auditory brainstem. *J Comp Neurol* 496: 214-228, 2006.

Rose JE, Greenwood DD, Goldberg JM, and Hind JE. Some discharge characteristics of single neurons in the inferior colliculus of the cat. I. Tonotopical organization, relation of spike-counts to tone intensity, and firing patterns of single elements. *J Neurophysiol* 26: 294-320, 1963.

Rothman JS and Manis PB. The roles potassium currents play in regulating the electrical activity of ventral cochlear nucleus neurons. *J Neurophysiol* 89: 3097-3113, 2003.

Ruggero MA and Temchin AN. Similarity of traveling-wave delays in the hearing organs of humans and other tetrapods. *J Assoc Res Otolaryngol* 8: 153-166, 2007.

Ryugo DK, Willard FH, and Fekete DM. Differential afferent projections to the inferior colliculus from the cochlear nucleus in the albino mouse. *Brain Res* 210: 342-349, 1981.

Saint Marie RL, Luo L, and Ryan AF. Effects of stimulus frequency and intensity on c-fos mRNA expression in the adult rat auditory brainstem. *J Comp Neurol* 404: 258-270, 1999.

Saint Marie RL, Schneiderman A, and Stanforth DA. Glycine-immunoreactive projections of the cat lateral superior olive: possible role in midbrain ear dominance. *J Comp Neurol* 389: 264-276, 1997.

Saldaña E and Merchán MA. Intrinsic and Commissural Connections of the Inferior Colliculus. In: *The inferior colliculus*, edited by Winer JA and Schreiner CE. New York: Springer, 2005, p. 155-181.

Salvi RJ, Wang J, and Ding D. Auditory plasticity and hyperactivity following cochlear damage. *Hear Res* 147: 261-274, 2000.

Santi PA and Mancini P. Cochlear Anatomy and Central Auditory Pathways. In: *Otolaryngology Head & Neck Surgery* (4th ed.), edited by Cummings CW. Philadelphia: Elsevier Mosby, 2005, p. 3373-3401.

Schofield BR. Superior Olivary Complex and Lateral Lemniscal Connections of the Auditory Midbrain. In: *The inferior colliculus*, edited by Winer JA and Schreiner CE. New York: Springer, 2005, p. 132-154.

Schofield BR and Cant NB. Descending auditory pathways: projections from the inferior colliculus contact superior olivary cells that project bilaterally to the cochlear nuclei. *J Comp Neurol* 409: 210-223, 1999.

Schreiner CE and Langner G. Periodicity coding in the inferior colliculus of the cat. II. Topographical organization. *J Neurophysiol* 60: 1823-1840, 1988.

Schwartz MS, Otto SR, Shannon RV, Hitselberger WE, and Brackmann DE. Auditory brainstem implants. *Neurotherapeutics* 5: 128-136, 2008.

Semple MN and Aitkin LM. Physiology of pathway from dorsal cochlear nucleus to inferior colliculus revealed by electrical and auditory stimulation. *Exp Brain Res* 41: 19-28, 1980.

Seyfried TN, Todorova MT, and Poderycki MJ. Experimental models of multifactorial epilepsies: the EL mouse and mice susceptible to audiogenic seizures. *Adv Neurol* 79: 279-290, 1999.

Shaddock Palombi P, Backoff PM, and Caspary DM. Responses of young and aged rat inferior colliculus neurons to sinusoidally amplitude modulated stimuli. *Hear Res* 153: 174-180, 2001.

Shaikh AG and Finlayson PG. Hyperpolarization-activated (I_h) conductances affect brainstem auditory neuron excitability. *Hear Res* 183: 126-136, 2003.

Sharp AA, O'Neil MB, Abbott LF, and Marder E. Dynamic clamp: computer-generated conductances in real neurons. *J Neurophysiol* 69: 992-995, 1993.

Sinex DG, Henderson J, Li H, and Chen GD. Responses of chinchilla inferior colliculus neurons to amplitude-modulated tones with different envelopes. *J Assoc Res Otolaryngol* 3: 390-402, 2002.

Sinex DG, Li H, and Velenovsky DS. Prevalence of stereotypical responses to mistuned complex tones in the inferior colliculus. *J Neurophysiol* 94: 3523-3537, 2005.

Sivaramakrishnan S and Oliver DL. Distinct K currents result in physiologically distinct cell types in the inferior colliculus of the rat. *J Neurosci* 21: 2861-2877, 2001.

Smith M and Perrier J-F. Intrinsic properties shape the firing pattern of ventral horn interneurons from the spinal cord of the adult turtle. *J Neurophysiol* 96: 2670-2677, 2006.

Smith PH. Anatomy and physiology of multipolar cells in the rat inferior collicular cortex using the *in vitro* brain slice technique. *J Neurosci* 12: 3700-3715, 1992.

Söhl G, Maxeiner S, and Willecke K. Expression and functions of neuronal gap junctions. *Nat Rev Neurosci* 6: 191-200, 2005.

Spangler KM, Cant NB, Henkel CK, Farley GR, and Warr WB. Descending projections from the superior olivary complex to the cochlear nucleus of the cat. *J Comp Neurol* 259: 452-465, 1987.

Stiebler I and Ehret G. Inferior colliculus of the house mouse. I. A quantitative study of tonotopic organization, frequency representation, and tone-threshold distribution. *J Comp Neurol* 238: 65-76, 1985.

Suga N. Analysis of frequency-modulated sounds by auditory neurons of echo-locating bats. *J Physiol* 179: 26-53, 1965.

Suga N. Classification of inferior collicular neurons of bats in terms of responses to pure tones, FM sounds and noise bursts. *J Physiol* 200: 555-574, 1969.

Suga N and Schlegel P. Coding and processing in the auditory systems of FM-signal-producing bats. *J Acoust Soc Am* 54: 174-190, 1973.

Sun H and Wu SH. Modification of membrane excitability of neurons in the rat's dorsal cortex of the inferior colliculus by preceding hyperpolarization. *Neuroscience* 154: 257-272, 2008.

Syka J. Plastic changes in the central auditory system after hearing loss, restoration of function, and during learning. *Physiol Rev* 82: 601-636, 2002.

Tan AY, Zhang LI, Merzenich MM, and Schreiner CE. Tone-evoked excitatory and inhibitory synaptic conductances of primary auditory cortex neurons. *J Neurophysiol* 92: 630-643, 2004.

Tan ML and Borst JGG. Comparison of responses of neurons in the mouse inferior colliculus to current injections, tones of different durations, and sinusoidal amplitude-modulated tones. *J Neurophysiol* 98: 454-466, 2007.

Tan ML, Theeuwes HP, Feenstra L, and Borst JGG. Membrane properties and firing patterns of inferior colliculus neurons: an in vivo patch-clamp study in rodents. *J Neurophysiol* 98: 443-453, 2007.

Thompson AM. Descending Connections of the Auditory Midbrain. In: *The Inferior Colliculus*, edited by Winer JA and Schreiner CE. New York: Springer, 2005, p. 182-199.

Tibesar RJ and Shallop JK. Auditory Neuropathy. In: *Otolaryngology Head & Neck Surgery* (4th ed.), edited by Cummings CW. Philadelphia: Elsevier Mosby, 2005, p. 3503-3521.

Traub RD, Draguhn A, Whittington MA, Baldeweg T, Bibbig A, Buhl EH, and Schmitz D. Axonal gap junctions between principal neurons: a novel source of network oscillations and perhaps epileptogenesis. *Rev Neurosci* 13(1): 1-30, 2002.

Valiante TA, Perez Velazquez JL, Jahromi SS, and Carlen PL. Coupling potentials in CA1 neurons during calcium-free-induced field burst activity. *J Neurosci* 15: 6946-6956, 1995.

Verkhratsky A, Krishtal OA, and Petersen OH. From Galvani to patch clamp: the development of electrophysiology. *Pflugers Arch* 453: 233-247, 2006.

Viana F, Bayliss DA, and Berger AJ. Repetitive firing properties of developing rat brainstem motoneurons. *J Physiol* 486: 745-761, 1995.

Vigmond EJ, Perez Velazquez JL, Valiante TA, Bardakjian BL, and Carlen PL. Mechanisms of electrical coupling between pyramidal cells. *J Neurophysiol* 78(6): 3107-3116, 1997.

Voytenko SV and Galazyuk AV. Intracellular recording reveals temporal integration in inferior colliculus neurons of awake bats. *J Neurophysiol* 97: 1368-1378, 2007.

Wagner T. Intrinsic properties of identified neurones in the central nucleus of mouse inferior colliculus. *Neuroreport* 6: 89-93, 1994.

Walton JP, Frisina RD, and O'Neill WE. Age-related alteration in processing of temporal sound features in the auditory midbrain of the CBA mouse. *J Neurosci* 18: 2764-2776, 1998.

Walton JP, Simon H, and Frisina RD. Age-related alterations in the neural coding of envelope periodicities. *J Neurophysiol* 88: 565-578, 2002.

Webster WR. Auditory System. In: *The Rat Nervous System* (2nd ed.), edited by Paxinos G: Academic Press, 1995, p. 797-831.

Wehr M and Zador AM. Balanced inhibition underlies tuning and sharpens spike timing in auditory cortex. *Nature* 426: 442-446, 2003.

Wenstrup JJ. The Tectothalamic System. In: *The Inferior Colliculus*, edited by Winer JA and Schreiner CE. New York: Springer, 2005, p. 200-230.

Willott JF. Focus: Diversity of the Mouse Central Auditory System. In: *Handbook of mouse auditory research: from behavior to molecular biology*, edited by Willott JF. New York: CRC Press, 2001, p. 239-242.

Willott JF. Hearing Loss and the Inferior Colliculus. In: *The Inferior Colliculus*, edited by Winer JA and Schreiner CE. New York: Springer, 2005, p. 585-602.

Willott JF, Bross LS, and McFadden SL. Morphology of the inferior colliculus in C57BL/6J and CBA/J mice across the life span. *Neurobiol Aging* 15: 175-183, 1994.

Willott JF, Hnath Chisolm T, and Lister JJ. Modulation of presbycusis: current status and future directions. *Audiol Neurotol* 6: 231-249, 2001.

Willott JF, Parham K, and Hunter KP. Comparison of the auditory sensitivity of neurons in the cochlear nucleus and inferior colliculus of young and aging C57BL/6J and CBA/J mice. *Hear Res* 53: 78-94, 1991.

Willott JF and Urban GP. Response properties of neurons in nuclei of the mouse inferior colliculus. *J Comp Physiol [A]* 127: 175-184, 1978.

Winer JA. Three Systems of Descending Projections to the Inferior Colliculus. In: *The Inferior Colliculus*, edited by Winer JA and Schreiner CE. New York: Springer, 2005, p. 231-247.

Winer JA and Schreiner CE. The Central Auditory System: a Functional Analysis. In: *The Inferior Colliculus*, edited by Winer J and Schreiner C. New York: Springer, 2005, p. 1-68.

Wu SH. Biophysical Properties of Inferior Colliculus Neurons. In: *The inferior colliculus*, edited by Winer JA and Schreiner CE. New York: Springer, 2005, p. 282-311.

Wu SH, Ma CL, and Kelly JB. Contribution of AMPA, NMDA, and GABA(A) receptors to temporal pattern of postsynaptic responses in the inferior colliculus of the rat. *J Neurosci* 24: 4625-4634, 2004.

Xia YF, Qi ZH, and Shen JX. Neural representation of sound duration in the inferior colliculus of the mouse. *Acta Otolaryngol* 120: 638-643, 2000.

Xie R, Gittelman JX, Li N, and Pollak GD. Whole cell recordings of intrinsic properties and sound-evoked responses from the inferior colliculus. *Neuroscience* 154: 245-256, 2008.

Xie R, Gittelman JX, and Pollak GD. Rethinking tuning: in vivo whole-cell recordings of the inferior colliculus in awake bats. *J Neurosci* 27: 9469-9481, 2007.

Yin TCT and Chan JCK. Interaural time sensitivity in medial superior olive of cat. *J Neurophysiol* 64: 465-488, 1990.

Yu X, Wadghiri YZ, Sanes DH, and Turnbull DH. In vivo auditory brain mapping in mice with Mn-enhanced MRI. *Nat Neurosci* 8: 961-968, 2005.

Zappalà A, Cicero D, Serapide MF, Paz C, Catania MV, Falchi M, Parenti R, Pantò MR, La Delia F, and Cicirata F. Expression of pannexin1 in the CNS of adult mouse: cellular localization and effect of 4-aminopyridine-induced seizures. *Neuroscience* 141: 167-178, 2006.

Zhang H and Kelly JB. AMPA and NMDA receptors regulate responses of neurons in the rat's inferior colliculus. *J Neurophysiol* 86: 871-880, 2001.

Zhang LI, Tan AY, Schreiner CE, and Merzenich MM. Topography and synaptic shaping of direction selectivity in primary auditory cortex. *Nature* 424: 201-205, 2003.